SOME PHYSICAL PROPERTIES OF CRYSTALLINE SODIUM: AN X-RAY INVESTIGATION

by

D. W. FIELD, B.Sc. (Hons.)

A Thesis

submitted for the Degree of

Doctor of Philosophy

in the Department of Physics

University of Adelaide

December 1971

CONTENTS

SUMMARY

This thesis describes an accurate and detailed X-ray study of crystalline sodium. Two previous papers on the temperature dependence of the intensities are reviewed and their limitations discussed. Accurate measured structure factors are presented for the first time, and an accurate X-ray Debye temperature is determined at room temperature.

Methods for determining real space distributions from limited amounts of reciprocal space data while avoiding termination effects have been investigated. An easy, rapid and sensitive integral method for the determination of the real space distribution for spherically symmetric atoms was developed and tested. The three dimensional summation analogue is also presented.

Single crystals of sodium of 3N purity were grown. A total of six sets of integrated Weissenberg photographic intensities were recorded from two crystals at two wavelengths at room temperature. The intensities were measured using a Joyce-Loebl microdensitometer and corrected for various effects. Considerable care was taken in recording and measurement to ensure the greatest possible accuracy.

Considerable anisotropy in the intensities at room temperature was observed. This was considered to be due to anharmonic vibration of the atoms and was analysed using a fourth order potential

expansion. This is the first time that such anharmonic vibration anistropy in a body-centred-cubic solid has been analysed in this way. The atoms were found to be vibrating with greater amplitude towards the next nearest neighbours and with less amplitude towards the nearest neighbours. An isotropic Debye parameter and a single anisotropic vibration parameter were determined for each of five data sets. An accurate value of the X-ray Debye temperature at room temperature was found from the average of the five isotropic Debye parameters. A re-analysis of previous work on the basis of anharmonic vibration theory gave potential parameters which were in reasonable agreement with those obtained from the present measurements. An alternative description of the anisotropy as being due to electron density distortion for an isotropically vibrating atom was found to give an almost equally good mathematical description, indicating that it provides a good description of the time averaged electron density. Structure factors were calculated after taking account of this anisotropy and are presented for all six sets of data. An accuracy of 2 - 3% is claimed.

Considerable extinction was present in all samples. The extinction was investigated using a wavelength dependent mathematical treatment, and corrected structure factors are presented for two data sets. Evidence for room temperature annealing over a period of several weeks due to the thermal motion of the atoms is presented.

The contribution of the 3s electron to the structure factors was confirmed to be unobservable.

Seven structure factors were measured from a small spherical crystal of sodium using an absolute counting technique. Intensities were corrected and structure factors calculated and presented. The above observations have been confirmed but on a relative basis.

DECLARATION

The work described in this thesis was carried out in the Department of Physics between February 1968 and December 1971. No material contained in this thesis has been submitted for the award of any other degree or diploma in this or any other University. To the best of the author's knowledge and belief, the thesis contains no material previously published or written by another person except where due reference is made in the text.

D. W. Field

ACKNOWLEDGEMENTS

I would like to thank my supervisor, Dr. E. H. Medlin for suggesting the project and for his guidance and insight throughout the work.

The facilities of the Physics Department were generously provided by Professor J. H. Carver.

I would like to thank Mr. K. Metcalfe on the Defence Standards Laboratories, Adelaide, for his help with xerographic recording, and Dr. M. R. Snow (Physical and Inorganic Chemistry Department (Adelaide)) for his help with two programs in the crystallographic computing library at Adelaide. I am indebted to Dr. S. W. Kennedy of the Physical and Inorganic Chemistry Department of the Univetsity of Adelaide, who provided facilities including the X-ray generator, horizontal goniometer and some of the electronic equipment used for the work described in Chapter 6. I am also grateful to Drs. R. E. Dingle and P. M. Colman for helpful discussions and to Miss H. Barrow for assistance with calculations.

This work was made possible by the tenure of a Commonwealth Postgraduate Award (1968-1971).

CHAPTER 1

INTRODUCTION

1.1 The Aim of the Project

There has been considerable interest in recent years in accurate measurement of the X-ray structure factors of various elements. Such measurements may be expected to give information about the effect of the crystal field on the electron distribution and vibrational properties of the atoms. For example, measurements of "forbidden" reflections in diamond-type structures gives information about the covalent bonding (Dawson (1967b)). Measurements of low angle reflections in metals provide information about the effect of the crystal field on the valence electrons (e.g. Raccah and Henrich (1969) for aluminium). Finally, measurements of a number of reflections at the same temperature, or more usually of the same reflection at several temperatures, provide information about the effect of the crystal field on the vibrations of the atoms in the lattice.

Alkali metals are of considerable interest in theoretical physics because their characteristic electronic structure of an inert gas core and single valence electron makes them the most fundamental of metals and enables various solid state calculations to be performed with relative simplicity. On the other hand, their

somewhat intractable chemical and physical properties have meant that very little definitive X-ray or neutron diffraction work has been done for comparison.

The aim of the project was to measure as accurately as possible X-ray structure factors for one or more of the alkali metals in order to determine crystal field effects, and to relate these results to relevant known information about the alkali metals.

It was decided to measure accurate relative intensities photographically, with the possible measurement of absolute structure factors by counter techniques for comparison. Indeed, both measurements were made, the photographic relative intensity measurements being described in Chapters 3 to 5 and the absolute counter measurements being described in Chapter 6.

1.2 Properties of Sodium

Sodium is a soft, silvery, metallic, polycrystalline solid at room temperature. It has a specific gravity of .971 and a melting point of 97.81^{o}C. Single crystals of 99.9% purity have been grown as part of this work.

Hull (1917) found the crystal structure to be body-centred-cubic at room temperature. The space group is Im3m and there are two atoms per unit cell. The value of the lattice parameter used

throughout this work was 4.2906Å at room temperature (American Institute of Physics Handbook, 2nd Ed. (1963)). This value is in good agreement with a recent value of 4.28860Å at 25°C (Feder and Charbnau (1966)), determined from a thermal expansion method using X-ray and interferometric techniques.

The electronic structure for the eleven electrons in free sodium atoms is $1s^2$, $2s^2$, $2p^6$ (neon core), $3s^1$. An energy diagram for atomic and solid sodium is shown in Figure 1.1. The energies for the 1s and 2s, 2p levels were obtained from X-ray emission wavelengths and that for the 3s level in the atom from the ionisation energy. The value of -2.3 eV used for the top of the 3s band was considered the best for a range of values from 2.06 to 2.47 eV for the work function for sodium. The width of 3.4 eV for the 3s band in the solid is given by the width of the soft X-ray emission band. This latter agrees fairly well with the value of 3.2 eV calculated on the basis of the free electron theory (Seitz (1940)).

A number of other properties of sodium are consistent with the simple free electron theory of metals, the number of free electrons in this case being one. Among these are values for the electrical resistivity of solid sodium (5.23×10^{-6} ohm-cm at 29.4°C (Handbook of Chemistry and Physics (1967))) and the Hall coefficient ($-23.6 \times 10^{-11} m^3$/coulomb) (Kittel (1971)). (The calculated single free electron value for the Hall coefficient is $-24.7 \times 10^{-11} m^3$/

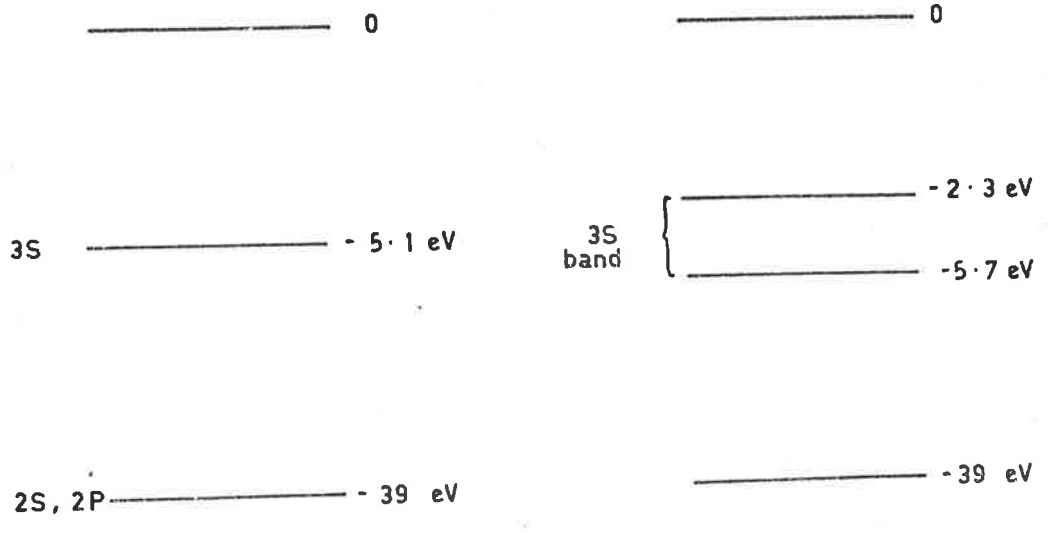

FIG. 1·1 ENERGY LEVEL DIAGRAM FOR SODIUM. (not drawn to scale)

coulomb. The negative sign indicates that the charge carriers are electrons and the density of charge carriers measured by the Hall effect is 1.05 per atom). This theory is also supported by thermoelectric power measurements in that they are negative and tend to zero at low temperatures.

Further, a considerable amount of evidence has shown that the Fermi surface of sodium is spherical to a very good degree of approximation. (Were it to be entirely spherical, the behaviour of the outer electron of sodium could be described entirely by the free electron theory of metals). Such evidence is obtained from the positron annihilation experiments of Donaghy and Stewart (1967), the cyclotron resonance experiments of Grimes and Kip (1963), and the de Haas-van Alphen effect measurements of Shoenberg and Stiles (1964). Such techniques have measured the sphericity of the Fermi surface to $\sim$1%. This evidence is in accordance with the prediction of Cohen and Heine (1958) on the basis of pseudopotential calculations.

Moreover, the ground state outer electron momentum density distributions measured by Phillips and Weiss (1968) by means of a Compton line-shape technique give the momentum density in sodium as "essentially spherically symmetric".

However, sodium is, elastically, a very anisotropic material.

The most accurate values of its elastic constants are considered to be those given by Martinson (1969). These are

$$c_{11} = 76.9 \times 10^9 \text{ dynes/cm}^2$$
$$c_{12} = 64.7 \times 10^9 \text{ dynes/cm}^2$$
$$\text{and } c_{44} = 43.4 \times 10^9 \text{ dynes/cm}^2$$

Using these values, the anisotropy factor, which is given by

$$A = \frac{2c_{44}}{c_{11}-c_{12}}$$

is 7.1. (An elastically isotropic cubic crystal has an anisotropy factor of 1). The relatively low values of the elastic constants mean that elastic moduli such as the compressibility K, Young's modulus Y and the shear modulus n are relatively high (for K) and low (for Y and n), and explain the softness exhibited by the metal. The formulae and the values obtained on substituting for the elastic constants are

$$K = \frac{3}{c_{11}+2c_{12}}$$
$$= .0145 \times 10^{-9} \text{cm}^2/\text{dyne}$$
$$Y = \frac{(c_{11}-c_{12})(2c_{12}+c_{11})}{c_{11}+c_{12}}$$
$$= 178 \times 10^9 \text{ dynes/cm}^2$$

and $n = c_{44}$ for a shearing strain in the [100] cube direction $= 43.4 \times 10^9$ dynes/cm^2. Finally, the Cauchy relation given by $c_{12} = c_{44}$ holds if the interaction between atoms are due to central forces and if each atom is at a centre of symmetry. Since the second of these two conditions holds for the sodium structure, the fact that the Cauchy relation breaks down implies that the forces between the atoms are not central.

1.3 Wave Function and Scattering Factor Calculations for Sodium

A number of wave function calculations have been made for atomic sodium. The earliest was the self-consistent-field determination of Hartree (1928), on which were based the scattering factor calculations of James and Brindley (1931). A later wave function calculation by Hartree and Hartree (1948) was a solution of Fock's equations for the self-consistent-field with an exchange correction. It formed the basis of subsequent calculations of atomic scattering factors by Berghuis et al. (1955) and Freeman (1959).

Scattering factor calculations have been the subject of a review by Cromer (1965b). The most recently published values have been those of Cromer and Mann (1968), based on numerical Hartree-Fock wave functions calculated by Mann (1967), and those of Doyle and Turner (1968). These last values, which were calculated from

an Hartree-Fock atomic wave function due to Coulthard (1967), with allowance for relativistic effects, could be expected to be the most reliable published values.

However, the relativistic effect is negligible for wave functions of elements with low atomic numbers, as can be seen from Table 1.1.

TABLE 1.1

Calculated Scattering Factors for Sodium

$\frac{\sin\theta_B}{\lambda}$	Present Work	Doyle-Turner
.20	8.337	8.335
.25	7.621	7.618
.30	6.884	6.881
.35	6.159	6.156
.40	5.475	5.471
.45	4.851	4.848
.50	4.297	4.293
.60	3.401	3.398

The values labelled Doyle-Turner were taken from the paper of Doyle and Turner (1968). The values labelled Present Work were calculated by the author. Program SCATFAC (Appendix 1) was written to carry out the numerical calculation using the Hartree and

Hartree (1948) wave function values. Doyle and Turner comment that the fourth and probably the third figures in their calculation have no physical significance, and are useful merely for interpolation purposes. It can be seen that the two sets of values agree to better than .01%. Therefore the values of calculated scattering factors used in this work are those calculated by the author from the Hartree and Hartree (1948) wave functions.

1.4 The Debye Temperature and X-ray Scattering

It is convenient in crystallography to describe the temperature variation of the scattered intensity in terms of the Debye-Waller factor thus:

$$I_T \sim \exp\left|-2W\right|$$

$$\sim \exp\left|-2B_B s^2\right|$$

where B is known as the Debye parameter and $s = \frac{\sin\theta_B}{\lambda}$

This theory assumes that the atoms are vibrating harmonically. This is never true, even at $0^{\circ}K$, but is often a sufficiently good approximation to enable a value of the X-ray Debye temperature θ_D to be obtained. This estimate of the Debye temperature is similar to the characteristic temperature obtained from specific heat measurements (Zener and Bilinsky (1936)). For a cubic monatomic

crystal the relation between B and θ_D may be written

$$B = \frac{6h^2T}{km\theta_D^2}\left|\phi(x) + \frac{x}{4}\right| \qquad \ldots(1.4.1)$$

where $x = \frac{\theta_D}{T}$

T is the temperature in ^oK

ϕ is the function $\frac{1}{x}\int_o^x \frac{y\,dy}{e^y-1}$

and the other symbols have their usual meanings.

Walford and Schoeffel (1970) point out that if harmonic vibrations of the atoms are assumed, there are at least three ways of determining the X-ray Debye temperature of a crystal. These are:

(a) The measurement of the integrated intensity of a Bragg reflection at two or more temperatures. A plot of $\ln\left(\frac{I_{Ti}}{I_{To}}\right)$ versus temperature will give a straight line from which can be determined the Debye temperature θ_D. Here I_{Ti} represents the integrated intensity of the reflection at temperature T_i, and I_{To} represents the integrated intensity of the reflection at some reference temperature T_o.

(b) The measurement of the integrated intensities of a large number of Bragg reflections at the same temperature. The graph of $\ln\left(\frac{I_i}{F_c^2}\right)$ versus $\left(\frac{\sin\theta_B}{\lambda}\right)^2$ gives a straight line, the slope of which yields the temperature factor B and hence

θ_D can be found. Here I_i is the measured integrated intensity for the ith reflection, and F_c its calculated structure factor. An example of the use of method (b) for the accurate determination of the Debye temperature of aluminium at room temperature is given in the paper of Dingle and Medlin (1971). The third method for determination of X-ray Debye temperature is:

(c) The determination of the inversion temperature of first order thermal diffuse scattering near a Bragg reflection hkl (Canut and Amoros (1961)). For the temperature range $\theta_D < T < T_{mp}$, where T_{mp} is the melting point, the relation for inversion temperature T_{inv} is given by

$$T_{inv} = \frac{km}{3h^2} \theta_D^2 d_{hkl}^2 \qquad \ldots(1.4.2)$$

where d_{hkl} is the spacing of the hkl Miller planes and the other symbols have their usual meaning.

Little experimental work has been done using this last method, probably because of the difficulties associated with measuring thermal diffuse scattering intensities accurately. In addition, because the inversion temperature depends on the plane spacing (equation 1.4.2), measurements of diffuse scattering near a low angle reflection, such as 211 for sodium, would have to be made to

obtain T_{inv} near room temperature. Because extinction or temperature changes of the mosaic structure would make either this or the first method less accurate, the second method was chosen for this work.

1.5 Review of Previous X-ray Investigations of Sodium

Few X-ray diffraction investigations of sodium or any of the alkali metals have been attempted. Hull (1917) determined the space group and the location of the single atoms at special positions in the unit cell, Lonsdale (1942) mapped the thermal diffuse scattering observed in the Laue diffraction patterns of sodium, and Barrett (1956) showed that for some of the alkali metals, including sodium, a partial martensitic transformation to an hexagonal-close-packed structure occurs at temperatures below about 50°K. However, the only Bragg intensity studies and Debye temperature determinations have been those of Dawton (1937) and Geshko et al. (1968).

Dawton studied the temperature variation of the intensities of six reflections from single crystals for the temperature range 120°K to 370°K. His observations and conclusions include the following:

(a) A "temperature hysteresis" effect was present in the intensities of lower order reflections for temperatures between 293°K and the melting point of ∿370°K. This effect disappeared when the crystal was chilled with liquid air.

(b) A "permanent" increase was found in the intensities of the lower angle reflections with a splitting of the single crystals into smaller grains when chilled with liquid air.

(c) A Debye temperature was calculated at five temperatures, the value at room temperature being 119°K ± 4°K (read from a graph). (This corresponds to a B factor of $10.6^{-.7}_{+.8}$).

(d) The temperature dependence of the intensities was found to obey the empirical relation

$$I_T \sim \exp-(0.04044\ T + 17.08 \times 10^{-5} T^2)\ \mathrm{Sin}^2\theta_B$$

for filtered molybdenum radiation.

(e) Extinction was found to be present in the crystals.

(f) Scattering factor curves were drawn after absorption corrections were made to the intensities, both with and without allowance for extinction effects. These curves were considerably lower than a theoretical Hartree scattering factor curve.

The results of Dawton on the temperature dependence of the intensities referred to in (d) above were re-analysed for comparison with the present results (see Section 5.9).

Geshko et al. investigated the temperature dependence of the intensity of the 200 reflection for polycrystalline samples of sodium in the temperature range 115°K to 353°K. Their main findings were:

(a) The presence of anharmonic effects was found as revealed by the non-linearity with temperature of the curve

$$f(T) = \ln \left(\frac{I_{Ti}}{I_{To}}\right)$$

where the symbols are as before. This anharmonicity was described in terms of the temperature dependence of the Debye temperature as

$$\theta_D(T) = \theta_D(To) \{ 1-2.1\gamma_G\chi(T-To) \}$$

where $\theta_D(T)$ represents the Debye temperature at a temperature T°K

γ_G is the Gruneisen parameter

and χ is the volume expansion coefficient.

This is equivalent to the "quasi-harmonic" theory approach outlined in section 2.3.

(b) A Debye temperature of $154^{\circ}K \pm 8^{\circ}K$ at $T = 293^{\circ}K$ was determined. (This corresponds to $B = 6.22^{-.59}_{+.70}$).

Thus no reliable measurements of the structure factors of sodium have been made and, in addition, there is a large difference in the value of the available Debye temperatures. This can be attributed to the fact that both measurements are inaccurate, that of Dawton being uncorrected for TDS, and that of Geshko et al. involving the assumption that there was no extinction present in the polycrystalline sample, which, as will be seen from the present work is unlikely to be true (see Section 5.7).

1.6 Previous Determinations of the Debye Temperature of Sodium

Table 1.2 gives a summary of various experimental measurements of the Debye temperature of sodium, including the two X-ray measurements already mentioned. Different experimental methods measure different quantities known as the Debye temperature, thus accounting for some of the differences between different methods. The generally lower Debye temperature as measured by X-ray diffraction techniques is consistent with the experiences of other authors for several other metals (for example, the work of Wilson et al. (1966) on nickel and chromium).

TABLE 1.2

SUMMARY OF DEBYE TEMPERATURE DETERMINATIONS FOR SODIUM

Debye Temperature	Method	Reference
159°K	Specific heat at low temperature	Simon and Zeidler (1926)
155-163°K from T = 17-58°K Extrapolated to 135°K at 0°K	Calculated from elastic constants at low temperature	Fuchs (1936)
160°K	Selected from specific heat curve	Blackman (1955)
153-158°K (from T = 0°K to T = 20°K)	Heat capacity measurements at low temperature	Roberts (1957)
158°K	Heat capacity measurements at low temperature	Gammer and Heer (1960)
156°K	Heat capacity measurements	Lien and Phillips (1960)
152.5 ± 2°K	Specific heat at low temperature	Martin (1965)
202°K	Electrical conductivity	Meissner (1935)
118-140°K	X-ray measurement	Dawton (1937)
154 ± 8°K	X-ray measurement	Geshko et al. (1968)

Calculations of the Debye temperature for sodium have also been made recently. One such calculation is that of Sharma and Mehrota (1969) using a non-Debye distribution approach with the elastic constant data of Daniels (1960). Although a value for θ_D is not explicitly given, some agreement with Dawton's results below 200°K is claimed, with discrepancies at higher temperatures.

A second calculation is that of Konti and Varshni (1969). The elastic constant data of Diederich and Trivisonno (1966) were used in three different methods of calculation. Their average "best theoretical value" for the Debye temperature was found to be 144.3°K.

1.7 Summary of the Present Work

Various methods for analysing limited amounts of diffracted intensity data are presented in Chapter 2. Both integral and summation methods for determining real space distributions are considered. The application of the generalised structure factor formalism of Dawson (1967a) to the present case is presented.

A total of six sets of relative intensities have been recorded photographically from two cylindrical crystals of sodium at two different wavelengths at room temperature. After correction for absorption, Lorentz-polarisation, TDS and anomalous dispersion

effects, the intensities showed considerable anisotropy. This was accounted for in terms of the theory of anharmonic vibrations of atoms due to Willis (1969). The anisotropy was also discussed in terms of the electron density distortion theory of Weiss (1966).

Considerable extinction was present in all samples, and room temperature annealing was observed. A Zachariasen type extinction correction was applied. Structure factors are presented for the data both corrected and uncorrected for extinction. The recording of the relative intensities, analysis and discussion are presented in Chapters 3, 4 and 5.

An absolute intensity measurement technique described by Burbank (1965) was used to measure the intensities of seven independent reflections from a small spherical single crystal of sodium. Structure factors were calculated and compared with the results obtained from the photographic measurements. This work is described in Chapter 6.

CHAPTER 2

METHODS OF ANALYSING AND INTERPRETING DATA

At an early stage of the project it became apparent that the number of observable reflections was limited (Chapter 3). Accordingly, consideration was given to the investigation of methods for analysing and interpreting small quantities of reflection data. Indeed, remembering how the X-ray method "oversolves the structure", the amount of observational information was still sufficient for the determination of a dozen or so parameters. Analysis in both real space and reciprocal space was considered, and various methods are presented in this chapter. These methods are suitable for use with monatomic solids, or simple structures where charge transfer has taken place.

2.1 The Crystal Field and the Determination of Real Space Distributions; Integral Transforms

If a simple solid with accurately known structure is assumed to consist of a condensed array of spherically symmetric atoms, there is a simple relation between the X-ray structure factors and atomic scattering factors. For a monatomic body-centred-cubic solid such as sodium, this relation is given by

$$F(hkl) = \delta\, f(hkl) \qquad \ldots(2.1.1)$$

where δ = 0 if h+k+l is odd; = 2 if h+k+l is even

The radial charge density distribution U(r) may then be determined from the scattering factors by the integral transform (James (1965))

$$U(r) = 4\pi r^2\rho(r) = 32\pi r\int_0^S sf(s)\,\mathrm{Sin}(4\pi sr)\,ds \qquad \ldots(2.1.2)$$

where $s = \frac{\mathrm{Sin}\theta_B}{\lambda}$ and S is the upper limit of s. This can be compared with the radial probability density distribution P(r), which for a single free atom in an array of free atoms, each with independent non-interacting electrons is obtained from the atomic wave function by

$$P(r) = \sum_i n_i R_i^* R_i \qquad \ldots(2.1.3)$$

where the sum is over i subshells of electrons in the atom and R_i is the radial wave function for each of the n_i electrons in the ith subshell.

The integral transform of equation 2.1.2 has been used by Medlin et al. (1969) to determine the conduction electron probability density distribution for solid aluminium. However the nature of scattering factor curves and the presence of the sf(s) term in the integrand of equation 2.1.2 mean that the integral converges very slowly. This means a large value of the integration limit S is required in order to avoid termination ripple. Indeed, Medlin

et al. used observed values of f to s $\sim 1.4\text{Å}^{-1}$, and calculated free atom values of f to s $\sim 12\text{Å}^{-1}$ in their calculation for aluminium. It is not immediately obvious which regions in real space are most affected by this theoretical extrapolation. If only for this reason this technique needs to be handled with some care.

The term sf(s) in the integrand of equation 2.1.2 bears some resemblance to the term which arises on differentiation of one member of a Fourier pair. That is, if two general functions f(r) and F(s) are a Fourier pair, then $\frac{\partial f(r)}{\partial r}$ and $i2\pi sF(s)$ are also a Fourier pair. It was decided to investigate the derivative properties of Fourier transforms in order to try to find a more rapidly converging real space distribution function than that given by equation 2.1.2.

Two functions $F_1(R)$ and $F_2(R)$ were considered, where

$$F_1(R) = \int_0^R 4\pi r\rho(r)dr \qquad \ldots(2.1.4)$$

and

$$F_2(R) = \int_0^R 4\pi r^2\rho(r)dr \qquad \ldots(2.1.5)$$

It follows from these functions that the radial density distribution may be determined at r = R as

$$4\pi R^2\rho(R) = R\frac{\partial F_1(R)}{\partial R} \qquad \ldots(2.1.6)$$

and $$4\pi R^2\rho(R) = \frac{\partial F_2(R)}{\partial R} \qquad \ldots(2.1.7)$$

Now an expression for $F_1(R)$ in terms of the scattering factor may be determined from equations 2.1.4 and 2.1.2 as follows. Substituting for $4\pi r^2\rho(r)$ from equation 2.1.2 into equation 2.1.4 and reversing the order of integration gives

$$F_1(R) = 32\pi\int_0^S sf(s)\int_0^R \mathrm{Sin}(4\pi sr)dr\,ds$$

$$= 32\pi\int_0^S sf(s)\,\frac{1-\mathrm{Cos}(4\pi sR)}{4\pi s}\,ds$$

$$= 16\pi^2\int_0^S f(s)\,\mathrm{Sin}^2(2\pi sR)\,ds \qquad \ldots(2.1.8)$$

Similarly for $F_2(R)$, if we substitute from equation 2.1.2 into equation 2.1.5 and reverse the order of integration, we have

$$F_2(R) = 32\pi\int_0^S sf(s)\int_0^R r\,\mathrm{Sin}(4\pi sr)\,dr\,ds$$

Integrating the term $\int_0^R r\,\mathrm{Sin}(4\pi sr)dr$ by parts gives

$$F_2(R) = 32\pi\int_0^S sf(s)\left|\frac{\mathrm{Sin}\,(4\pi sr)}{4\pi s^2} - \frac{r\mathrm{Cos}(4\pi sr)}{4\pi s}\right|_0^R ds$$

$$= 8R\int_0^S f(s)\left|\frac{\mathrm{Sin}(4\pi sR)}{4\pi sR} - \mathrm{Cos}(4\pi sR)\right| ds$$

$$\ldots(2.1.9)$$

It can be seen that the integrands in both equations 2.1.8 and

2.1.9 involve only the term f(s) rather than s f(s) and the higher order spectra are not weighted. Therefore both the functions $F_1(R)$ and $F_2(R)$ are more rapidly convergent than the integral in equation 2.1.2.

Physically, only the function $F_2(R)$ seems to have any obvious significance. It represents the total number of electrons inside a sphere of radius R. It should be therefore a useful function for interpreting charge transfers or core contractions in spherical atoms. The function $F_1(R)$ has units of inverse length.

The analytic wave function for the hydrogen ground state is given by

$$\psi_{1s} = \frac{1}{\sqrt{\pi} a_o^{3/2}} e^{-r/a_o} \qquad \ldots(2.1.10)$$

where a_o is the Bohr radius. ψ_{1s} was used to find both $F_1(R)$ and $F_2(R)$ by the integral equations 2.1.4 and 2.1.5. The radial density distributions were then determined analytically from these functions by the differential equations 2.1.6 and 2.1.7. These distributions were then compared with the analytic distribution given by the special form of equation 2.1.3 for this one-electron atom in order to check the validity of the functions and the method.

A numerical check was provided for $F_1(R)$ by calculating the function by equation 2.1.8 from scattering factors calculated from

the Hartree and Hartree (1948) wave functions for the complete sodium atom. The limit of integration S was 14Å^{-1}. The radial density distribution was then determined by equation 2.1.6. The resultant curves in each case are shown in Figures 2.1(a) and 2.1(b). The radial density distribution curve in Figure 2.1(b) is in agreement with that obtained from the Hartree and Hartree wave functions to within the accuracy of the graph. Similar agreement was obtained for the radial density distribution curve determined from a calculated $F_2(R)$ function for sodium. Although nothing is claimed to have been established to this stage the technique has been shown not to have generated any artefacts. It is reasonable therefore to expect to be able to use the method for limited experimental reciprocal space data where convergence of the transform is desirable without the use of extrapolated theoretical data.

(It should be noted here that the functions $F_1(R)$ and $F_2(R)$ were calculated at about 50 points in each case, then interpolated at a large number of points depending on the mesh size required for differentiation purposes. This was done because interpolation is a much less time consuming computer procedure than integration. The interpolation method used in this work was a fourth order polynomial fitting procedure such as that used in program SCATFAC (Appendix 1). The numerical integration was carried out by a one dimensional Simpson's rule procedure as for program SCATFAC, and

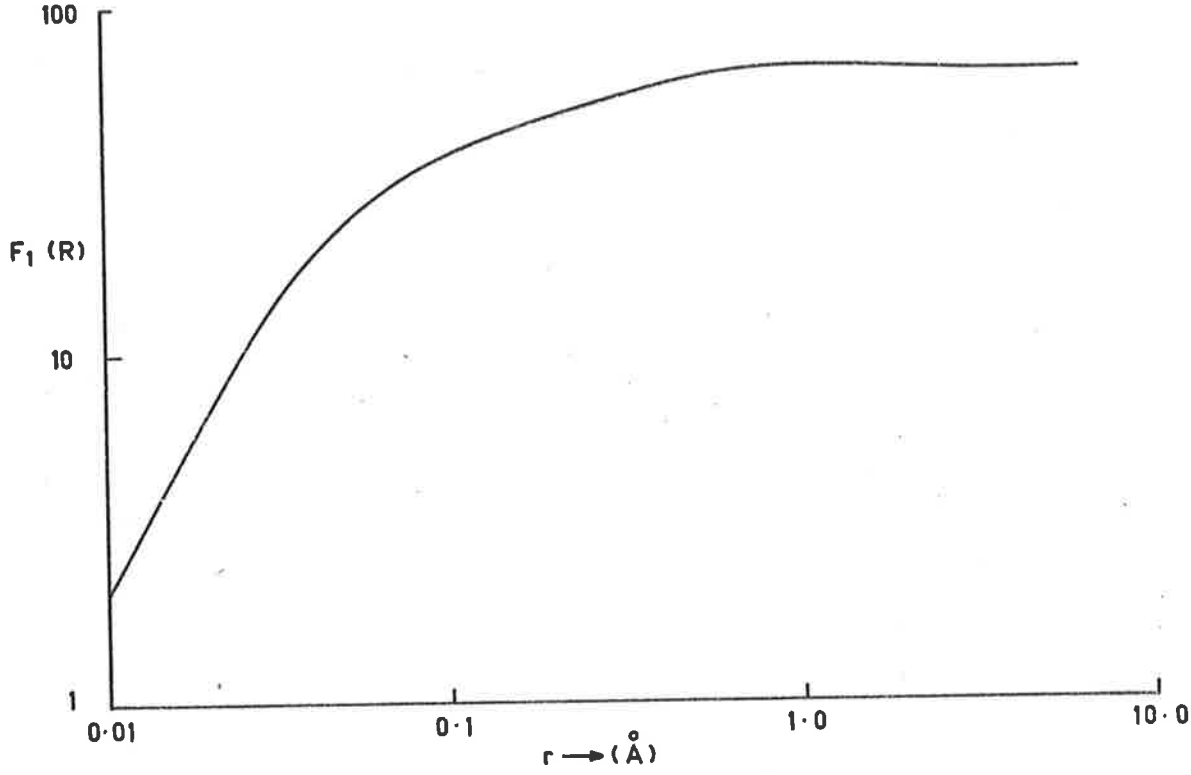

FIG. 2·1(a) FUNCTION F_1 (R) FOR SODIUM (11 ELECTRONS).

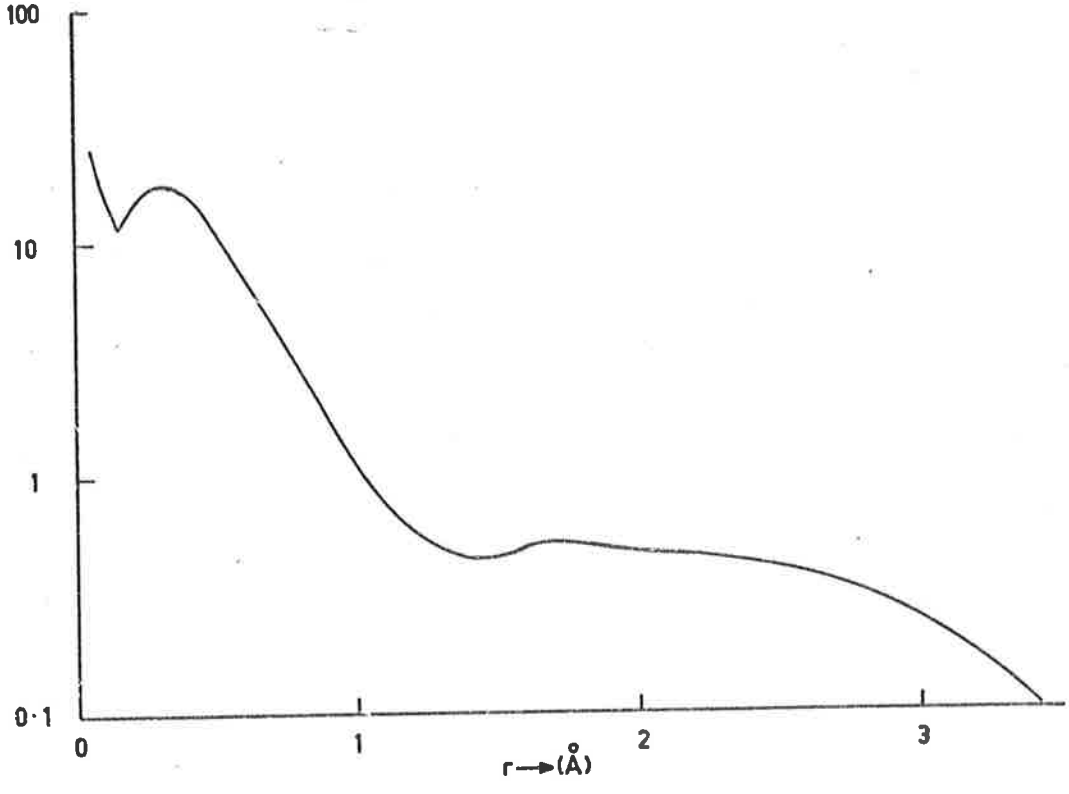

FIG. 2·1(b) RADIAL PROBABILITY DENSITY DISTRIBUTION FOR SODIUM (11 ELECTRONS) CALCULATED FROM F_1 (R).

the numerical differentiation was carried out by a backward difference procedure, and was similar to that used in program EXTINCT (Appendix 1)).

The function $F_2(R)$ had more physical significance than $F_1(R)$ and was therefore investigated more fully and in particular to determine its stability for small amounts of reciprocal space information. The analytic hydrogen wave function for the 1s state as given in equation 2.1.10 and the 3s state given by

$$\psi_{3s} = \frac{1}{81\sqrt{3\pi a_o^{3/2}}} \left(27 - \frac{18r}{a_o} + \frac{2r^2}{a_o^2}\right) e^{-r/3a_o}$$

were used. In each case, the scattering factors were determined from the wave functions and $F_2(R)$ was calculated by equation 2.1.9. Finally, the radial density distribution was calculated by equation 2.1.7. The radial probability density distribution calculated from the ψ_{1s} wave function is shown in Figure 2.2.(b). The distribution is fairly broad and spread out a little more than the distribution expected, for example, for low atomic number atoms in the solid state. The $F_2(R)$ function was calculated for integration limits S of 1, 2 and 3Å^{-1} in equation 2.1.9. The three curves obtained are shown in Figure 2.2 (a), and are identical within the accuracy of the graph. The distributions obtained from each are identical within the accuracy of the graph to the

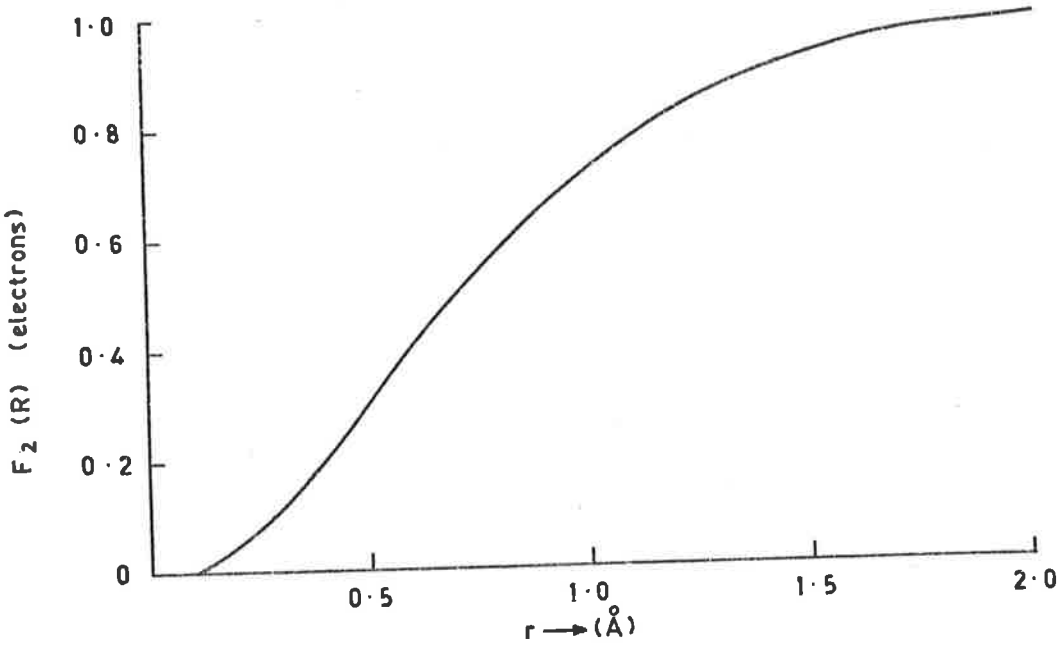

FIG. 2·2(a) F_2 (R) FOR HYDROGEN 1S STATE.

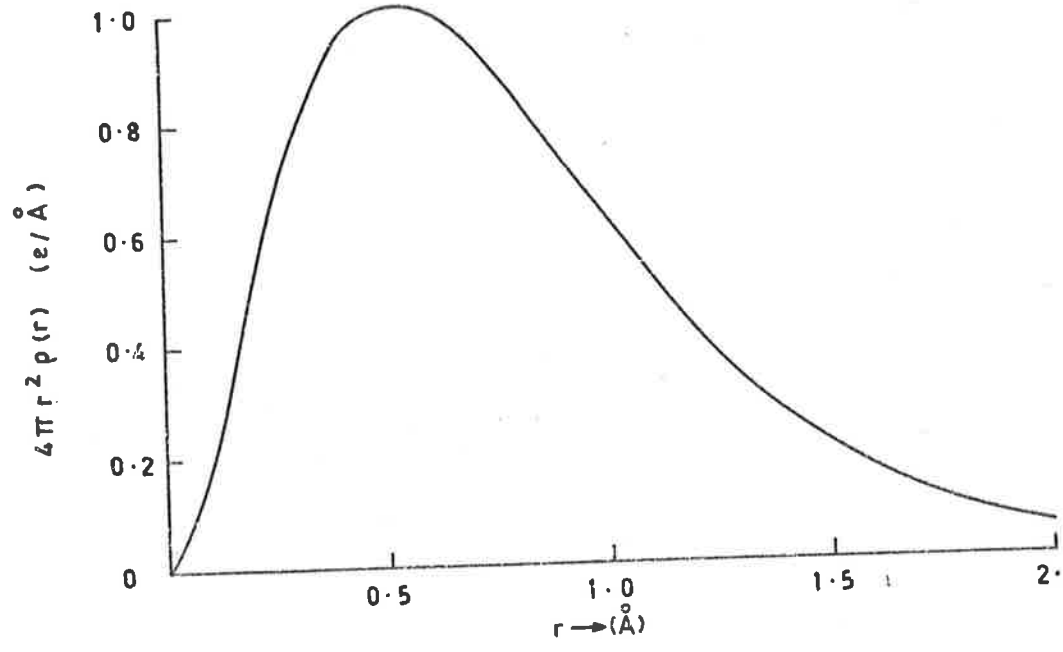

FIG. 2·2(b) RADIAL DENSITY DISTRIBUTION FOR HYDROGEN 1S STATE.

probability density distribution shown in Figure 2.2(b). The ability of the $F_2(R)$ to handle extremely spread out distributions was then tested in the case of the hydrogen 3s state. The radial probability density distribution is shown in Figure 2.3(b). This is an extreme test of the type of distribution that might be expected for the valence electron of a metal crystal such as sodium, where, although the core electrons may be distributed inside about 1Å, the valence electron distribution may be spread out over ~4Å if there is no solid state distortion of this distribution (see Figure 2.4(b)). The $F_2(R)$ function for the hydrogen 3s state was determined for a very small numerical integration limit of $S = .05Å^{-1}$, and is shown in Figure 2.3(a). The distribution obtained from it is shown in Figure 2.3(b). The $F_2(R)$ function has no obvious termination ripple, nor does the radial density distribution. The latter, however, does not have sufficient resolution to show the three peaks in the probability distribution and indeed was not expected to show this because the $F_2(R)$ function was calculated in the region 0 to 4Å with only 1Å resolution, and elsewhere with only 0.5Å resolution. However, the distribution peak is at the radial distance expected and the width is also as for the probability distribution. At this stage it appeared that the method provided stable values of $F_2(R)$ and also gave a good method for determining the radial density distribution provided that the $F_2(R)$ function was calculated at sufficient points.

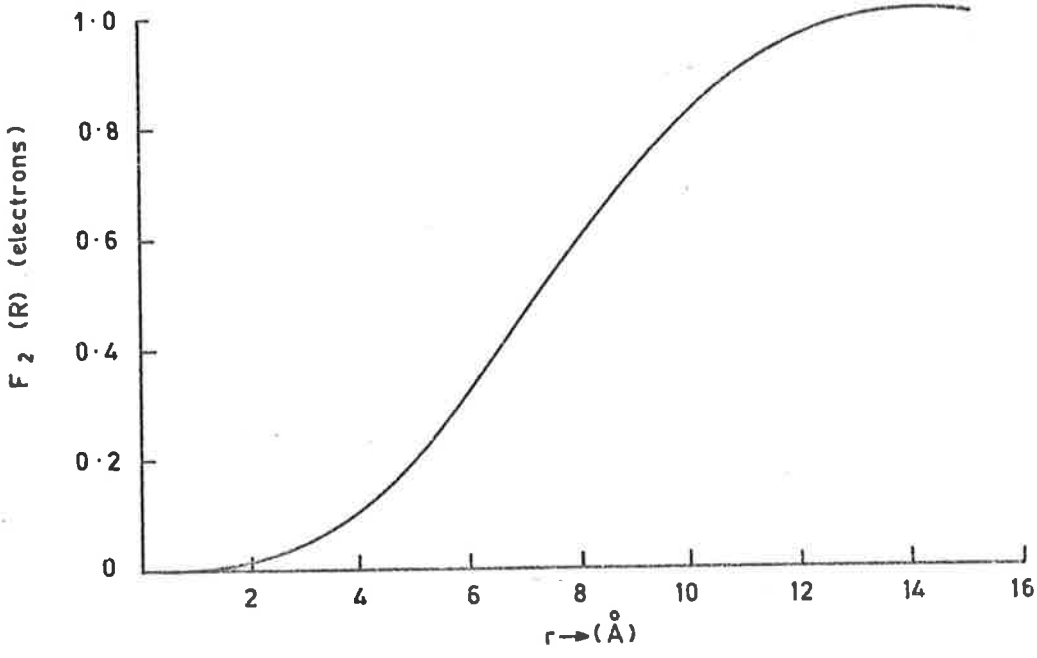

FIG. 2·3(a) F_2 (R) FOR HYDROGEN 3S STATE.

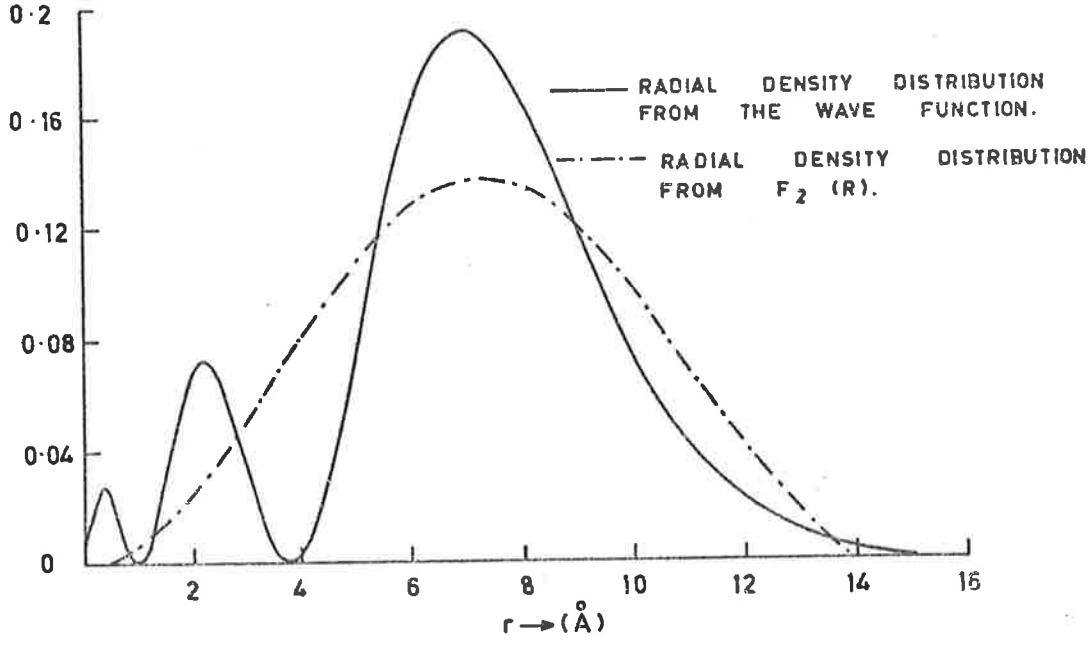

FIG. 2·3(b) RADIAL DENSITY DISTRIBUTION FOR HYDROGEN 3S STATE.

A final check was obtained by calculating the function $F_2(R)$ from the numerical Hartree and Hartree (1948) wave functions for the sodium 3s electron for integration limits S of (a) 6Å^{-1}, (b) 1.4Å^{-1} and (c) $.64\text{Å}^{-1}$. These last two values correspond to the edges of the MoK_α and CuK_α reflecting spheres respectively. The resultant curve is shown in Figure 2.4(a). The difference in the curve for case (b) from that for case (a) was less than .1%, and for case (c) less than 1%. The corresponding density distributions were obtained and that corresponding to case (c) is shown in Figure 2.4(b) together with the radial density distribution obtained from the wave function. The density distribution for cases (a) and (b) were almost identical to that calculated directly from the wave function. A calculation of the radial density distribution using equation 2.1.2 with an integration limit of $.64\text{Å}^{-1}$ yielded an identical curve to that in Figure 2.4(b) obtained from the $F_2(R)$ curve calculated with the same integration limit.

It can be concluded that the function $F_2(R)$ is, as expected, more stable to limited reciprocal space information than the distribution function given by equation 2.1.2. A radial density distribution curve may be calculated from $F_2(R)$ and will give similar results to that calculated from equation 2.1.2 provided $F_2(R)$ is calculated at sufficient values of R to give the resolution required.

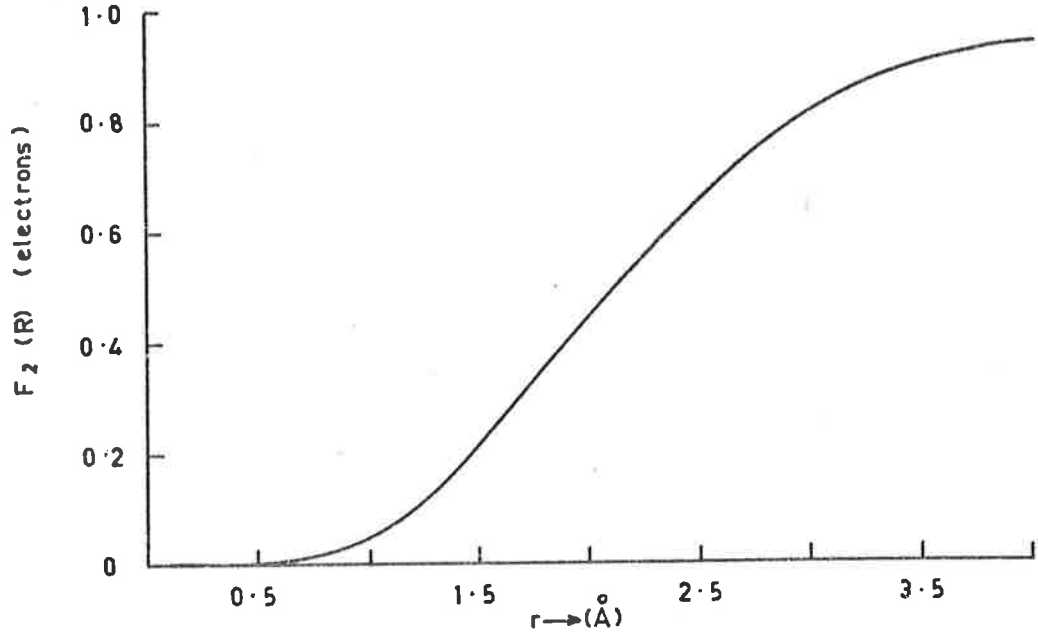

FIG. 2·4 (a) F_2 (R) FOR Na 3S ELECTRON.

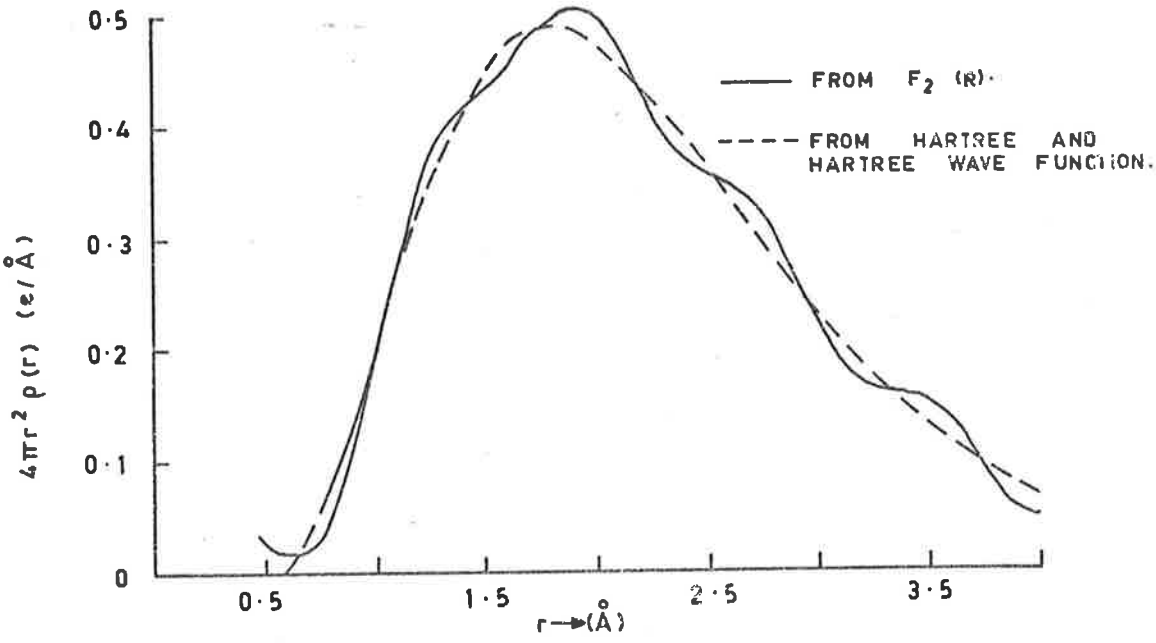

FIG. 2·4 (b) RADIAL DENSITY DISTRIBUTION FOR Na 3S ELECTRON.

The sensitivity of the $F_2(R)$ function to different types of scattering factor curve may be ascertained from calculations, for example, on the $O^{=}$ ion in MgO. The $O^{=}$ ion is unstable in the free state; it is stabilised by the crystal field. There has been interest in the past in the way the $O^{=}$ is bound in MgO (e.g. Togawa (1965), Raccah and Arnott (1967) and Sanger (1969)). Two theoretical determinations of the $O^{=}$ scattering factor have provided the basis for the analysis of experimental data in most cases published. The first of these scattering factor determinations was calculated by Suzuki (1960) for an $O^{=}$ ion artifically stabilised at the centre of a sphere of uniform charge +2. The second was calculated by Tokonami (1965) from a variational wave function for $O^{=}$ in MgO specifically. It was suggested by Tokonami that the charge distribution in this second case is slightly contracted. Calculation of $F_2(R)$ functions for the two scattering factor models gives an indication of the sensitivity of the function to different reciprocal space information. The difference between the two sets of scattering factor values is only about 5%. The calculated $F_2(R)$ functions are shown in Figure 2.5(a), where an $F_2(R)$ curve calculated from the relativistic Hartree-Fock atomic scattering factors for oxygen of Doyle and Turner (1968) is presented also for comparison. A model picture for the two ionic electrons in the $O^{=}$ ion is given by Figure 2.5(b), where curve (a) represents $F_2(R)$ (Suzuki) - $F_2(R)$ (Doyle and Turner) and curve (b) represents $F_2(R)$ (Tokonami) -

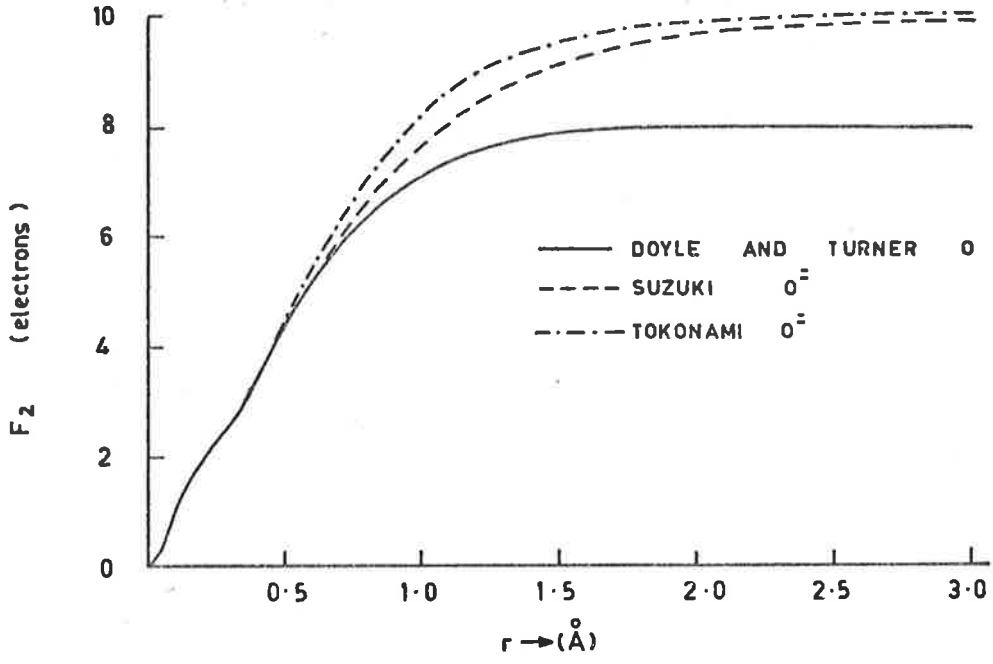

FIG. 2·5(a) F_2 CURVES.

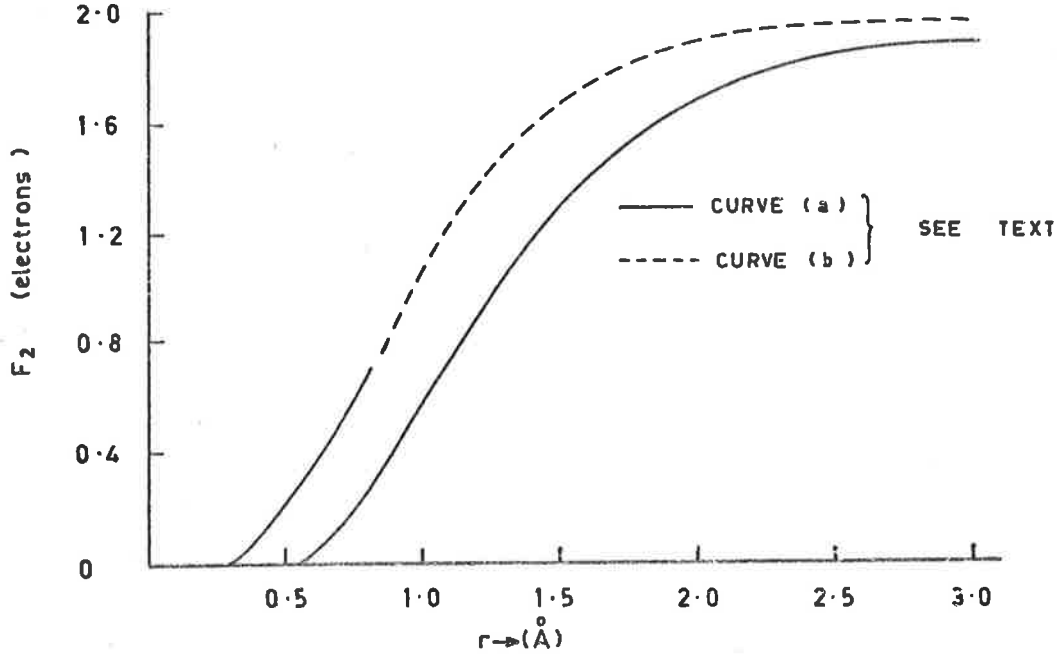

FIG. 2·5(b) DIFFERENCE F_2 CURVES.

$F_2(R)$ (Doyle and Turner). (Sanger (1969) has shown using the formalism of Dawson (1967a) (section 2.3) that there is no evidence of distortion of the ion from spherical symmetry. The $F_2(R)$ method is, then, a valid way of representing the distribution). It can be seen from Figure 2.5(b) that there is a considerable difference in the two curves despite the small difference in scattering factor. Indeed, there is a difference of almost half an Angstrom, for example, in the radius of the sphere which encloses 1.6 electrons.

In summary, the function $F_2(R)$ is much more stable for small amounts of reciprocal space information than the radial density distribution determined by equation 2.1.2. A radial density distribution may be determined from the $F_2(R)$ function via equation 2.1.7, provided sufficient values of $F_2(R)$ are generated to give the required resolution. This distribution is, however, no more stable than the distribution determined by equation 2.1.2. The $F_2(R)$ function is particularly sensitive to small changes in the scattering factor curve. This function may therefore be useful for simple structures where a relation such as 2.1.1 exists, or for compounds where charge transfers or charge distributions are of some significance.

An example of the use of the function with experimental scattering factors is in the case of aluminium, where several authors have shown that the low angle scattering factors are not in agreement with calculated Hartree-Fock values. The function $F_2(R)$

was calculated for the three valence electrons for aluminium. The experimental distribution was determined by using the difference between interpolated values of the measured scattering factors of Raccah and Henrich (1969) and of the theoretical Al^{+++} scattering factors of Freeman (1959). A theoretical distribution for comparison was calculated in a similar way from the Al and Al^{+++} scattering factors of Freeman. The two curves are shown in Figure 2.6. The experimental distribution is narrower than the theoretical one and is pushed further out from the core. It might be argued that the curve is a mathematical consequence of the interpolation procedure used between $s = 0\text{Å}^{-1}$ and the first reflection. This is partly true for that part of the distribution at distances greater than about 1.5Å, but that part of the distribution inside about 1.5Å is determined by the difference in experimental scattering factor from the theoretical value and so is real.

This method would provide an easy, rapid and sensitive means of determining relative distributions for, say, the alkali metals in a variety of bonding states, provided the scattering factor curves could be obtained from the observed structure factors. For example, the fully ionised state would be represented by NaCl. The scattering factors for sodium are obtained from the structure factors by solving by interpolating the equations

$$F_{hkl} = 4(f_{Cl} \pm f_{Na})$$

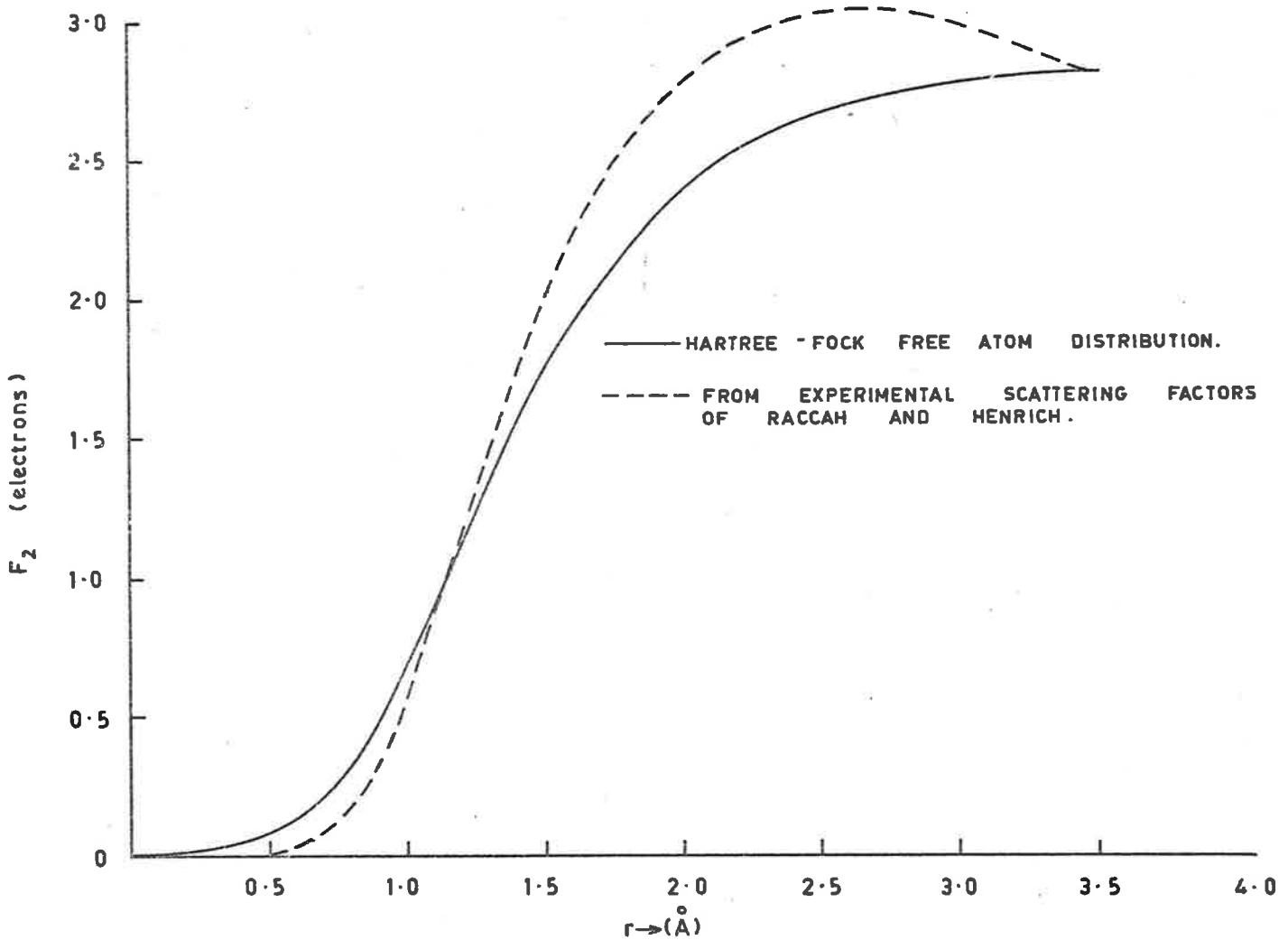

FIG. 2·6 F_2 CURVES FOR ALUMINIUM.

where the plus sign is applicable for h,k,l all even and the minus sign for h,k,l all odd (Brill (1967)). The virtually unionised state would be represented by, for example, the clathrate structure of Na_8Si_{46} (Kasper et al. (1965)). In between would be various organic compounds (for example, the cryptates (Truter and Pederson (1971))), minerals (for example, the alkali silicates (Bragg and Claringbull (1965))), alloys and possibly protein structures. Given these distributions it should then be possible to predict the behaviour of the electrons in various types of bonding states. Comparative studies of this type have recently been carried out on the second row hydrides (Cade et al. (1969)).

2.2 The Crystal Field and Determination of Real Space Distributions: Summation Methods

If an electron density distribution is required for atoms which cannot be regarded as being spherically symmetric, that is, there are anisotropic features in the structure factors, then the use of the integral functions may lead to misinterpretation of the information present. In this case a summation method must be used. The most usual is that given by

$$\rho(x,y,z) = \frac{1}{V} \sum_{-\infty}^{+\infty} \sum\sum_{hkl} F(hkl) \exp \left| -2\pi i(hx+ky+lz) \right| \qquad \ldots(2.2.1)$$

where V is the volume of the unit cell, and x, y, z are the fractional coordinates of the point in the unit cell at which the density is being determined.

Equation 2.2.1 suffers from termination errors. These may be reduced by taking a difference density or by using extrapolated values of the structure factors beyond the experimentally observable range. Each of these latter methods, however, involves some assumptions about the structure factors beyond the observable range of data, and as a result may give rise to misleading information.

There are two similar methods for using as little extrapolated information as possible, and reducing the series termination error. These are to find the average density in a small cube of side δ centred at the point x,y,z in the unit cell, or the average density in a sphere of radius δ, centred similarly. In each case δ is measured as a fraction of the lattice parameter. The first procedure was suggested by Calder et al. (1962) in determining the charge transfer in LiH and described more fully by Weiss (1966) for LiH and MgO. The average density can be expressed as

$$\bar{\rho}(x,y,z) = \frac{1}{V} \sum_{-\infty}^{\infty}\sum\sum F(hkl)\ \exp\left[-2\pi i(hx+ky+lz)\right]$$

$$\times \left(\frac{\sin\pi h\delta}{\pi h\delta}\right)\left(\frac{\sin\pi k\delta}{\pi k\delta}\right)\left(\frac{\sin\pi l\delta}{\pi l\delta}\right) \qquad \ldots(2.2.2)$$

Here, the normal expression for the electron density has been modified by the Lanczos smoothing factor $\frac{\mathrm{Sin}\alpha}{\alpha}$, in three dimensions. This procedure is actually an application of the use of Lanczos smoothing factors in the suppression of the Gibbs phenomenon in Fourier series. Physically, the Lanczos factor as used in three dimensions in equation 2.2.2 represents the Fourier transform of a cube of side δ centred at the origin. This means that for small δ, the smoothing function is spread out, and the error in $\bar{\rho}$ is still large. Alternatively, as δ gets larger, any non-spherical details in the density will be lost. Hence a compromise must be reached which is just wide enough to admit the available scattering data, that is, having a fairly large box, and applying a much broader smoothing function corresponding to a much smaller box size.

The second procedure, introduced here, is to find an average electron density over a sphere. This is a better approach to the smoothing of reciprocal space data than the box of Calder et al. and Weiss, because the spherical symmetry of the transformed smoothing function is a better approximation to the shape of the atom than the box. The average electron density over a sphere is given by

$$\bar{\rho}(x,y,z) = \frac{1}{V} \sum_{-\infty}^{\infty}\sum\sum_{hkl} F(hkl) \exp\left[-2\pi i(hx+ky+lz)\right] \times \frac{3(\mathrm{Sin}(2\pi R) - 2\pi R\,\mathrm{Cos}(2\pi R))}{(2\pi R)^3} \qquad \ldots(2.2.3)$$

where $R = \delta(h^2+k^2+l^2)^{\frac{1}{2}}$. Similar comments on the size of the sphere apply here as in the case of the average density in the box.

We now see that the expression for the average density over a sphere of radius δ bears a close relation to the function $F_2(R)$. It has been shown that $F_2(R)$ represents the total number of electrons inside a sphere of radius R, thus the average density over the sphere will be

$$\bar{\rho}(R) = \frac{F_2(R)}{\frac{4}{3}\pi R^3} \qquad \ldots(2.2.4)$$

Thus we have series and integral analogues for finding average densities in a sphere. As has already been remarked, these may find some use in determination of charge transfers etc. in structures, for example, similar to LiH.

2.3 The Effect of the Crystal Field in Reciprocal Space

Although chemical crystallographers traditionally are interested in real space distributions, involving such things as charge transfers in bonding etc., and therefore are interested in transforms of the type discussed in the previous two sections, the search for purely crystal field effects may be better carried out in reciprocal space (e.g. Kurki-Suonio (1968)). Dawson (1967a) has described a

general structure factor formalism to account for crystal field effects. Its use for diamond and fluorite structures has been described by Dawson and others in a series of papers. This formalism was found to be suitable for the analysis of the sodium data, and is outlined below.

The effect of the crystal field is to change the atomic potential function. This in turn can have two effects. The first is that the electron density distribution may be distorted from the spherical symmetry usually assumed for the free atom state, and the second is that the atomic vibrations become anharmonic. The effect these have on the scattered intensities can be taken into account using the following general formalism due to Dawson (1967a).

The structure factor may be expressed in two forms, thus

$$F(\underset{\sim}{S}) = \sum_j f_j(\underset{\sim}{S}) T_j(\underset{\sim}{S}) \exp 2\pi i(\underset{\sim}{S}.\underset{\sim}{r}_j) \qquad \ldots(2.3.1)$$

and

$$F(\underset{\sim}{S}) = A(\underset{\sim}{S}) + iB(\underset{\sim}{S}) \qquad \ldots(2.3.2)$$

Here

$$|\underset{\sim}{S}| = \frac{2\mathrm{Sin}\theta_B}{\lambda} \qquad \ldots(2.3.3)$$

$f_j(\underset{\sim}{S})$ is the X-ray atomic scattering factor for the jth atom, and $T_j(\underset{\sim}{S})$ is its temperature factor. Now $f_j(\underset{\sim}{S})$ and $T_j(\underset{\sim}{S})$ can be further separated into centrosymmetric and antisymmetric parts, thus

$$f_j(\underset{\sim}{S}) = f_{c,j}(\underset{\sim}{S}) + if_{a,j}(\underset{\sim}{S}) \qquad \ldots(2.3.4)$$

$$T_j(\underset{\sim}{S}) = T_{c,j}(\underset{\sim}{S}) + iT_{a,j}(\underset{\sim}{S}) \qquad \ldots(2.3.5)$$

This leads to

$$A(\underset{\sim}{S}) = \sum_j (f_c T_c - f_a T_a)_j \, \mathrm{Cos}2\pi \underset{\sim}{S}.\underset{\sim}{r}_j - (f_c T_a + f_a T_c)\mathrm{Sin}2\pi \underset{\sim}{S}.\underset{\sim}{r}_j \qquad \ldots(2.3.6)$$

where the notation has been shortened in an obvious way. There is a corresponding term for $B(\underset{\sim}{S})$.

It is convenient to note here that for neutron diffraction, the X-ray scattering factor must be replaced by the isotropic neutron scattering length b_j. There is no possibility of separating b_j as for f_j in equation 2.3.4 and no possibility of observing electron density distribution distortions.

If the symmetry of the particular structure, i.e. sodium, is now taken into account, it is found that because each atom has centrosymmetric m3m point symmetry, the terms $B(\underset{\sim}{S})$, f_a and T_a are all zero, and the structure factor becomes

$$F(\underset{\sim}{S}) = A(\underset{\sim}{S}) = \sum_j f_c T_c \, \mathrm{Cos}2\pi \underset{\sim}{S}.\underset{\sim}{r}_j \qquad \ldots(2.3.7)$$

As a consequence of the centrosymmetry, there is no possibility of finding "forbidden" reflections as in the diamond structure, because these can only arise from cross-combinations of antisymmetric scattering terms with centrosymmetric vibrational terms and vice versa.

The two effects of the crystal field on the centrosymmetric scattering and vibrational factors in sodium will now be considered specifically in (a) and (b) below.

(a) The crystal field may distort the electron density from the normally assumed spherical shape. This can be taken into account by expanding the electron density in terms of functions having the expected symmetry of the structure. For bcc sodium, there are eight nearest neighbours in the <111> body diagonal directions. The density is expanded in terms of functions which point toward the eight nearest neighbours, thus

$$\rho_c = \bar{\rho}_c + \delta\rho_{c,4} \qquad \ldots(2.3.8)$$

where $\delta\rho_{c,4}$ is a fourth order anisotropic correction term to the normal spherically symmetric density $\bar{\rho}_c$. This transforms to

$$f_c = \bar{f}_c + \delta f_{c,4} \qquad \ldots(2.3.9)$$

where again, $\delta f_{c,4}$ is a fourth order anisotropic correction term to the normal spherically symmetric $\bar{f}_c$. The term $\delta f_{c,4}$ can be represented as

$$\delta f_{c,4} = A(\theta,\phi) \times \langle j_4(4\pi s r)\rangle \qquad \ldots(2.3.10)$$

where $A(\theta,\phi)$ has directional properties and $\langle j_4(4\pi s r)\rangle$ is the expectation value of the fourth order spherical Bessel

function with respect to some wave function which depends on the function used in expanding the density. Dawson (1967b) has expanded the density in terms of Kubic Harmonic functions which give the form

$$\langle j_4(4\pi sr)\rangle = 4\pi(-1)^4\int_0^\infty r^2(r^q\exp(-\alpha r^m))j_4(4\pi sr)dr \qquad \ldots(2.3.11)$$

Weiss (1966) uses a slightly different approach in using

$$\langle j_4(4\pi sr)\rangle = \int_o^\infty R^2(r)\ j_n(4\pi sr)\ dr \qquad \ldots(2.3.12)$$

where R(r) are the radial wave functions for the electron shell being distorted. This latter approach will now be developed more fully.

The orbital part of the charge density is expanded in terms of a simple function that points in the eight <111> directions, thus

$$\rho \sim 1+\alpha\left(\frac{(xy)^2+(xz)^2+(yz)^2}{(x^2+y^2+z^2)^2}\right) \qquad \ldots(2.3.13)$$

where α is an adjustable constant that depends on the asphericity. If this is converted to spherical coordinates and the scattering factor calculated in the usual way as

$$f(s) = \left\langle \frac{\mathrm{Sin}(4\pi sr)}{4\pi sr} \right\rangle \qquad \ldots(2.3.14)$$

where the wave function used is

$$\Psi(r,\theta,\phi) = 2\pi r R(r)\Xi(\theta)\Phi(\phi)$$

where $s = \frac{\mathrm{Sin}\theta_B}{\lambda}$

R(r) is the radial part of the wave function and $\Xi(\theta)$ and $\Phi(\phi)$ are the two angular parts, the result is

$$f(s) = \langle j_o(4\pi sr)\rangle - \frac{\frac{1}{3} A\langle j_4(4\pi sr)\rangle}{1 + \frac{15}{4\alpha}} \qquad \ldots(2.3.15)$$

where A is given in terms of the Miller indices h,k,l as

$$A = \frac{3(h^4+k^4+l^4) - 9(h^2k^2+h^2l^2+k^2l^2)}{(h^2+k^2+l^2)^2} \qquad \ldots(2.3.16)$$

and

$$\langle j_n(4\pi sr)\rangle = \int_o^\infty 4\pi r^2 R^2(r) j_n(4\pi sr)\, dr \qquad \ldots(2.3.17)$$

The $j_n(4\pi sr)$ are the spherical Bessel functions (see Appendix 1), where

$$j_o(4\pi sr) = \frac{\mathrm{Sin}(4\pi sr)}{4\pi sr}$$

Thus it can be seen that in equation 2.3.15 above $\langle j_o(4\pi sr)\rangle$ is the familiar scattering factor for a spherically symmetric charge density, which is modified by the crystal field by the second

term

$$-\frac{\frac{1}{3}A\langle j_4(4\pi sr)\rangle}{1+\frac{15}{4\alpha}}$$

If α is 0, the charge density is spherically symmetrical and the scattering factor is given by the usual equation.

Similar expansions to that in equation 2.3.13 can be set up to give charge densities pointing in the other directions in a cubic crystal. The scattering factor calculated as above will always be given in terms of the expectation values of the spherical Bessel functions, the parameter α, and a directional function similar to A.

(b) The effect of the crystal field on the atomic potential may alter the vibrations of the atom from harmonic to give some anharmonic component. This phenomenon has been examined by Willis (1969), as follows.

The potential for harmonic vibrations is parabolic in terms of the atomic displacement, but the anharmonic factors can be taken into account by expanding to higher orders. Truncating at fourth order terms gives the potential for the Kth atom as

$$V_K(u_1,u_2,u_3) = V_o + \tfrac{1}{2}\alpha_K r^2 + \beta_K u_1u_2u_3 + \gamma_K r^4 + \delta_K(u_1^4 + u_2^4 + u_3^4 - \tfrac{3}{5}r^4) \qquad \ldots(2.3.18)$$

where

$$r^2 = u_1^2 + u_2^2 + u_3^2$$

and u_1, u_2, u_3 are the components of displacement $\underset{\sim}{u}$ from the equilibrium position. If the atom is at a centre of symmetry $\beta_K = 0$. This leads to a general expression for centrosymmetric temperature factor given by

$$T_c = N_K \exp\left(\frac{-Q^2 k_B T}{2\alpha_K}\right)\left\{1-15k_BT\left(\frac{\gamma_K}{\alpha_K^2}\right)+10(k_BT)^2\left(\frac{2\pi}{a_o}\right)^2\left(\frac{\gamma_K}{\alpha_K^3}\right)(h^2+k^2+l^2)\right.$$

$$-(k_BT)^3\left(\frac{2\pi}{a_o}\right)^4\left(\frac{\gamma_K}{\alpha_K^4}\right)\ (h^2+k^2+l^2)^2$$

$$\left.-(k_BT)^3\left(\frac{2\pi}{a_o}\right)^4\left(\frac{\delta_K}{\alpha_K^4}\right)\ \left(h^4+k^4+l^4-\frac{3}{5}\ (h^2+k^2+l^2)\right)\right\}$$

...(2.3.19)

where

$$N_K = \left(1-15k_BT\ \left(\frac{\gamma_K}{\alpha_K^2}\right)\ \right)^{-1}$$

a_o is the lattice parameter, and the other symbols have their usual meanings. If the vibrations were harmonic, then $\gamma_K = \delta_K = 0$, and the temperature factor reduces to the familiar

$$T_c = \exp\left(-\tfrac{1}{2}Q^2u_K^2\right)$$

$$= \exp\left(- B \frac{\mathrm{Sin}^2\theta_B}{\lambda^2}\right) \qquad \ldots(2.3.20)$$

Thus the additional terms which occur in the temperature factor for anharmonic crystals are either isotropic in reciprocal space with magnitudes determined by γ_K, or anisotropic with magnitudes determined by δ_K.

I have applied this theory of anharmonicity to the specific case of sodium in order to separate the anisotropic and isotropic thermal vibrations. The anisotropic features can be observed in intensity measurements at a single temperature, but the isotropic features can be observed only for intensity measurements at several different temperatures. Since the atoms in sodium are all in identical symmetry positions in the lattice, the subscript K will be dropped in the following. Now putting

$$A = N\{1-15k_BT\left(\frac{\gamma}{\alpha^2}\right)+10(k_BT)^2 \left(\frac{2\pi}{a_o}\right)^2 \left(\frac{\gamma}{\alpha^3}\right) (h^2+k^2+l^2)$$

$$-(k_BT)^3 \left(\frac{2\pi}{a_o}\right)^4 \left(\frac{\gamma}{\alpha^4}\right) (h^2+k^2+l^2)^2\} \qquad \ldots(2.3.21)$$

$$Y = N (k_BT)^4 \left(\frac{2\pi}{a_o}\right)^4 \left(\frac{\delta}{\alpha^4}\right)$$

where Y is a constant at constant temperature T,

$$D = h^4+k^4+l^4 - \frac{3}{5} (h^2+k^2+l^2)^2$$

then

$$T_c = A \exp\left(- B \frac{\sin^2\theta_B}{\lambda^2}\right)\left(1 - \frac{YD}{A}\right) \qquad \ldots(2.3.22)$$

If the isotropic anharmonic parameters are fairly small, the factor A can be taken into account as a small change ΔB in the harmonic Debye temperature parameter B thus

$$T_c = \exp\left(- B' \frac{\sin^2\theta_B}{\lambda^2}\right)(1 - PD) \qquad \ldots(2.3.23)$$

where $B' = B + \Delta B$

and $P = \frac{Y}{A}$

The temperature factor can now be written in a similar way to the scattering factor as in equation 2.3.9 thus,

$$T_c = \overline{T_c} + \delta T_{c,4} \qquad \ldots(2.3.24)$$

where now, $\delta T_{c,4}$ is a fourth order correction term for anisotropic anharmonic vibrations only, whilst $\overline{T_c}$ is not a harmonic Debye temperature factor, but involves isotropic anharmonic factors.

Now equation 2.3.19 is not in a convenient form to enable a calculation of the relative magnitudes of δ and α to be made. This can be done however if the Debye parameter is expressed in terms of the temperature explicitly by using the "quasi-harmonic" approximation as follows (Willis (1969)).

If the crystal expands on heating, it is assumed that there is a relative reduction in the frequencies of the normal modes of vibration proportional to the relative change in volume of the crystal thus:

$$\frac{\Delta\omega}{\omega} = -\gamma_G \frac{\Delta v}{v} = -\gamma_G \chi T \qquad \ldots(2.3.25)$$

where ω represents frequency, v volume

γ_G = Gruneisen constant,

and χ = volume coefficient of expansion.

This yields

$$T_c \text{ (quasi-harmonic)} = T_c \text{ (harmonic)} \ (1+2\gamma_G \chi T) \qquad \ldots(2.3.26)$$

This is equivalent in terms of the previous symbolism, to assuming a temperature dependence of parameters α, γ, δ of

$$\frac{\alpha}{\alpha_o} = \frac{\gamma}{\gamma_o} = \frac{\delta}{\delta_o} = 1 - 2\gamma_G \chi T \qquad \ldots(2.3.27)$$

where α_o is the value of α for no expansion, and it is assumed that $2\gamma_G \chi T \ll 1$. The expression for the exponent of the Debye-Waller factor for a cubic monatomic solid can then be written as

$$2W = \left(\frac{2\pi}{a_o}\right)^2 (h^2+k^2+l^2) \left(\frac{1}{\alpha_o}\right) k_B T$$

$$+ \left(\frac{2\pi}{a_o}\right)^2 (h^2+k^2+l^2) \left(\frac{2\gamma_G \chi}{\alpha_o k_B}\right) (k_B T)^2$$

$$- \left(\frac{2\pi}{a_o}\right)^2 (h^2+k^2+l^2) \left(\frac{20\gamma_o}{\alpha_o^3}\right) (k_B T)^2$$

$$+ \left(\frac{2\pi}{a_o}\right)^4 (h^2+k^2+l^2)^2 \left(\frac{2\gamma_o}{\alpha_o^4}\right) (k_B T)^3$$

$$- \left(\frac{2\pi}{a_o}\right)^4 (h^2k^2+h^2l^2+k^2l^2 - \tfrac{1}{3}(h^4+k^4+l^4)) \left(\frac{12\delta_o}{5\alpha_o^4}\right) (k_B T)^3$$

...(2.3.28)

If we now apply this expression to the case of sodium, and assume that in equation 2.3.23 PD << 1, we can rewrite that equation as

$$T_c = \exp\left(- B' \frac{\mathrm{Sin}^2\theta_B}{\lambda^2}\right) \exp(-PD) \qquad \ldots(2.3.29)$$

(The assumption that exp (-PD) ∿ (1-PD) is in fact quite reasonable even for a relatively highly anharmonic solid such as sodium).

If we now equate the anisotropic parts of the exponents as given by equations 2.3.28 and 2.3.29, and substitute for D, we have

$$\frac{\delta_o}{\alpha_o^4} = - P \frac{\left(\frac{a_o}{2\pi}\right)^4}{(k_B T)^3} \qquad \ldots(2.3.30)$$

The effect of the crystal field on the scattering and vibrational

parts of the structure factor, as summarised in equations 2.3.9 and 2.3.24, can be inserted in equation 2.3.7 to give

$$F(\underset{\sim}{S}) = \sum_j (\bar{f}_c + \delta f_{c,4}) (\bar{T}_c + \delta T_{c,4}) \cos 2\pi(\underset{\sim}{S}.\underset{\sim}{r}_j) \quad \ldots(2.3.31)$$

Ignoring the product of the two δ terms, anisotropic features in the structure factor can arise from cross-combinations of isotropic scattering and anisotropic vibrational terms or vice versa.

Now $\delta f_{c,4}$ and $\delta T_{c,4}$ currently can be found only by determining an ajustable parameter from the experimental observations and since the symmetry produces the same directional effect in each case, there is no way of determining from the experimental observations which of the two possible effects is present. That is, an arbitrary judgement must be made.

Distortions of the electron density distributions have been claimed to have been observed for the 3d outer electrons in bcc V (Weiss and De Marco (1965)) and also bcc Fe (Weiss (1966)). The measurements were made at room temperature and θ_D was found to be $323^{\circ}K$ for V. The electronic configuration of V is $.....3s^2, 3p^6, 3d^3, 4s^2$ and of Fe is $.....3s^2, 3p^6, 3d^6, 4s^2$. The 3d electrons are the least tightly bound in each case, the binding energy being $\sim$10eV. In this case anisotropic anharmonic contributions to the Debye-Waller factor were considered to be negligible on the basis of Maradudin and Flinn's (1963) estimates of such a contribution in

lead at $T \sim \theta_D$. However, Wolfe and Goodman (1969) suggest that the anisotropic contribution to the Debye-Waller factor is considerably larger than the estimate of Maradudin and Flinn, and might in fact be observable. In the case of diamond, where the binding energy of the bonding electrons is also $\sim$ 10 eV, it is considered by Dawson (1967b) that the distortion of the binding electron density is the cause of the observed "forbidden" structure factor 222. The possibility of observable anharmonic effects is considered to be very small because the large value of the Debye temperature for diamond ($\theta_D \sim 1800^{\circ}K$) implies that the atomic vibrations will be small and essentially isotropic at room temperature.

On the other hand, anharmonic vibrations are claimed to be the cause of anisotropic features in neutron diffraction measurements of UO_2 and CaF_2 which have fluorite structures (Dawson, Hurley and Maslen (1967)). As noted previously, there is no possibility that electron density distribution distortions are being measured if neutron diffraction is used.

In general, anisotropic features in the structure factors will probably be due either to anharmonic vibrations if $T \geq \theta_D$, or to distortions of the bonding electron density distribution for low angle reflections.

2.4 The Contribution of the 3s Electron to the Structure Factor for Sodium

Interest has been shown in the last few years in the effect of the crystal field on the valence or bonding electrons in metals. Aluminium has been one of the most extensively studied metals in this respect, and it has been found that the lowest angle scattering factors have values about 4% lower than calculated values from theoretical free atom wave functions (e.g. Raccah and Henrich (1969)) and Medlin, Dingle and Field (1969) have shown that the radial density distribution for the three valence electrons in solid aluminium more closely approximates a theoretical distribution calculated from the pseudopotential data of Harrison (1966) than that calculated from the Hartree-Fock wave function for the free atom.

The situation in sodium is more difficult because there is only one valence electron per atom and only two atoms per unit cell. The free atom scattering factor for the 3s electron in sodium was calculated from the wave function of Hartree and Hartree (1948), and is shown in Figure 2.7. It can be seen that the contribution to the free atom scattering factor for the lowest angle reflection in sodium (the 110 reflection) is in fact slightly negative. This makes it unlikely that any solid state effects on the 3s electron in sodium will be observed by X-ray diffraction techniques; but not impossible, since the effect in aluminium was sufficient to reduce

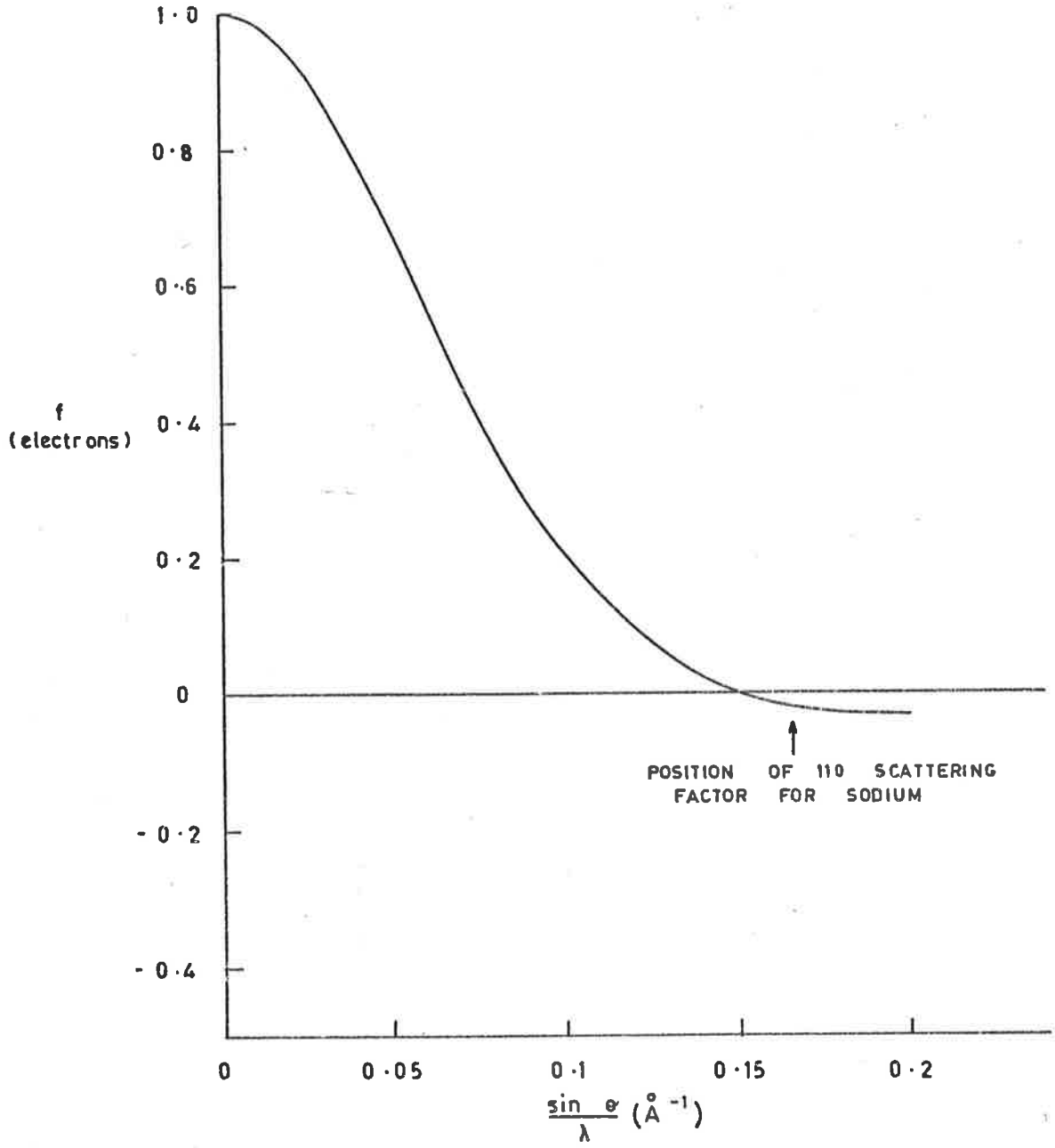

FIG. 2·7 ATOMIC SCATTERING FACTOR FOR Na 3S ELECTRON

the scattering factor for the first few reflections below both the free atom scattering factor and the neon core value.

In view of other evidence (Section 1.2) that sodium can of all metals be most nearly described by the free electron theory, it is unlikely that there would be a large solid state effect even if it were observable. On the other hand, the radial density distribution calculated for the valence electron from the Harrison (1966) pseudopotential data for sodium (see program PEDNA, Appendix 1) gives a different result from that calculated from the Hartree and Hartree (1948) wave functions. The two are shown for comparison in Figure 2.8. It should be possible to determine a solid state conduction electron density distribution from the momentum distribution determined by Phillips and Weiss (1968), but the experimental uncertainty is probably too large to give meaningful results.

Although the 3s electron contribution to the sodium structure factors is likely to be unobservable, much additional information on the properties of sodium in the solid state can be, and indeed, has been found by a study of all the available X-ray diffraction data.

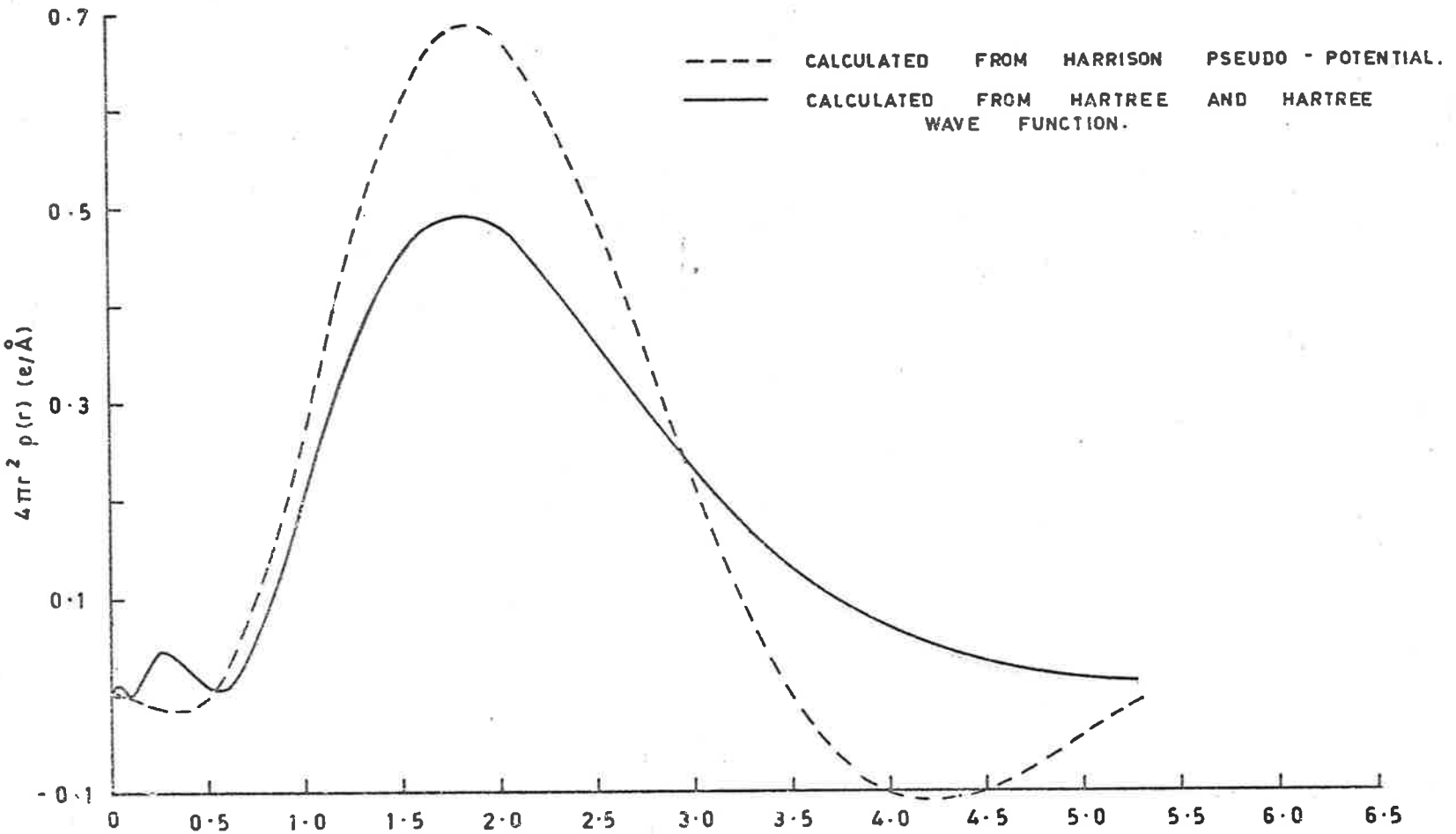

FIG. 2·8 RADIAL PROBABILITY DENSITY DISTRIBUTION FOR Na 3S ELECTRON.

CHAPTER 3

INTENSITY MEASUREMENT PROCEDURES

This chapter presents a discussion of the accuracy required, and obtainable by various experimental techniques to observe crystal field effects on diffracted intensities. The techniques used in crystal growth and recording and measuring the relative intensities are also presented.

3.1 Accuracy of Theoretical Scattering Factors and Experimental Techniques

It has been shown (e.g. Raccah and Henrich (1969)) that the crystal field effect on the valence electron distribution in metals is only a few percent. Crystal field effects of other types may also produce relatively small changes in structure factor (e.g. Dawson, Hurley and Maslen (1967) on anharmonic vibrations). Thus it was necessary to try to achieve the best accuracy available.

In any determination of relative experimental scattering factors, the final values will be influenced to some (generally undetermined) extent by scaling procedures. Accordingly it is necessary to know the accuracy of the theoretical free atom scattering factors used and also to have some insight as to how they

might depart from the experimental solid state values.

Absolute experimental measurements by Chipman and Jennings (1963) have verified that Hartree-Fock free atom scattering factors for the inert gases are accurate to about 1% over a range of $\frac{\sin\theta_B}{\lambda}$ up to 0.4Å^{-1}. It has been supposed in Section 1.3 that the relativistic Hartree-Fock free atom scattering factors of Doyle and Turner (1968) are the most accurate calculations of their type to have been published. It has been shown in Section 1.3 that the author's free atom scattering factors calculated from the wave functions of Hartree and Hartree (1948) for sodium are in excellent agreement with those of Doyle and Turner. It may be concluded, therefore, that relativistic effects are not significant. Free atom scattering factors accurate to 1% calculated from Hartree and Hartree wave functions have therefore been used in this work.

There has recently been considerable discussion on the accuracy available in experimental techniques, and on the relative merits of various techniques. Diffractometer techniques are generally supposed to be accurate to ∿1%. Young (1969) has reviewed the advantages and disadvantages of precise counting techniques, while Jeffery (1969) has reviewed evidence for an accuracy of 1% in photographic intensity recording. However, the report on inter-experimental agreement of the Single Crystal Intensity Measurement Project (Abrahams et al. (1970)), which was carried out on crystals of D(+) - tartaric acid using a wide range

of diffractometers and techniques, states that "two scaled experimental sets of structure factors, measured under circumstances similar to those of the project will most probably differ by 6%, agree no better than 3% and usually no worse than 10% except in cases of extreme systematic error". A cautious generalisation might be that it is improbable that any set of experimental structure factors will be accurate to 1%, however precise are the measurements.

One of the particular problems in recording intensities from sodium was the rapid falloff in intensity at higher angles due to the large thermal motion of the atoms. This required long recording times for higher angle reflections. It will be shown (Section 5.7) that sodium crystals may undergo internal mosaic changes when dipped in liquid air and may subsequently anneal at room temperature. This highlights one of the advantages of the photographic technique in that reflections are recorded virtually simultaneously, giving easy recognition of deficiencies in either crystal or apparatus. The photographic technique is also useful in that it allows some errors to be avoided easily, for example, multiple diffraction errors. These are particularly important in a very high symmetry crystal like sodium (Section 4.1).

It appeared that the photographic intensity measurement method outlined by Jeffery (1969) of photometry of integrated Weissenberg

photographs taken with CuK_α radiation was precise to 1%. It appeared also that photographic methods had some advantages in the present case. It was decided to measure the relative intensities by the method of Jeffery, using an integrating Weissenberg camera for recording and a Joyce-Loebl recording microdensitometer for measurement of the intensities. The experimental requirements for accurate X-ray intensity measurement by photographic means were reviewed by Jeffery and Whitaker (1965). Their suggestions on the stabilisation of the X-ray source, operation of the integrating camera, integrating limits, multiple diffraction and processing and photometry of films have been used.

It was decided also to measure absolute intensities for several reflections. The method described by Burbank (1965) was found to be the most suitable for the type of crystal available and was used for the work described in Chapter 6. The intensities in this case were recorded on a horizontal diffractometer with a proportional counter and pulse height analysing equipment.

3.2 Crystal Growth

Small single crystals of sodium have been grown by a number of experimenters. Andrade and Tsien (1937) and Weymouth and Soepano (1962) have grown crystals from the melt using cylindrical glass moulds. Spherical crystals have been grown at the Division of

Tribophysics of the C.S.I.R.O. by very slow cooling (Michell (1968)). Dawton (1937) grew crystals by methods similar to both those above.

Since sodium is very reactive and oxidises rapidly on exposure to air, some form of protective coating is necessary. This is normally of regular shape such as spherical or cylindrical to allow easy correction of the intensities for angle dependent effects. The optimum diameter of $2/\mu$, where μ is the linear absorption coefficient, is 0.64 cm for sodium, scattering MoK_α radiation, and 0.68 mm for sodium scattering CuK_α radiation. However, crystals of $\leq$ .5 mm diameter were required to comply with the assumption of the kinematical diffraction theory that the whole width of the crystal is bathed in the beam.

Initially spherical crystals were grown under "Vaseline" petroleum jelly by the method of Michell. They were then packed in petroleum jelly and mounted in gelatin capsules. The crystals were unsuitable, however, since they oxidised over a period of a few days.

Samples were then grown by slow cooling in capillaries drawn from large bore, thin-walled soft glass. The technique was unsuitable because the samples were polycrystalline, and the capillaries were impractical because the bore and wall thickness could not be made adequately uniform, and there was heavy diffuse scattering

from the glass. Capillaries made by coating a wire with liquid perspex were also unsuitable because the sodium oxidised when in contact with the perspex.

Finally, crystals were grown in commercial Lindemann glass capillaries designed for X-ray work (Siemens Cat. No. 176346). The diameter was 0.5 mm and the wall thickness 0.01 mm. The capillaries were found to give only small background scattering relative to the intensity of the Bragg reflections after long exposure. All the crystals used in the project were grown from 99.9% pure sodium supplied by Koch, Light Laboratories Ltd.

The final technique for the preparation of single crystals was as follows. The capillaries were first cleaned with chromic acid, rinsed with distilled water, and dried over a flame and in a desiccator. A few cubic centimetres of sodium were cut from a slab and the oxide coating removed. The sample was melted in a bath of liquid paraffin. This fluid was chosen because it produced the least rapid reoxidation of the freshly cut sodium of a number of fluids suitable for the purpose. Molten sodium, with a liquid paraffin covering, was drawn into the tube by means of an eyedropper and clamp, the tube removed and cut to a suitable length. The ends of the tube were then sealed in a flame. It was found essential to leave an air gap between the sealed end of the tube and the liquid paraffin protecting the crystal. Otherwise, when the crystal was mounted on a set of goniometer arcs, the mounting

cement was found to be able to mix with the liquid paraffin, causing rapid deterioration of the crystal.

Generally the specimen was polycrystalline at this stage. It was made to crystallise by drawing axially from a bath of paraffin oil held at a temperature a few degrees above the melting point of sodium. The bath was open to the atmosphere, thus a travelling temperature gradient was produced. Initially this procedure produced polycrystalline specimens. Honeycombe (1959) has suggested that better crystallisation is obtained using this type of technique by reducing supercooling at the solid-liquid interface. This can be done by increasing the temperature gradient and reducing the drawing rate. Satisfactory single crystals were grown by reducing the drawing rate to 2.2 cm/hour. This rate is comparable with the rate of 2.4 cm/hour used by Weymouth and Soepano (1962) in a similar method.

3.3 Alignment of the Crystals

Transmission Laue diffraction patterns of the crystals were photographed, using white radiation from a copper target. A stereographic projection was made of the resulting pattern, and sets of Bragg reflections belonging to zones of planes in the crystal were found. These reflections, and then all other Bragg reflections in the pattern were indexed.

Also clearly visible on the films were patterns of diffuse scattering and diffuse "extra reflections" due to thermal motion of the atoms.

If all the Bragg reflections were indexed unequivocally, and did not display evidence of internal structure, the specimen was a single crystal. The stereographic projection showed which of the three main rotation axes for a cube, <001>,<110> or <111> was nearest to the cylinder axes. The goniometer arc settings were then adjusted to give approximately that rotation axis, and the final adjustment was made by the "double oscillation" procedure of Davies (1950).

Weymouth and Soepano (1962) considered the possibility of preferred orientation in bcc crystals and in sodium in particular, and concluded that their cylindrical sodium crystals were more frequently oriented close to <111> than <110>. It has been this author's experience, however, that the reverse was more likely to be true, with a few crystals being oriented near an <001> axis. The relative distributions of orientations probably depend on the methods and conditions of growth of the crystals, such as the speed of travel of the temperature gradient.

3.4 Preliminary Observations

It was immediately apparent that there was a very rapid falloff of intensities with Bragg angle. At room temperature, non-integrating exposures of the order of 12 hours were required to record all the reflections in the CuK_α limiting sphere (14 independent reflections). However, non-integrating exposures of up to 64 hours in MoK_α radiation at room temperature produced only about 12 of the possible 112 independent reflections in the MoK_α limiting sphere. In addition to the already low definition of the higher angle reflections, background scatter from the glass capillaries became excessive at these long exposures.

It was supposed initially that the limited number of reflections obtained with MoK_α radiation was due in part to the Lorentz-polarisation effect as θ_B approached 45°, in which case, the use of a shorter wavelength such as AgK_α radiation would have been beneficial. Calculations showed, however, that the falloff in intensity was due rather to the high B factor produced by the large thermal vibrations in the solid. This can be seen from Table 3.1 where the intensity reduction factor Lp due to Lorentz-polarisation effect in MoK_α radiation and that due to thermal motion (e^{-M}) is given for various reflections. Here $e^{-M} = e^{-2B\frac{\sin^2\theta_B}{\lambda^2}}$ where the value of B used was 5.3, calculated from equation 1.4.1 on the basis of the harmonic theory, for temperature $T = 90^\circ K$, and assuming the Debye temperature $\theta_D = 150^\circ K$.

It is apparent from Table 3.1 that even at low temperatures there is considerable thermal motion of the atoms. This was confirmed by using a low temperature attachment on the Weissenberg camera. Various exposures were taken with temperatures as low as 120°K with a total of 5 crystals. (It was impractical to consider very low temperatures due to the martensitic transformation of the crystals observed by Barrett (1956)). The following observations were made:

(a) There was a "permanent" increase in intensity of the low angle reflections.

(b) The shape of the reflections on the photograph became very irregular on cooling, indicating change in the mosaic structure of the crystal.

(c) There were still heavy thermal diffuse scattering streaks at low temperatures.

(d) Long exposures were still required to record the high angle reflections.

It was found that the number of independent reflections obtained with MoK_α at the lowest temperatures was 16, or two more than were obtained with CuK_α radiation at room temperature. In view of the small gain in observable reflections, which indicated the essentially similar vibration properties of the solid at low temperatures as at room temperature, and the greater complexity of

TABLE 3.1

Lp AND THERMAL MOTION FACTORS

Reflection	e^{-M}	Lp
110	.75	8.5
200	.56	6.0
211	.42	4.9
220	.32	4.2
310	.24	3.8
222	.18	3.4
321	.13	3.2
400	.10	3.0
{330 411	.075	2.8
420	.056	2.6
332	.042	2.5
422	.032	2.5
{431 510	.024	2.3

low temperature recording, it was decided not to measure the intensities at low temperatures.

Xerographic recording of the X-rays was tried in an effort to increase the definition of the high angle reflections. Some success with this technique had been reported by Wolfe (1969). An ordinary piece of xerography paper was sensitised and a flat transmission Laue exposure of a sodium crystal was made. This was then developed in the usual way for xerographic paper. Several further exposures were made, varying initial charging voltage on the paper, type and length of developing and amount of exposure. Lead-barium sulphate screens were also used to try to reduce exposure time. However, although the technique was capable of detecting X-ray reflections, only a few of these were actually recorded, and the definition was much inferior to that obtained with ordinary film. Although this technique has scope for development, it was not considered further here.

A proportional counter was set up on a Unicam S-25 goniometer to determine whether counter techniques might be expected to give better definition. No evidence of greater definition was found.

Milledge (1969) has discussed the problem of poor definition in film techniques with particular reference to small crystals. One solution suggested was the use of intensifying screens, or some similar high sensitivity recording system such as that afforded by

Polaroid film. Unfortunately Polaroid film does not as yet produce a transparent negative directly suitable for densitometry. Milledge, however, reported good results with Ilford Industrial A film and Dupont "Lightning Special" screens in conjunction with MoK_α radiation; but CuK_α radiation did not produce encouraging results.

As Dupont screens were not immediately available, Ilford Fast Tungstate screens, which were recommended by Ilford for use with Industrial A film, were used as a comparison with the normally used Industrial G film. The results were unsatisfactory because in general the definition at high angles was greater for Industrial G film than Industrial A film with screens, and the exposure time was not greatly less for the latter case.

It was decided therefore to measure all the reflections available at room temperature using the integrating camera and Industrial G film.

3.5 Intensity Sets

Six sets of intensities were recorded from two different crystals. Details are given in Table 3.2.

Four film packs were used for each exposure, with black wrapping paper interleaved between each film for CuK_α radiation,

TABLE 3.2

Set	Crystal	Rotation Axis	Radiation	Exposure time/layer
1	1	<001>	CuK_α	24 hrs
2	1	<001>	MoK_α	48 hrs
3	2	<001>	CuK_α	24 hrs
4	2	<210>	CuK_α	20 hrs
5	2	<210>	MoK_α	24 hrs
6	2	<001>	MoK_α	24 hrs

and 0.05 mm tin sheets between each film for molybdenum radiation. This produced film factors of about 4 and reduced fluorescent radiation between films.

3.6 Apparatus; Developing and Handling of Films

A self-rectifying X-ray set with standard interchangeable Philips tubes was used for intensity sets 1 and 2. The tubes were run at 45 Kvp and 22 mA. All the other sets were recorded using a constant potential unit operated at 40 Kv and 20 mA. The input voltage for both these sets was supplied from a Stabilac M5000 voltage stabiliser with a rated stability of ± 1%. After allowing the stabiliser about an hour to warm up, the voltage and current

outputs could be held with no noticeable long term drift.

The Weissenberg goniometer used for all six sets of intensities was a Unicam S 35 model, but the integrating camera was designed and built in this laboratory by Dr. E. H. Medlin. This camera produced a series of ten step-shifts about the axis of rotation of the crystal for each of a series of ten step-shifts along the axial direction. One shift about the axis of rotation occurred each time the camera translation mechanism reversed direction. The amount of the step-shift could be adjusted in each case.

The film used throughout was Ilford Industrial G, the developer Ilford Phen-X and the fixer Ilford Ilfofix. All films were developed at a temperature within $1^{o}C$ of $20^{o}C$ for five minutes or its temperature equivalent. The films were washed for about one minute, fixed for 5 minutes and finally washed in running water for 20-30 minutes, and allowed to dry in the open air. All layers for each set of exposures were developed together under the same conditions.

3.7 Densitometry

The measurement of relative intensities was carried out on a Joyce-Loebl Mark IIIC Automatic Recording Microdensitometer. This was a conventional two beam instrument, with a null balance

obtained by a linear density wedge. The recording table and film table were driven at relative speeds determined by the variable ratio arm between the two. Three wedges were used. Most of the densities were measured using the A or 0-0.5D wedge, but a few of the most dense reflections were measured using the B or 0-1.0D wedge or the D or 0-2.0D wedge. The measured densities were never greater than 1.2D up to which point the film density versus X-ray intensity curve is linear (Jeffery (1969)). The ratio of recording table to film table movement used was 50 to 1, and the objective was a 20 x lens, giving a magnification of 44 times. The final slit width was 0.5 mm, giving a resolution of 11 microns.

There were two modes of operation of this densitometer. The first gave a differential forward movement of the recording table depending on the rate of change of amplitude of the pen. The second gave a uniform motion of the recording table, which allowed a measurement of the area under the traced curve by recording an integrated, digitised pen amplitude over the scan. This latter mode was used throughout.

The instrument was capable of reproducing readings to an absolute value of ± ½% for the more dense reflections. Each reflection and its background level were recorded twice and the final intensity was the average of the two. One or two reflections with unremoveable background interference were discarded,

otherwise all available reflections were recorded.

The wedges had been calibrated by the manufacturer. To put the densities recorded with the B and D wedges on the same scale as those recorded with the A wedge, the density of a suitable reflection was measured several times with each wedge, and an average taken. The ratios of the wedge densities found, and those listed by the manufacturer are listed in Table 3.3.

TABLE 3.3

Wedges	Manufacturer	Experimental
B:A	2.1	2.08
D:A	4.1	4.12

To determine the accuracy of the densitometry method, a reflection with medium density in the A wedge range was measured 13 times. Each time the film was moved away from its reading position, so that the errors involved were the random errors of trying to reposition the film at exactly the same position coupled with the errors due to the accuracy of the machine itself. The result was a density of 100.0 arbitrary units with standard deviation 3.5 units and standard error .86 units. This means, using Student's t test, that the mean density will be 100 ± 1.85 at the

95% confidence limit, for 13 samples.

3.8 Diffraction from Other Alkali Metals

It has been stated in Section 1.1 that sodium was the only alkali metal suitable for X-ray diffraction investigation. The reasons for this should be stated here. Firstly, the thermal motion of the atoms is large as indicated by the low Debye temperature. This vibrational motion increases with atomic number. It might be expected therefore, that for alkali metals with $Z \geq 11$, there would be even less observational information than for sodium, and extinction would be greater. On the other hand, the optimum diameter of $2/\mu$ for a lithium crystal is greater than 5 cm for CuK_{α} radiation, and so the diffraction from a crystal of $\sim$.5 mm would be weak. For these reasons this work concentrates on a careful analysis of diffraction data in sodium. An understanding of this metal should lead to informed speculation about the behaviour of the other alkali metals in similar bonding configurations.

CHAPTER 4

MEASURED INTENSITIES: CORRECTION FACTORS

Values of measured intensities, methods of correcting for various effects and values of the correction factors will be presented in this chapter. In general only results for set 3 will be presented, the other results being given in Appendix 2. Set 3 has the lowest calculated errors, but on the other hand shows the least effect of anharmonic vibration.

4.1 Multiple Diffraction

It has been pointed out in recent years (e.g. Jeffery and Whitaker (1965), Yakel and Fankuchen (1962) and Zachariasen (1965)) that the recording of intensities using equi-inclination geometry about any symmetry axis, and in particular about a crystal axis in a cubic structure, leads to the condition of multiple diffraction. For the particular case of a cube rotation axis, this involves all reflections on non-zero layers. Jeffery (1969) has suggested a simple way to overcome this difficulty by deliberately offsetting the equi-inclination angle by about $\frac{1}{2}^{o}$. This procedure was used for all non-zero layers for all six sets of intensities.

4.2 Film and Layer Scaling Factors

In all cases, least squares film factors were calculated from the measured intensities by program AUFAC, whilst the least squares layer factors were calculated by program AULAC after the intensities had been corrected for spot shape, Lorentz-polarisation, absorption and TDS effects. Programs AUFAC and AULAC are very similar, both being extensions of the SUFFAC least squares scale factor program coded by G. L. Paul. The two programs were adapted for the crystallographic program library of Adelaide University by Dr. M. R. Snow of the Physical and Inorganic Chemistry Department.

4.3 Spot Shape Corrections

It is well known (Phillips (1954)) that spots on upper layer equi-inclination photographs are extended on one half of the film and contracted on the other. The usual procedure for dealing with this problem for rotations about a symmetry axis, where reflections of a particular type occur on both sides of the film, is to find the harmonic mean intensity I_m, given by

$$I_m = \frac{2I_E I_c}{I_E + I_c} \qquad \ldots(4.3.1)$$

where I_E is the extended spot intensity and I_c the contracted spot intensity. On the other hand, if the rotation axis is not a

symmetry axis, reflections of the same type may not be present on both sides of the film. In this case the mean intensity I_m is given by

$$I_m = I_o(1 \pm K \cos\theta_B) \qquad \ldots(4.3.2)$$

where I_o is the observed intensity and K is an empirically determined correction factor (Rollett (1965)).

After film factor scaling, symmetry related reflections from each side of the film were averaged and the mean intensity from both sides of the film determined by equation 4.3.1 for intensity sets 1,2,3 and 6 where the rotation axis in each case was a highly symmetrical cube axis. In the case of intensity sets 4 and 5 where the rotation axis was a nonsymmetrical <210> axis, equation 4.3.2 was used to determine the mean intensity from both sides of the film.

The measured relative intensities after film factor scaling and spot shape correction are presented in Table 4.1.

4.4 Lorentz-Polarisation Corrections

Corrections were made for the Lorentz and polarisation effects simultaneously. The Lorentz correction factor, which takes into account the way the reciprocal lattice point hkl passes through

TABLE 4.1

RELATIVE INTENSITIES AFTER FILM FACTOR SCALING AND SPOT SHAPE CORRECTIONS

Set 3

Reflection	Layer 0	Layer 1	Layer 2
110	4251.5	3963.8	
200	2237.7		
211		948.5	1316.2
220	637.2		603.7
310	303.8	237.4	
222			163.8
321		78.4	89.5
400	50.8		
(330	35.4		
(			
(411		22.7	
420	20.9		20.0
332			13.3
422			8.6
(431		6.1	
(			
(510	5.7	5.1	
521		5.0	5.1

the reflecting sphere is given in the case of equi-inclination geometry by

$$L^{-1} = \xi \, Cos\Theta_B$$

where ξ is the radial cylindrical coordinate of the reciprocal lattice point in the usual notation as given by International Tables (1959). The polarisation factor takes account of the polarisation of the incident beam. If this radiation is unpolarised, the polarisation factor p is given by

$$p = \frac{1+Cos^2 2\theta_B}{2}$$

The total effect can therefore be taken into account by multiplying the observed intensities by the factor

$$(Lp)^{-1} = \frac{2\xi Cos\theta_B}{1+Cos^2\theta_B}$$

A program was written to carry out this procedure.

The offsetting of the equi-inclination angle could involve corrections to the intensities of up to about .85%. These were ignored on the grounds that they are insignificant in this case.

4.5 Absorption Corrections

Zero layer absorption correction factors A* are tabulated as a function of μR and θ_B for cylindrical crystals in International Tables (1959). Here, μ is the linear absorption coefficient, R is

the radius of the crystal, and θ_B the diffraction angle. These can be modified for upper levels of equi-inclination Weissenberg photographs by putting $\mu Sec\upsilon$ in place of μ and $\gamma/2$ in place of θ_B. Here, υ is the equi-inclination angle and γ is the angle between the projection of the incident beam and the projection of the diffracted beam on the equatorial plane of the reflecting sphere, and is given by

$$\text{Sin}\ \frac{\gamma}{2} = \text{Sec}\ \upsilon\ \sqrt{(\text{Sin}^2\theta_B - \text{Sin}^2\upsilon)}$$

The values of μ for sodium for both CuK_α and MoK_α radiation were calculated from values of mass absorption coefficient μ/ρ tabulated for various wavelengths in International Tables (1962).

A program was written to interpolate the tabulated values of A* for the present work and is briefly described in Appendix 1.

For both crystals used, the cylinder axis was inclined at a few degrees to the rotation axis. The absorption corrections calculated as above were therefore slightly inaccurate, but calculations showed that this inaccuracy was 3% at the worst, and was ignored.

Since μR was $\sim.7$ for a cylindrical crystal of radius $\sim.23$ mm, the absorption factor for CuK_α was ~ 3, and for MoK_α was ~ 1.

4.6 Thermal Diffuse Scattering Corrections

Thermal diffuse scattering (TDS) has been recognised over the last few years as one of the major sources of error as yet unconsidered by crystallographers in systematic correction procedures (e.g. Willis (1969)). A number of authors have presented successively more sophisticated treatments (e.g. Nilsson (1957), Annaka (1962), Schwartz (1964), Cooper and Rouse (1968), Rouse and Cooper (1969) and Lucas (1968, 1969, 1970)). Most of these have attempted to correct for TDS in terms of a correction ∇B to the isotropic Debye parameter B.

Lonsdale (1942) however, first pointed out that the TDS pattern for sodium is extremely complex, largely due to the elastically anisotropic nature of sodium. Thus any correction for TDS in this metal must take into consideration this anisotropy and will not be applicable as an adjustment to the isotropic Debye parameter, but must be calculated for each independent reflection. The only one of the above methods which does this is that of Rouse and Cooper (1969). Their treatment is for θ -2θ or ω scans on a diffractometer and depends only on knowing the way the reciprocal lattice point passes through the reflecting sphere, that is, the volume of reciprocal space swept out as the reflection passes through the reflecting sphere, and the scattering cross-section, which is derived from the elastic constants. The most accurate elastic constants for the case of sodium were those given by Martinson

(1969), and these were used for this correction procedure.

The geometry of equi-inclination photographic procedures is associated with the geometry for ω scans. Thermal diffuse scattering corrections for photographically recorded reflection intensities have been discussed by Annaka (1962). He used the width of the spot in each direction as the"receiving slit" on the film. Accordingly, unintegrated Weissenberg photographs were taken with both copper and molybdenum radiation. Densitometer traces across the film and from top to bottom taken under the same conditions as for intensity measurement gave a measure of the "aperture" height and width respectively. These readings were averaged for two separate spots. The spot sizes were found to be approximately linear with θ_B, and a straight line was fitted by means of a least squares routine.

The theory outlined by Rouse and Cooper is as follows. If I_o is the integrated Bragg intensity, then the total integrated intensity may be written

$$I = I_o (1 + \alpha_1 + \alpha_2 + \ldots)$$

where α_1, α_2 etc. are the contributions of TDS for one-, two- etc. phonon scattering. Values for α_1 etc. can be found by determining the differential scattering cross-section in each case and integrating over the solid angle swept out in the scan.

A program to calculate the first order anisotropic thermal diffuse scattering correction α_1 by the method of Rouse and Cooper was written and details are given in Appendix 1.

The calculated correction factors $(1 + \alpha_1)$ for set 3 are tabulated in Table 4.2. The procedure for set 3 was slightly different from that for the other five sets. The correction factor α will vary from layer to layer as the manner in which the reflection passes through the reflecting sphere and hence the swept volume varies. For set 3, spot sizes were measured for each layer and separate correction factors calculated for each layer on the basis of these spot sizes. (In order to save computing time this procedure was simplified for the other data sets by using correction factors calculated from the zero layer spot sizes only).

4.7 Layer Scaling

Values of the measured intensities for sets 3 and 4 after application of Lorentz-polarisation, absorption and TDS corrections are given in Table 4.3. It was initially planned that sets 3 and 4 and sets 5 and 6 could be layer scaled together, giving two sets of two-axis data for the second crystal, each at a different wavelength. This was done using the layer scaling program AULAC for sets 3 and 4, but it was immediately obvious that the two sets of data could not be put on the same scale. This can in fact be

TABLE 4.2

TDS Correction Factors (1+α) used in Correcting Relative Intensities

Set 3

Reflection	Layer 0	Layer 1	Layer 2
110	1.0166	1.0218	
200	1.0358		
211		1.0632	1.0431
220	1.0748		1.0589
310	1.0814	1.0931	
222			1.0769
321		1.0973	1.0785
400	1.1501		
(330	1.1107		
(411		1.1206	
420	1.1263		1.0955
332			1.0708
422			1.0916
(431		1.1468	
(510	1.2316	1.0981	
521		1.1000	1.1120

TABLE 4.3

Averaged Intensities after Correction for Lorentz-Polarisation, Absorption and TDS

Set 3

Reflection	Layer 0	Layer 1	Layer 2
110	7017.4	4720.8	
200	5527.9		
211		2796.8	2718.2
220	2567.5		1815.8
310	1330.1	995.5	
222			708.1
321		385.3	418.6
400	242.3		
(330	166.6		
(			
(411		104.6	
420	87.81		82.98
332			49.12
422			28.58
(431		13.78	
(			
(510	12.35	12.02	
521		4.364	4.317

TABLE 4.3 (Continued)

Set 4

Reflection	Layer 0	Layer 1	Layer 2	Layer 3	Layer 4
110		761.3	420.7	496.6	
200	827.87		454.9		309.9
211	751.0	622.8		433.5	425.4
220			333.0		325.9
310		305.2	196.7	242.5	
222			155.5		
321	208.0	148.8			109.1
400	109.0				75.72
(330				47.41	
(411		67.38	39.22	35.62	
420	48.91		33.00		30.18
332		28.31		20.28	18.25
422	20.66		9.067		
(431		7.292	5.093		
(510		5.372	4.181	5.125	

seen directly from Table 4.3, where the order of magnitude of intensity difference between the two sets for the 110 reflection is about 10, while that for the 431-510 pair is about two. The six data sets were then treated as separate sets, and layer scaled using AULAC assuming that symmetry related reflections on different layers were identical. Sets 3 and 4 were internally consistent when layer scaled in this way.

4.8 Anomalous Dispersion Corrections

The phenomenon of anomalous dispersion, which is due to the interaction between the frequency of the incident radiation and any natural absorption frequencies of the scattering atom, can be taken into account as follows (after James (1965)). The atomic scattering factor may be written as

$$f = f_o + \Delta f' + i\Delta f''$$

where $\Delta f'$ and $\Delta f''$ are the real and imaginary frequency dependent parts of the scattering factor, and f_o is the frequency independent scattering factor for no interaction of the incident and absorbing frequencies. For the correction of intensities, this may be written as

$$|f|^2 = (f_o + \Delta f')^2 + (\Delta f'')^2$$

and a first order correction for relative intensities is made by multiplying the observed intensities by the factor

$$\frac{f_o^2}{(f_o+\Delta f')^2+(\Delta f'')^2} \qquad \ldots(4.8.1)$$

where f_o is the calculated Hartree-Fock scattering factor.

Values for $\Delta f'$ and $\Delta f''$ have been calculated by Cromer (1965a) from relativistic Dirac-Slater wave functions for a number of elements for five wavelengths, including CuK_α and MoK_α. Although the wave functions used throughout this work for the calculation of scattering factors are Hartree-Fock type, there would be negligible difference in the values of $\Delta f'$ and $\Delta f''$ calculated from these wave functions than those calculated from the values of Cromer.

The values of $\Delta f'$ and $\Delta f''$ given by Cromer for each wavelength and used in the correction procedure are given in Table 4.4.

TABLE 4.4

	CuK_α	MoK_α
$\Delta f'$	.12	.04
$\Delta f''$	.14	.04

The values of $\Delta f'$ and $\Delta f''$ are relatively insensitive to changes in $\frac{\sin\theta_B}{\lambda}$, and are taken as constants.

A program to calculate the correction for anomalous dispersion for each reflection as given in equation 4.8.1 was written.

The values of the anomalous dispersion correction factors applied to the relative intensities for CuK_α and MoK_α radiation respectively are given in Table 4.5. The values of the intensities for set 3 after layer scaling and anomalous dispersion corrections were applied are given in Table 4.6.

The observed intensities have now been processed to the stage where they can be related with theoretical data for the determination of thermal parameters and solid state effects.

TABLE 4.5

Calculated Anomalous Dispersion Correction Factors

Applied to the Relative Intensities

Reflection	CuK_α Radiation	MoK_α Radiation
110	.97311	.99098
200	.96989	.98988
211	.96667	.98880
220	.96338	.98768
310	.96001	.98653
222	.95658	.98536
321	.95312	.98418
400	.94963	.98299
(330	.94613	.98179
(411	.94613	.98179
420	.94264	.98059
332	.93916	.97939
422	.93571	.97820
(431	.93231	.97702
(510	.93231	
521	.92564	

TABLE 4.6

Intensities after Layer Scaling and Correction for Anomalous Dispersion

Set 3

Reflection	Intensity
110	6177.9
200	5361.5
211	3458.4
220	2326.5
310	1250.5
222	860.0
321	481.5
400	230.1
(330	157.6
(411	128.7
420	89.74
332	57.95
422	33.59
(431	16.69
(510	13.24
521	5.184

CHAPTER 5

DEBYE PARAMETERS:
ANHARMONICITY AND EXTINCTION: ERRORS

In this chapter are presented details of the determination of the Debye and anharmonicity parameters, and information about the atomic potential which can be derived, a discussion of extinction, and an estimate of the experimental errors.

5.1 Wilson Plots

The experimental structure factors $F_o(hkl)$ can be determined from the observed relative intensities I(hkl) if these latter can be put on an absolute scale by finding the scaling factor K and the Debye parameter B in the expression

$$I(hkl) = KF_o^2(hkl) \exp\left(\frac{-2B\sin^2\theta_B}{\lambda^2}\right) \qquad \ldots(5.1.1)$$

As pointed out in Section 1.4, the method chosen for the determination of B, and the scaling of the intensities was that first described by Wilson (1942) and used here in the following form.

It is assumed that the F_o values are sufficiently similar to the F_c values that the parameters K and B can be determined using the equation

$$I(hkl) = KF_c^2\ (hkl)\ \exp\left(\frac{-2B\sin^2\theta_B}{\lambda^2}\right) \qquad \ldots(5.1.2)$$

Here $F_c(hkl)$ is the structure factor calculated from the Hartree-Fock spherically symmetric free atom wave function, and related to the X-ray scattering factor by

$$F_c(hkl) = 2f(hkl)$$

for a single atom bcc lattice (see equation 2.1.1). Equation 5.1.2 can be written as

$$\ln(I/F_c^2) = \ln K - \frac{2B\sin^2\theta_B}{\lambda^2}$$

Thus a plot of $\ln(I/F_c^2)$ versus $\frac{\sin^2\theta_B}{\lambda^2}$ should yield a straight line with a slope of 2B and an intercept of lnK. These values of B and K can then be used to calculate values of $F_o(hkl)$ from equation 5.1.1.

A least squares program was written to calculate structure factors and B and K parameters by this procedure.

A plot of $\ln(I/F_c^2)$ versus $\frac{\sin^2\theta_B}{\lambda^2}$ for set 3 is given in Figure

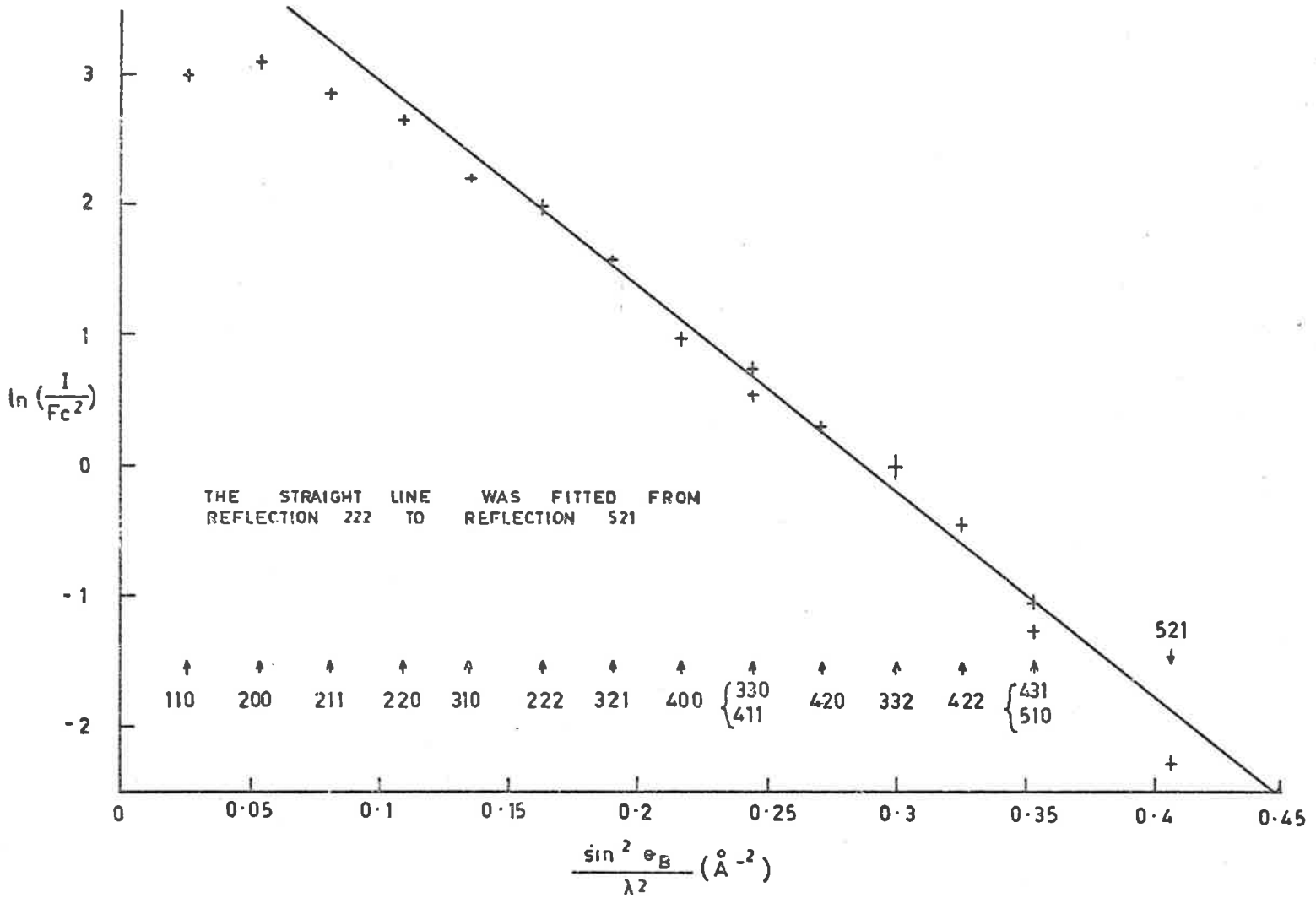

FIG. 5 · 1 WILSON PLOT FOR DATA SET 3.

5.1. The vertical bars indicate the estimated experimental errors. The errors will be discussed in Section 5.6.

5.2 Anisotropy of the Intensities

It was obvious from the Wilson plots, such as that for set 3 in Figure 5.1, that there was considerable anisotropy in the intensities. As seen in Section 2.3, such anisotropy features may be due either to electron density distortions or to anharmonic vibrations of the atoms. The error bars in Figure 5.1 indicate that the anisotropy is due to one of these causes and is not merely the result of inaccurate measurement.

Taking the anharmonic vibration theory first, equation 2.3.23 gives a temperature factor of

$$T_c = \exp\left(\frac{-B'\mathrm{Sin}^2\theta_B}{\lambda^2}\right)(1-PD) \qquad \ldots(5.2.1)$$

where

$$D = h^4 + k^4 + l^4 - \frac{3}{5}(h^2 + k^2 + l^2)^2$$

and P is an anharmonicity parameter.

Using the value of B' determined by the least squares Wilson plot procedure described in Section 5.1, a value of P was found from a least squares fit of F_l to the F_o's obtained from the Wilson

plot procedure, where

$$F_1 = F_c(1 - PD)$$

These values of F_1 were then used to recalculate B' using the Wilson method, and the procedure was cycled to find further values of B' and P until convergence was reached. This was generally after 2 - 3 cycles.

On the other hand, such anisotropic features could have been due to distortions of electron density from spherical. From equation 2.3.15 and using the notation of Section 2.3, this can be described by

$$f(s) = \langle j_o(4\pi sr)\rangle - \frac{\frac{1}{3}A\langle j_4(4\pi sr)\rangle}{1+\frac{15}{4\alpha}} \qquad \ldots(5.2.2)$$

where

$$A = \frac{3(h^4+k^4+l^4)-9(h^2k^2+h^2l^2+k^2l^2)}{(h^2+k^2+l^2)^2}$$

and α is a parameter describing the extent of the distortion.

At the values of $\frac{\sin\theta_B}{\lambda}$ at which the anisotropy is apparent, only the core electron density could contribute to the anisotropy via such a mechanism as that above, since the valence electrons do not contribute to the scattering at such high angles. It was assumed in the present case that because the experiment was carried out at a high temperature relative to both the Debye temperature and

the melting point, and because the least tightly bound electrons in the sodium core are the $2p^6$ electrons which are still relatively tightly bound at ∿39eV, that most of the anisotropic effects were due to the anharmonic vibrations rather than the electron density distortion. However, to provide a comparison, a least squares value of α was calculated for each data set, using the final value of B' obtained for each data set from the cyclic determination of B' and P described above, and assuming P = 0, that is, none of the anisotropy was due to anharmonic vibrations.

5.3 Debye and Anharmonicity Parameters

As outlined in Sections 5.1 and 5.2, the Debye parameter B' and the anharmonicity parameter P were determined simultaneously by alternate application of least squares procedures. This method was convergent for sets 1 to 5. For set 6 the method was not convergent. However, only four reflections were available in this set for the least squares fitting procedure. In this case arbitrary values of B' = 8.50 and P = -10×10^{-4} were applied and gave a reasonable fit.

The values of the Debye parameters and scaling factors and their respective standard errors determined from the least squares Wilson plot procedure for each set are given in Table 5.1. Also given in Table 5.1 are the anharmonicity parameters P for each set.

TABLE 5.1

Debye Parameters, Scaling Factors and their Standard Errors, and Anharmonicity Parameters

Set	B	α_B	k	α_k	P(X 10^{-4})
1	8.48	.30	474.3	90.2	-9.83
2	8.95	.34	39.10	8.81	-19.2
3	7.86	.12	92.53	6.62	-7.01
4	7.54	.46	41.57	11.13	-9.37
5	7.97	.56	1.923	.506	-11.19
6	8.50		44.56		-10.

The average room temperature value of B' obtained from the values derived from sets 1 to 5 is 8.16 ± .25. This must be regarded as being more accurate than the value of $10.2^{-.7}_{+.8}$ read from a graph given by Dawton (1937) because the thermal atomic vibration effects of TDS and anharmonicity were unknown and uncorrected for at that time. It must also be regarded as being more accurate than the value of $6.2^{-.6}_{+.7}$ given by Geshko et al. (1968). The work of these latter authors was done using the 200 reflection from a polycrystalline sample. It was assumed that no extinction was present because the sample was initially dipped in liquid air. However, in the present single crystal case, the 200 reflection intensity is considerably affected by extinction even after the

crystal had been treated with liquid air. This can be seen from the Wilson plot for set 3 in Figure 5.1. It seems unlikely that extinction would have been totally removed in the polycrystalline case merely by dipping the specimen in liquid air.

If we assume that it makes physical sense to calculate a harmonic Debye temperature at room temperature from the isotropic B' value of 8.16 ± .25 for what is obviously a highly anharmonic solid, the Debye temperature value obtained is 134 ± 2°K. This is considerably lower than Debye temperatures listed in Table 1.2, Section 1.6, but as remarked in that section, this is consistent with the experience of other authors for other metals, including nickel and chromium.

The calculated anharmonicity parameters P are listed in Table 5.1. They are all of the same magnitude, but the value for set 2 is numerically about twice as big as the rest. The average value for the first five sets is $-11.3 \pm 2.1 \times 10^{-4}$. Equation 2.3.30 gives the relation between the anisotropic quartic anharmonic, and harmonic parameters of the potential expansion. Substituting the appropriate values for sodium gives

$$\frac{\delta_o}{\alpha_o^4} = 15.3 \text{eV}^{-3}\ \text{Å}^4$$

5.4 The Structure Factors

The observed absolute zero structure factors F_o calculated from equation 5.1.1 are given for set 3 in Table 5.2. Also listed are F_c and F_1, where these are as before. It can be seen that overall, the observed structure factors more closely agree with the F_1 than the F_c. This is seen also in the values of the indices R and R_1, where these are

$$R = \frac{\sum_j |F_{c,j} - F_{o,j}|}{\sum_j |F_{o,j}|}$$

and

$$R_1 = \frac{\sum_j |F_{1,j} - F_{o,j}|}{\sum_j |F_{o,j}|}$$

where the sums were taken over only the non-extinction affected reflections j. The calculated effect of anisotropic anharmonicity on the structure factor is a maximum of 15% for set 3, which has the lowest calculated anharmonicity parameter. Also listed in Table 5.2 are the calculated errors (σ_F) in the structure factors F_o, and the structure factors F_2. These are discussed in Sections 5.6 and 5.5 respectively.

TABLE 5.2

Observed and Calculated Structure Factors

Set 3

Reflection	F_o	F_c	F_1	F_2	σ_F(%)
110	10.12	17.65	17.65	17.66	2.2
200	11.67	15.74	15.68	15.64	3.3
211	11.60	14.20	14.23	14.25	1.9
220	11.78	12.90	12.95	12.98	2.1
310	10.69	11.80	11.65	11.58	1.7
222	10.98	10.85	11.03	11.18	3.3
321	10.17	10.03	10.15	10.18	1.6
400	8.70	9.32	8.77	8.64	2.7
(330	8.91	8.71	8.76	8.90	2.6
(411	8.06	8.71	8.38	8.33	2.0
420	8.33	8.16	8.01	7.99	1.9
332	8.28	7.68	8.19	8.21	5.4
422	7.85	7.36	7.61	7.50	2.9
(431	6.81	6.88	7.16	7.14	2.5
(510	6.07	6.88	6.00	6.05	2.8
521	5.82	6.25	5.87	5.93	2.3

$R = .049$

$R_1 = .019$

$R_2 = .020$

5.5 Electron Density Distortion Approach

For comparison with the anharmonicity approach to the observed anisotropies, the density distortion parameter α (Section 5.2) was calculated for each set. These are listed in Table 5.3. These parameters have no physical significance except that the sign of α indicates that the distribution is distorted inwards along the <111> directions and outward along the <100> directions. Again, the parameters are all of the same order of magnitude, but vary by a factor of up to 4 from smallest to largest.

The values of F_2 and R_2 are given in Table 5.2 for comparison with the values F_1 and R_1. Here $F_2 = 2f(s)$, where $f(s)$ is given by equation 5.2.2, and

$$R_2 = \frac{\Sigma_j |F_{o,j} - F_{2,j}|}{\Sigma_j |F_{o,j}|}$$

where the summation is taken, as for R_1, only over those reflections j which are unaffected by extinction. From Table 5.2 it can be seen that the values of F_1 and F_2 are very similar. As a consequence the values of R_1 and R_2 are almost identical. This result does not mean that the electron distribution is distorted from spherical symmetry, but rather that the time averaged electron density produced by the thermal motion is distorted inwards in the <111> directions, or nearest neighbour directions, i.e. the atomic

TABLE 5.3

Electron Density Distortion Parameter α

Set	α
1	-7.74
2	-5.79
3	-16.7
4	-16.7
5	-8.57
6	-22.1

vibration amplitude is greater in the <100> directions, or the directions of the next nearest neighbours.

Table 5.4 gives the values of A, and $\langle j_4(4\pi sr)\rangle$ as calculated in program SCATFAC (Appendix 1) from the sodium $2p^6$ wave functions.

5.6 The Errors in the Structure Factors

The errors presented are standard errors calculated from the spread in the measured intensities, and do not include any estimate of the errors involved in calculating the parameters B' and K. The formalism is as follows. If observations x_j, j = 1,2 .....n of a variable (the intensity of a reflection) are made and the mean is $\bar{x}$, the standard error is

TABLE 5.4

Values of Electron Density Anisotropy Parameter A, and $\langle j_4(4\pi sr)\rangle$ for Na $2p^6$ Electrons

Reflection	A	$\langle j_4(4\pi sr)\rangle$
110	-.75	.01196
200	3.0	.03993
211	-.75	.07588
220	-.75	.11510
310	1.65	.15484
222	-2.0	.19349
321	-.75	.23017
400	3.0	.26439
(330	-.75	.29595
(411	1.4722	.29595
420	.6	.32483
332	-1.7417	.35106
422	-.75	.37479
(431	-.75	.39615
(510	2.4453	.39615
521	.85	.43241

$$\sigma = \left(\frac{1}{n(n-1)} \sum_{j=1,n} (x_j - \bar{x})^2\right)^{\frac{1}{2}} \qquad \ldots(5.6.1)$$

Then the standard error of any function of a number of measured means $m_1, m_2 \ldots\ldots m_n$, e.g. $f(m_1, m_2 \ldots\ldots m_n)$ is

$$\sigma = \left(\left(\frac{\partial f}{\partial m_1}\right)^2 \sigma_1^2 + \left(\frac{\partial f}{\partial m_2}\right)^2 \sigma_2^2 + \ldots \left(\frac{\partial f}{\partial m_n}\right)^2 \sigma_n^2\right)^{\frac{1}{2}} \qquad \ldots(5.6.2)$$

where $\sigma_1, \sigma_2 \ldots\ldots \sigma_n$ are the standard errors corresponding to the means $m_1, m_2 \ldots\ldots m_n$ respectively. These two relations form the basis of the error estimation.

In calculating average relative intensities, the film factors were calculated and applied to the intensities read from each four-film-pack. Mean intensities and the standard errors were then calculated by means of equation 5.6.1 for each side of the film from all symmetry related reflections of a particular type hkl. Equation 5.6.2 was then used to calculate the standard errors in the mean intensities after spot shape corrections were applied. Similarly, equation 5.6.2 was used to calculate the standard errors in the mean intensities after Lorentz-polarisation, absorption and TDS correction factors, layer scaling and anomalous dispersion corrections were applied. In calculating the errors due to the layer scaling procedure, the errors in the layer scaling factors were taken as the standard deviations of the scaling factors as

produced by program AULAC. The Lorentz-polarisation, absorption, TDS and anomalous dispersion corrections were assumed to be absolutely accurate. The estimated errors in the structure factors as in Table 5.2 are then just half the estimated errors in the intensities.

The standard errors σ_B and σ_K in the parameters B' and K respectively obtained in the Wilson plot were determined from the relations

$$\frac{\sigma_a^2}{n} = \frac{\sigma_b^2}{[xx]} = \frac{\sigma^2}{\Delta}$$

$$\sigma^2 = \frac{[dd]}{(n-2)}$$

$$\Delta = n[xx] - [x]^2$$

where we are fitting the straight line

$$y = ax + b$$

to n points. The symbols σ_a and σ_b represent the standard errors in the coefficients a, b respectively, d_j represents $ax_j + b - y_j$ and the symbol [ ] represents $\sum_{j=1,n}$.

The procedure for calculation of errors in structure factors does not take explicit account of errors in film factors, but these are implicitly considered in the spread in the intensity values averaged after film factor scaling. Likewise, no explicit account need be taken of the errors in the actual densitometering process, provided these are smaller than the spread of errors in the intensities. It has already been shown that these errors are probably ∿2%, and since the standard error in the intensity spread is in general greater than this, these errors are considered to be implicitly accounted for.

The error involved in taking the Lorentz-polarisation correction as absolutely accurate is negligible because the cell spacing is known accurately and all the relevant coordinates can be calculated to a much higher degree of accuracy than is available in the data. Likewise there is negligible error in the absorption correction, as it is relatively small, even for CuK_{α} radiation. A similar argument applies for the anomalous dispersion corrections.

It is more difficult to estimate errors in the TDS correction because a number of assumptions are made. Firstly, the "aperture" used is taken as the size of the spot as determined by the least squares fit of a straight line to measured spot sizes on film. Secondly, it was assumed that second and higher order TDS scattering was removed in the background, since these corrections are considerably more difficult to compute than the already difficult first

order correction. The largest error is likely to be in calculating the volume of reciprocal space swept out in a scan. Correction factors of up to 40% were calculated for sodium. But even if these are in error by 10%, the greatest error in the corrected intensities will be 3% for the highest angle reflections.

Finally, the calculated errors (as in Table 5.2 for set 3 and Appendix 2 for the other five sets) may be an overestimate of the errors in the structure factors. This may be inferred from the fact that on the average, the calculated errors are greater than the index R_1 for each of the sets of data by a factor of about 1½.

5.7 Extinction

For convenience, various relevant details of the intensity measurement for the various data sets are tabulated in Table 5.5. In this table, "Time Elapsed" for any intensity set means the time elapsed between the measurement of that set and the previous set. The extent of the extinction present for each data set can be seen from Table 5.6 where the calculated extinction parameters

$$y_j = \left(\frac{F_{o,j}}{F_{c,j}(1-PD_j)}\right)^2$$

have been tabulated. It can be seen that sets 3 and 4 could not be scaled together as was originally planned (Section 4.7) because

TABLE 5.5

Experimental Conditions

Data Set	Crystal	Radiation	Rotation Axis	Time Elapsed
1	1	CuK_α	[001]	-
2	1	MoK_α	[001]	-
3	2	CuK_α	[001]	-
4	2	CuK_α	[210]	1 month
5	2	MoK_α	[210]	1 week
6	2	MoK_α	[001]	1 week

TABLE 5.6

Extinction Factor y

Reflection	Set 1	Set 2	Set 3	Set 4	Set 5	Set 6
110	.07	.11	.33	.09	.10	.07
200	.10	.22	.55	.17	.23	.13
211	.19	.42	.66	.30	.42	.23
220	.32	.62	.83	.43	.52	.33
310	.36	.63	.84	.52	.66	.48
222	.40	.78		.62	.70	.72
321	.74			.74		.81
400	.66					

there was considerably less extinction present in set 3 than set 4. This was due to the fact that the crystal was dipped in liquid air, thus increasing the imperfections, before the recording of the set 3 intensities. In the interval between the two sets of data, the extinction had increased markedly. Lonsdale (1948) has suggested that the large thermal vibration of the atoms was responsible for the "self-annealing" of sodium observed by Dawton (1937) as a hysteresis in intensity with cycles of heating and cooling between room temperature and the melting point (Section 1.5). The time scale for this hysteresis was up to 3 hours. It is not unreasonable to assume that a similar effect has been observed in the present case over a time scale of several weeks at room temperature.

It is interesting to note that Feder and Charbnau (1966) discovered an irreversible temperature effect in the macroscopic expansion properties of sodium crystals when the sodium surface had acquired a coating of oxide. Also it was found that isothermal specimen shrinkage and growth occurred in sodium specimens after heating and cooling respectively. The temperature range being investigated was $-25^{\circ}C$ to the melting point, which was about the same range as that observed to produce hysteresis effects in X-ray intensities by Dawton.

There is, in fact, some evidence to suggest that the crystal underwent further annealing after measurement of data set 4. We

expect the data sets measured with MoK_α radiation to show less extinction than data sets measured with CuK_α radiation, if all other conditions are identical. This is true for sets 5 and 2 when compared with sets 4 and 1 respectively. However the difference in extinction factors between sets 4 and 5 compared with the difference in extinction factors between sets 1 and 2 is small. This seems to indicate that further annealing took place in the week or so between the measurement of data sets 4 and 5. Finally, the difference in extinction factors between sets 5 and 6, measured from the same crystal with the same radiation, seems to indicate that further annealing took place in the week or so between the measurement of data sets 5 and 6. Thus it appears that sodium may anneal at room temperature over a period of some weeks.

5.8 The Extinction Correction Program

As seen from Table 5.6, extinction was present in all intensity sets recorded, and correction procedures were investigated. Recent descriptions of extinction have been given by Weiss (1966), Hamilton (1969), and Zachariasen (1967, 1968) with extensions to the latter by Cooper and Rouse (1970). This latter method was suitable for use with data collected at two wavelengths from a single cylindrical crystal, provided that the positional parameters of the atoms in the unit cell were accurately known. As these conditions were

fulfilled in the present case, this was the method used. It is briefly outlined below, with a full description of the mathematics and programming given in Appendix 1.

The assumptions of the Zachariasen method for a spherical crystal are that the imperfect crystal is made up of spherical mosaic blocks of mean radius r, with their orientation characterised by the Gaussian function

$$W(\Delta) = \sqrt{2}\ g\ \exp(-2\pi^2 g^2 \Delta^2)$$

It is assumed that the higher angle reflections are unaffected by extinction, and average values of r and g are calculated from the low angle reflections from two sets of data at different wavelengths. These average values are then used to determine the corrections to be applied to each of the sets of data. The Cooper and Rouse modifications are firstly to take account of an angle dependence of the extinction factor, and secondly to adapt the Zachariasen theory for cylindrical crystals.

Zachariasen (1968) states that it may not be possible to justify the assumption of isotropy of shape and orientation of the mosaic domains for some crystals. Hamilton (1969) has discussed anisotropic extinction corrections. Cooper and Rouse (1970) point out however, that such corrections may lead to misinterpretations of other effects. ~~This would be particularly so in sodium, which~~

The case of sodium is particularly relevant here since considerable anistropic effects other than extinction are present yet, because of its elastically anisotropic nature, sodium might be considered likely to display anisotropic extinction. Hamilton's method was therefore not considered.

The Cooper and Rouse extinction treatment was applied to sets 1 and 2, and sets 4 and 5. The annealing previously described prevented any corrections being applied to sets 3 and 6. Table 5.7 gives F_1, the corrected observed structure factors for set 1, F_2, the corrected observed structure factors for set 2, and F_1' and F_2', the calculated Hartree-Fock structure factors with corrections for anharmonicity. It can be seen that the corrected structure factors are over corrected for the higher angle reflections and under corrected for the low angle reflections to a marked degree in both cases. It seems that the theory cannot handle heavy extinction as is present in this case. This is probably a consequence that the physical assumption underlying the theory is inappropriate. The real crystal is unlikely to consist of small spherical perfect crystal blocks, but this probably is a sufficiently good approximation where the number of imperfections in the crystal is large, and extinction small. The calculated domain size and spread parameters r and g respectively are 4.7×10^{-5} cm and 8.8×10^{3} for sets 1 and 2, which support Zachariasen's statement that "extinction effects will be very severe if $r > 5 \times 10^{-5}$ cm and $g > 5 \times 10^{3}$". It is also possible that the parameters r and g calculated from the low angle reflections are in error because the

TABLE 5.7

Reflection	F_1	F_2	F_1^1	F_2^1
110	15.04	11.17	17.66	17.66
200	13.16	11.39	15.66	15.58
211	14.20	13.13	14.24	14.28
220	15.13	13.54	12.97	13.04
310	13.08	11.07	11.59	11.38
222	12.38	12.06	11.11	11.35
321	14.36	12.06	10.19	10.35
400	10.36	8.46	8.54	7.80
(330	13.08	10.52	8.94	9.16
(411	11.52	8.33	8.25	7.82
420	11.37	8.71	7.95	7.74
332	12.13	9.11	8.39	9.07
422	10.80	8.99	7.71	8.04
(431	10.27	8.22	7.26	7.63
(510	7.46		5.64	
521	7.32		5.72	

extinction is anisotropic.

The results for sets 4 and 5 were similar.

5.9 Reanalysis of Dawton's Work

In view of the obvious anharmonicity shown by sodium in the present case, it was thought worthwhile to reanalyse Dawton's (1937) data on the temperature dependence of the intensities in sodium, since this leads to information about the parameters in the potential expansion.

Dawton listed ratios at three different pairs of temperatures of the intensities of the five reflections, 110, 200, 220, 310 and 400. The temperature ratios were 117/180°K, 117/291°K and 117/368°K. The ratio of intensities at 117°K and 180°K was also measured for the 440 reflection. Dawton showed that the data could be approximately fitted by an empirical formula of the type

$$I_T \sim \exp - (.04044T + 17.08 \times 10^{-5}T^2)\mathrm{Sin}^2\theta_B \qquad \ldots(5.9.1)$$

for molybdenum radiation, but no physical interpretation of this result was made.

By comparison with equation 2.3.28, it can be seen that such coefficients are related to the potential parameters α_o, γ_o and

δ_o . The intensities listed by Dawton were not corrected for TDS, and insufficient is known about the experimental arrangement to enable corrections to be made. It has already been seen that such corrections are of considerable importance in the case of sodium, and any determination of the potential parameters without this correction will be approximate only.

Taking equation 2.3.28, the exponential of the Debye-Waller factor at temperature T is given as

$$
\begin{aligned}
2W(T) = {} & \left(\frac{2\pi}{a_o}\right)^2 (h^2+k^2+l^2) \left(\frac{1}{\alpha_o}\right) k_B T \\
& + \left(\frac{2\pi}{a_o}\right)^2 (h^2+k^2+l^2) \left(\frac{2\gamma_G \chi}{\alpha_o k_B}\right) (k_B T)^2 \\
& - \left(\frac{2\pi}{a_o}\right)^2 (h^2+k^2+l^2) \left(\frac{20\gamma_o}{\alpha_o^3}\right) (k_B T)^2 \qquad \ldots(5.9.2) \\
& + \left(\frac{2\pi}{a_o}\right)^4 (h^2+k^2+l^2)^2 \left(\frac{2\gamma_o}{\alpha_o^4}\right) (k_B T)^3 \\
& - \left(\frac{2\pi}{a_o}\right)^4 (h^2k^2+h^2l^2+k^2l^2-\tfrac{1}{3}h^4-\tfrac{1}{3}k^4-\tfrac{1}{3}l^4) \left(\frac{12\gamma_o}{5\alpha_o^4}\right) (k_B T)^3
\end{aligned}
$$

where the symbols have the same significance as in Section 2.3. Then, putting

$$p(hkl) = h^2k^2+k^2l^2+h^2l^2- \frac{1}{3}h^4- \frac{1}{3}k^4- \frac{1}{3}l^4$$

$$a(hkl) = \left(\frac{2\pi}{a_o}\right)^2 (h^2+k^2+l^2) \left(\frac{1}{\alpha_o}\right) k_B$$

$$b(hkl) = \left(\frac{2\pi}{a_o}\right)^2 (h^2+k^2+l^2) \left(\frac{2\gamma_G\bar{x}}{\alpha_o k_B}\right) k_B^2 \qquad \ldots(5.9.3)$$

$$c(hkl) = \left(\frac{2\pi}{a_o}\right)^2 (h^2+k^2+l^2) \left(\frac{20\gamma_o}{\alpha_o^3}\right) k_B^2$$

$$d(hkl) = \left(\frac{2\pi}{a_o}\right)^4 (h^2+k^2+l^2)^2 \left(\frac{2\gamma_o}{\alpha_o^4}\right) k_B^3$$

$$f(hkl) = \left(\frac{2\pi}{a_o}\right)^4 p(hkl) \left(\frac{12\gamma_o}{5\alpha_o^4}\right) k_B^3$$

we can write

$$\ln\left(\frac{I(T_2)}{I(T_1)}\right) = -\left[a(hkl)(T_2-T_1)+(b(hkl)-c(hkl))(T_2^2-T_1^2)\right.$$
$$\left. + (d(hkl)-f(hkl))\ (T_2^3-T_1^3)\right] \qquad \ldots(5.9.4)$$

where I(T) is the observed intensity at temperature T. Then observations of ratios of intensities at three or more pairs of temperatures will allow the coefficients a(hkl), b(hkl) - c(hkl) and d(hkl) - f(hkl) to be determined.

Although Dawton has shown that his empirical formula 5.9.1 fits all six reflections reasonably well, it was decided in the present case to use the 400 reflection for computing the parameters since the present work has shown that this reflection is the least likely of the five to be affected by extinction. The values of the parameters found using equations 5.9.3 and 5.9.4 and the values of $I(T_2)/ I(T_1)$ for 400 as given by Dawton are

$$\alpha_o = .6 \text{ eV } \text{Å}^{-2}$$

$$\gamma_o = -.9 \text{ eV } \text{Å}^{-4}$$

$$\delta_o = -3. \text{ eV } \text{Å}^{-4}$$

The value of

$$\left(\frac{12\delta_o}{5\alpha_c^4}\right) = -47 \text{ eV}^{-3} \text{ Å}^4$$

is in qualitative agreement with the value of $-37 \text{ eV}^{-3} \text{ Å}^4$ obtained in the present work.

The value of the other parameters required in equation 5.9.2 were

$$a_o = 4.2906 \text{ Å and}$$

$$\gamma_G = 1.25$$

$$\chi = 20.1 \times 10^{-5} \text{ }^oK^{-1}$$

These latter two values were taken from Geshko et al. (1968).

Using the fact that for a cubic crystal

$$s^2 = \mathrm{Sin}^2\theta_B/\lambda^2$$

$$= \frac{h^2+k^2+l^2}{4a_o^2}$$

the exponent of the Debye-Waller factor can be written

$$2W = 2.2 \times 10^{-2} s^2 T + 1.1 \times 10^{-5} s^2 T^2 + 9.1 \times 10^{-5} s^2 T^2$$

$$- 2.0 \times 10^{-7} s^4 T^3 + \frac{P}{(2a_o)^4} \times 7.5 \times 10^{-7} T^3$$

...(5.9.5)

where these terms correspond in order to the terms given in equation 5.9.2. This formula corresponds reasonably with the empirical formula of Dawton (equation 5.9.1) of

$$2W = 2.03 \times 10^{-2} s^2 T + 8.59 \times 10^{-5} s^2 T^2$$

From equation 5.9.5 it can be seen that the second term, due to thermal expansion only, is much smaller than the third term, which depends on the fourth order potential parameter γ_o. Similarly, the fourth and fifth terms, which depend on the fourth order potential parameters γ_o and δ_o respectively, will become of the same order as the thermal expansion term for values of s^2T greater

than about $50^{\circ}K\ \text{Å}^{-2}$, or about $120^{\circ}K$ for s^2 at the edge of the copper reflecting sphere.

It seems then, that any explanation of anharmonic phenomena in sodium crystals which merely uses the "quasi-harmonic" approach, or merely includes the thermal expansion term only, is not likely to give a very accurate account. TDS of order n will affect terms in T^n. The values of α_o in particular will be smaller.

5.10 On the Determination of Low Angle Scattering Information from Neutral Sodium Atoms

For reasons given in Section 2.4, there is little likelihood of observing any contribution to the low angle Bragg intensities from the 3s electron in metallic sodium. Even if it were not for this reason, the particular vibrational properties of sodium, which give rise to large extinction and TDS, preclude accurate low angle scattering data being measured. Any low angle X-ray diffraction investigation of bound sodium atoms would need to be undertaken for a solid with a large unit cell, and where the sodium is loosely bound, with virtually no charge transfer. Such a structure is that of Na_8Si_{46} reported by Kasper et al. (1965). It is cubic, with $a = 10.2$ Å and space group Pm3n. The eight sodium atoms are in two sets of special positions, one atom at each of the equivalent origin and body-centred positions, and six atoms at the ¼ ½ 0 set

of positions. The structure is an analogue of the gas hydrate clathrate type structure 46 H_2O.8M. In the present case, the two types of sodium atoms occur at the centres of polyhedral cages of silicon atoms. The sodium-silicon distances are relatively large at 3.5 Å, which implies that the sodium atoms are uncharged. Unfortunately, Kasper et al. have not refined the structure fully, or given accurate observed structure factors. If accurate data were available, it would be possible to investigate the scattering from sodium atoms at two crystallographically non-equivalent types of sites down to a lower limit in reciprocal space of $\frac{\sin\theta_B}{\lambda} \sim .07$ Å^{-1}. This is sufficiently small to enable a contribution from the sodium 3s electron to be observed in the first several reflections.

This completes the main work based on the relative intensity data. A supplementary set of absolute intensity data was measured for comparison and is presented in the next chapter.

CHAPTER 6

ABSOLUTE INTEGRATED INTENSITY MEASUREMENTS

6.1 Introduction

Absolute intensity measurements of X-ray diffraction from metals have become more frequent in recent years, due to interest in solid state effects. Most of these investigations have been carried out on powders or thin crystal plates. However neither of these methods is suitable for sodium because the type of specimen required cannot be prepared. A method suitable for small single crystals was that described by Burbank (1965). This, with some modifications, was the method adopted by this author.

6.2 Outline of the Method

The method is for a crystal which is small enough to be completely bathed in the incident X-ray beam and has ideal mosaic texture. The absolute integrated intensity is then given by (James (1965))

$$\frac{E\omega}{I_o} = N^2\lambda^3 \, |F|^2 \left(\frac{e^2}{mc^2}\right)^2 \frac{1+\mathrm{Cos}^2 2\theta_B}{2\mathrm{Sin}2\theta_B} \, AV \qquad \ldots(6.2.1)$$

where E is the reflected energy

ω is the angular velocity of crystal rotation

I_o is the incident beam energy per unit area and unit time

N is the number of cells per unit volume

A is the transmission factor

V is the volume of the crystal, and the other symbols have their usual meanings.

Burbank (1964, 1965) has discussed methods of measurement of absolute intensities from small crystals and has concluded that certain conditions are most suitable. These are that the crystal and focal spot define the collimation, the spectral distribution is determined by balanced filters and the θ-2θ scanning technique is used with relatively long wavelength radiation.

Accordingly, nickel and cobalt balanced filters were used with copper radiation. The integrated intensities were recorded for the zero layer using a θ-2θ scan. The direct beam was measured using a pin-hole and attenuators.

6.3 Apparatus

The work was carried out manually on a horizontal goniometer with a Philips PW1010 constant potential generator. The counter was a 20th Century xenon-filled proportional counter linked to Ekco electronics, consisting of an amplifier,pulse height analyser (P.H.A.), scaler, ratemeter and a chart recorder.

The balanced filter foils, supplied by Goodfellow Metals Ltd., were 99.9% pure foils of nickel (0.0093 mm) and cobalt(0.01002 mm). They were nominally balanced for CuK_β at 10% transmission. Attenuation foils were aluminium (5 mil) and nickel (0.75 mil).

The crystal "viewed" the focal line of 10 x 1 mm as a spot at a take-off angle of 6^o through a pair of 3 mm circular apertures in one of which was mounted one of the pair of balanced filter foils. These, as were the aluminium and a set of six nickel attenuation foils, were mounted between two 1 mm thick lead strips shaped to fit into the incident and diffracted beam tunnels in place of the normal slits. The other nickel attenuating foils used were mounted on brass holders such that they could be placed perpendicular to the diffracted beam between the crystal and the counter. The receiving aperture immediately in front of the counter was a 3 mm square aperture in two 1 mm thick lead strips mounted in the diffracted beam tunnel in place of the usual slits.

6.4 The Wavelength Spectrum

The wavelength spectrum was determined using the goniometer as a spectrometer with an LiF crystal plate cut parallel to the 200 planes. The scanning speed was $4^o 2\theta$/min.

The amplifier and P.H.A. were adjusted to centre on the CuK_α peak. The effect of the P.H.A. can be seen in Figures 6.1 and 6.2, where Figures 6.1(a) and 6.1(b) show the spectrum with no P.H.A. for the Ni and Co filter foils respectively, and Figures 6.2(a) and 6.2(b) show the spectrum with P.H.A. for the two foils respectively. Wavelengths far from CuK_α, in particular the short bremmstrahlung wavelengths, have been reduced. Figure 6.1 shows also a slight imbalance of the foils at CuK_β, and a small peak due to WL_α contamination in the source. The imbalance was improved by placing a $\sim$ .75 mil nickel foil between the crystal and the receiving slit for all measurements. The resulting wavelength spectrum is shown in Figures 6.3(a) and 6.3(b). The CuK_β and WL_α peaks have become negligible.

The spectrum was measured also with the aluminium attenuator and each of the filter foils in turn in place to check that the filter balance was not affected by the aluminium attenuator. The results are shown in Figures 6.4(a) and 6.4(b).

6.5 Operating Conditions

There was an optimum voltage at which to work which was determined by the following statistical considerations. Suppose the direct beam is measured with suitable apertures and attenuating foils. If β and α are the direct beam intensities measured with

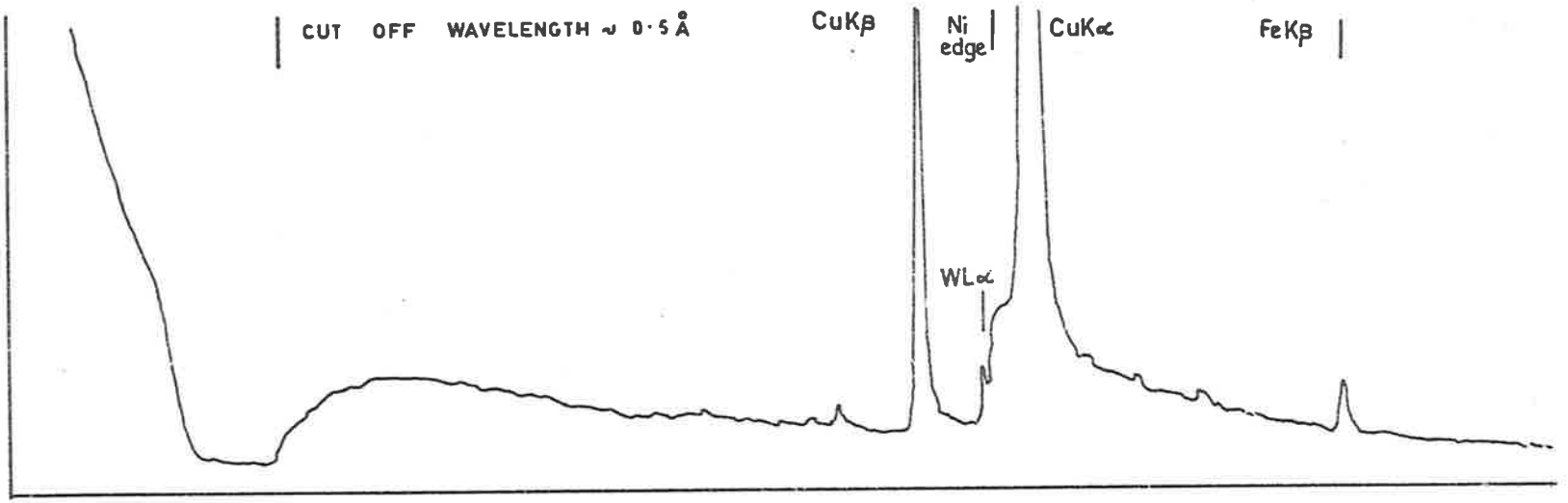

FIG. 6·1 (a) WAVELENGTH SPECTRUM; Ni FILTER; NO P. H. A.

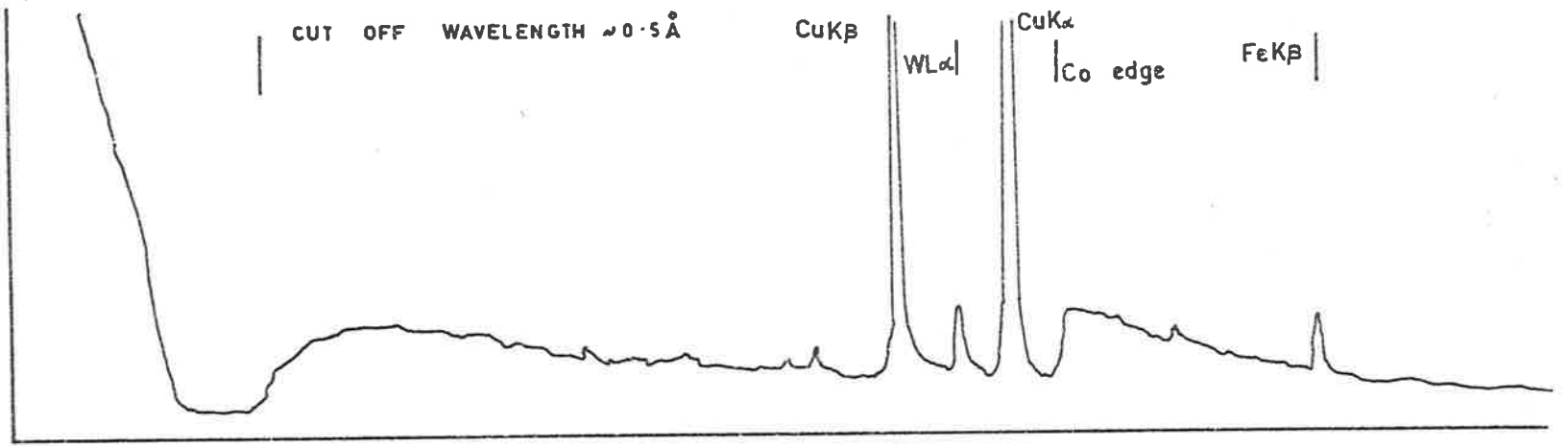

FIG. 6·1 (b) WAVELENGTH SPECTRUM; Co FILTER; NO P. H. A.

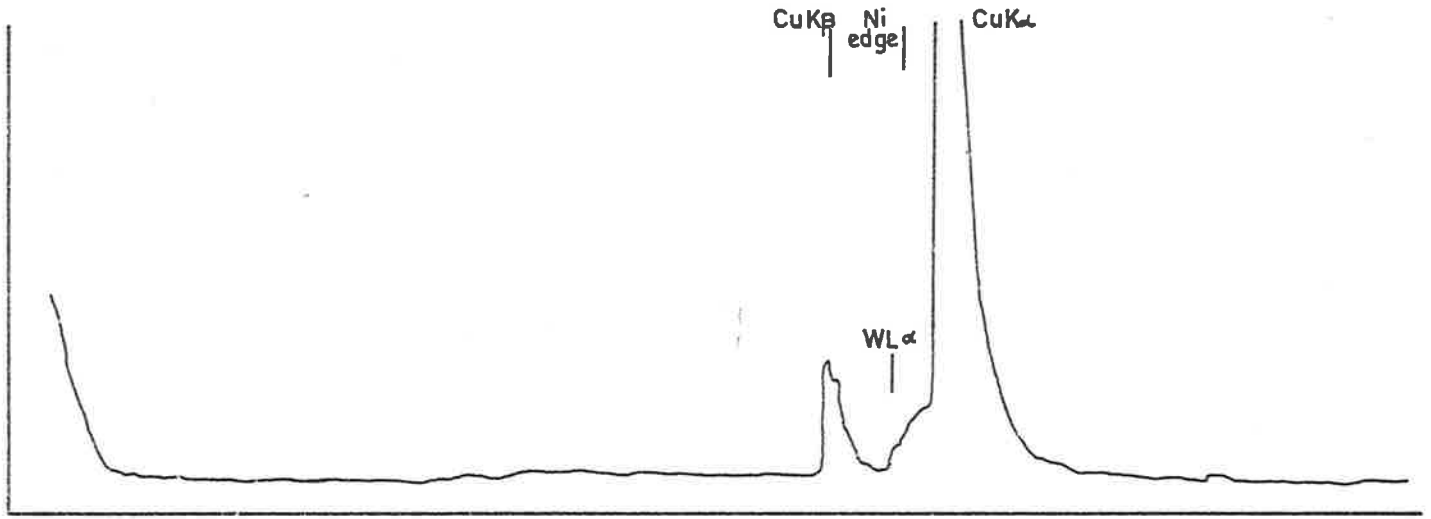

FIG. 6·2 (a) WAVELENGTH SPECTRUM; Ni FILTER; WITH P. H. A.

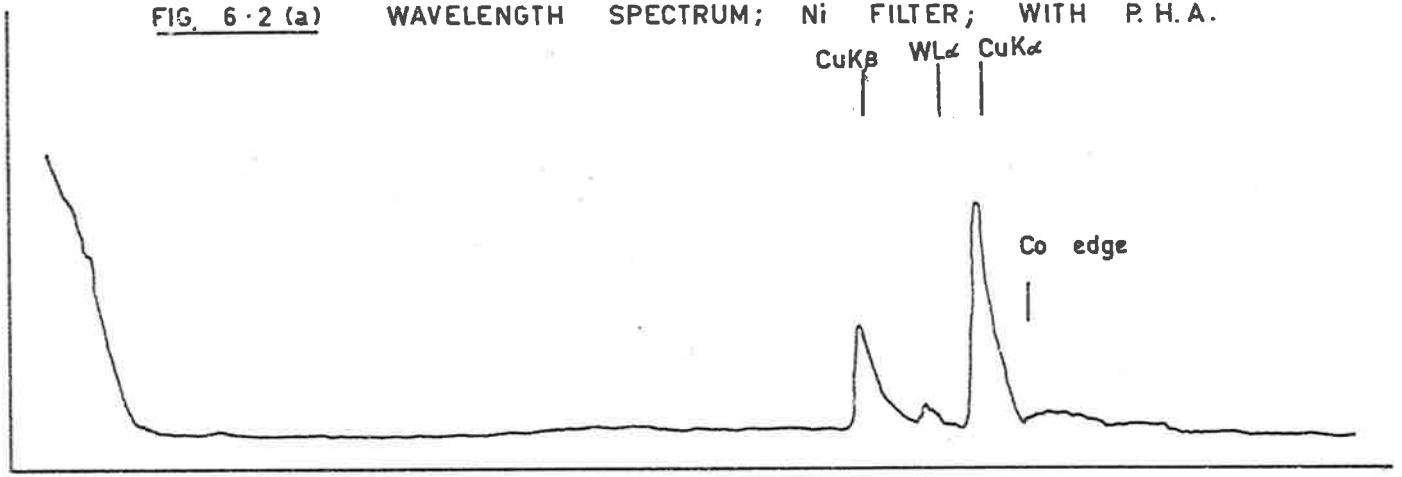

FIG. 6·2 (b) WAVELENGTH SPECTRUM; Co FILTER; WITH P. H. A.

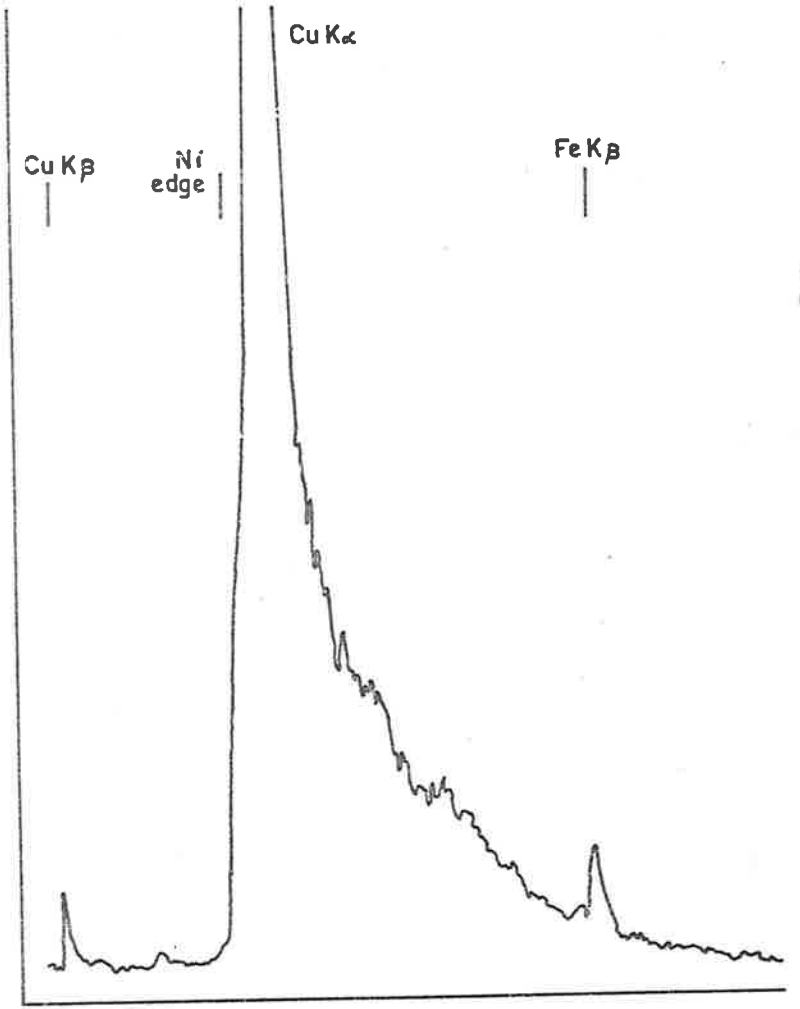

FIG. 6·3(a) WAVELENGTH SPECTRUM; Ni FILTER; Ni ATTENUATOR; WITH P.H.A.

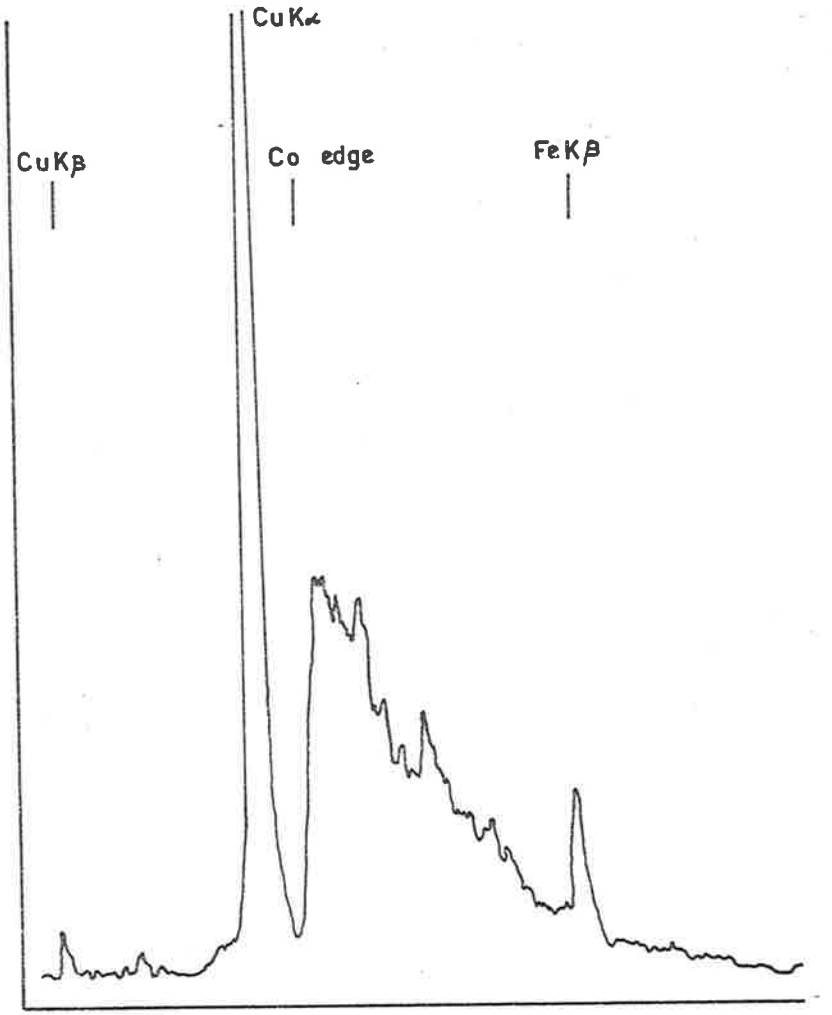

FIG. 6·3(b) WAVELENGTH SPECTRUM; Co FILTER; Ni ATTENUATOR; WITH P.H.A.

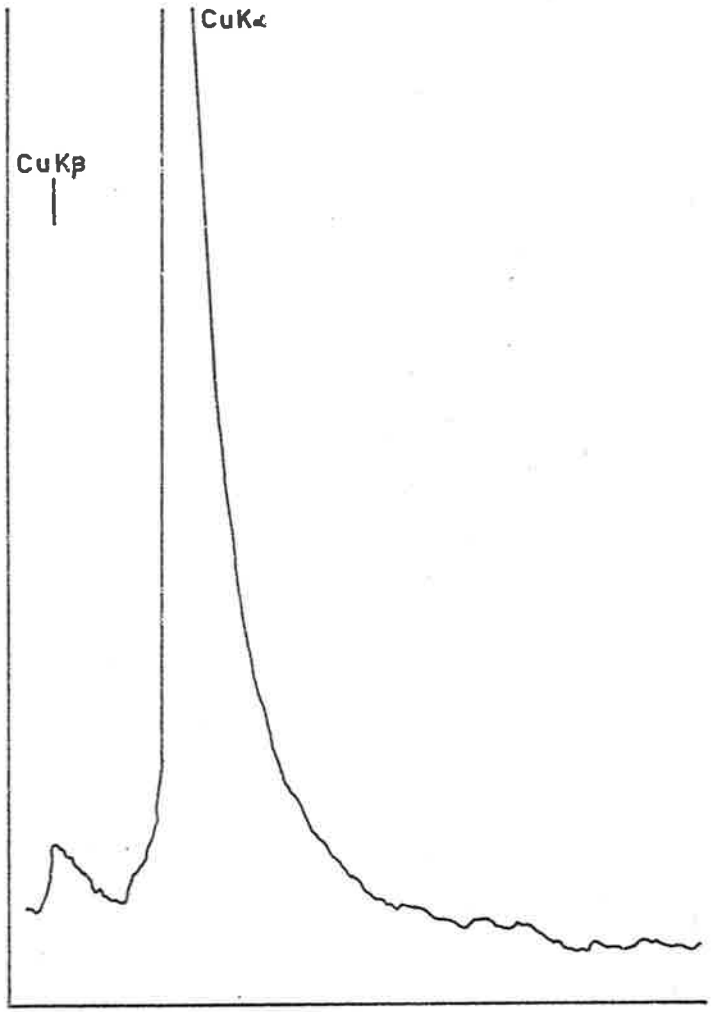

FIG. 6·4 (a) WAVELENGTH SPECTRUM; Ni FILTER; Al ATTENUATOR; WITH P. H. A.

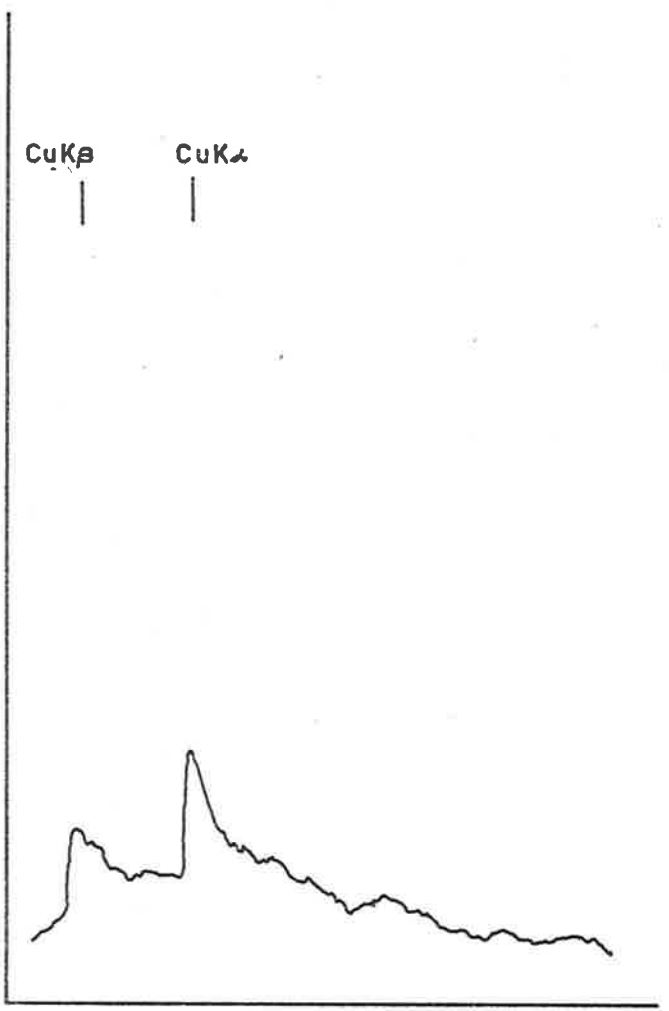

FIG. 6·4 (b) WAVELENGTH SPECTRUM; Co FILTER Al ATTENUATOR; WITH P. H. A.

the Ni and Co filter foils respectively, then the net count is given by N, where

$$N = \beta - \alpha$$

If $\beta \sim \alpha$, $\beta >> N$, $\alpha >> N$, the error in N given by

$$\sigma_N = \sqrt{\beta+\alpha}$$

will be unreasonable, whereas if $\beta > \alpha$, $N \sim \beta$, $N > \alpha$, the relative statistical error will be much smaller. Burbank (1965) suggests an optimum working voltage of 23 Kv for CuK_α, with Ni and Co balanced filters.

Values of β and α for direct beam measurements were obtained at a number of voltages. Table 6.1 shows the ratio of β/α for various constant potential accelerating voltages, with 30 mA current.

TABLE 6.1

Voltage (Kv)	β/α
20	4.50
22	3.38
24	2.60
26	1.98
28	1.50
30	1.23

The lowest available accelerating voltage of 20 Kv was used at 30 mA, because the measured β/α ratio was highest for this voltage. These and all other experimental conditions were kept constant where possible throughout the experiment to minimise scale factors.

6.6 Counter Calibration

The overall dead time of the counter and electronics system was required in order to estimate the"linear" counting range. The following procedure was used. The LiF spectrometer was first set to the CuK_α peak. The count rate was then measured using from zero to eight nickel attenuation foils of nominal thickness .75 mil. It was assumed initially that because these foils were cut from the same strip of nickel, they were of the same thickness and therefore had identical absorption coefficients. This was later verified (Section 6.7) to a tolerance of 1.5%.

Values of $\ln\left(\frac{N_j}{N_{j-1}}\right)$ were calculated, where N_j is the count rate with j attenuating foils in place. At low count rates (~300 cps) the value of $\ln\left(\frac{N_j}{N_{j-1}}\right)$ had become constant at -.629, indicating that dead time counting losses were negligible. Using this constant value, values of $N_{c,j}$ were calculated, where

$$N_{c,j-1} = \frac{N_j}{\exp(-.629)}$$

A value of the dead time τ for a particular j was then obtained from the usual formula

$$\tau = \left(\frac{1 - \frac{N_j}{N_{c,j}}}{N_j}\right)$$

An average value of τ obtained from count rates up to 7000 cps was ± 7.38 μsecs. This gives a "linear" counting range to within 5% up to 4000 cps. In general, maximum count rates used were below 2500 cps.

6.7 Calibration of Attenuating Foils

The attenuating coefficients of each of the eight nickel foils used for the counter calibration (Section 5.6) were checked separately for CuK_α. The average coefficient was found to be 1.92 ± .03 with a counting statistical error of 1%. It was concluded that the assumption of identical thickness for each of the foils was valid.

The attenuation coefficient at CuK_α of the .5 mil aluminium foil was measured under a variety of conditions. The average was found to be 6.66 ± .11.

Attenuation foils having an absorption edge near the wavelength of interest are normally used in work of the type being described because they prevent hardening of the radiation. However, attenuating foil such as aluminium, which has relatively flat absorption characteristics near CuK_α, can be used in the present case because the P.H.A. discriminates against the hardening effect of the attenuating foils.

6.8 The Growth of the Crystals

Small spheres of sodium were shaken from a mass under paraffin oil, and sucked into glass capillaries of the type used for cylindrical crystals (Section 3.2). The tubes were sealed as previously described. The molten sample was plunged into liquid air. This treatment provided a reasonable chance that a single crystal with reasonable spot shape would be formed. (If this treatment were applied to larger, cylindrical specimens in the hope of producing a powder, the result was a polycrystalline sample).

It was found necessary to grow the crystal sufficiently large to touch the sides of the tube on cooling; otherwise the crystal moved inside the tube.

The crystal was dipped in liquid air a second time before use. A subsequent photograph showed that the spot shape had become irregular with this treatment.

The crystal grown for this work was found to be oriented near a <311> axis, and was aligned photographically by the method described in Section 3.3. It was then transferred to the horizontal goniometer and aligned finally by the method of Furnas (1957).

6.9 Measurement of the Integrated Reflection Intensities

The horizontal and vertical dimensions of the aperture required

(T_h and T_v respectively) are given by (Burbank (1964))

$$T_h \sim S_h + 2C_h + 2M$$

$$T_v \sim S_v + C_v + M$$

Here S is the source size expressed as the angle subtended at the crystal ($.28^o$), C is the crystal diameter expressed as the angle subtended at the source ($.14^o$) and M is the angular width of the mosaic spread. Taking S_h equivalent to S_v and C_h to C_v, we have $T_h \sim .56 + 2M$ and $T_v \sim .42 + M$. To allow for mosaic irregularities and mis-setting of the crystal a 1.43^o square aperture was used.

The theoretical range of integration is similarly given in terms of S,C and M (Burbank (1965)) as from $2\theta_1$ to $2\theta_2$ where

$$2\theta_1 < 2\theta_{Ni(K\ edge)} - S - C - M$$

$$2\theta_2 > 2\theta_{Co(K\ edge)} + S + C + M$$

It was found that the scan range required was less than the theoretical range. This was possibly because the two liquid air treatments given the crystal before its use had effectively reduced the mosaic spread M to zero, and also because the wavelength dispersion was less than that defined by the balanced filters, due to the P.H.A.

The working procedure adopted was first to make a tracing with the chart recorder using each filter in turn. From this the maximum scan range and limits $2\theta_1$ and $2\theta_2$ for each reflection were determined. Further scans were then made with each filter in turn, and the integrated count recorded with the scaler. Fixed counts were then made for 100 seconds with each filter in turn at $2\theta_1$ and $2\theta_2$. Each count was immediately duplicated. A few measurements were rejected as being affected by local electronic interference. An average was taken when two suitable readings were obtained. Superimposed traces of the 110 reflection for each of the filter foils are shown in Figure 6.5.

Now suppose β is the integrated count from $2\theta_1$ to $2\theta_2$ with the nickel filter foil and α similarly for the cobalt foil. Suppose also that β_1, α_1 and β_2, α_2 refer to fixed counts recorded with the Ni and Co foils at $2\theta_1$ and $2\theta_2$ respectively. Then β_1 and α_1 will not be identical, nor will β_2 and α_2, because there will be additional background scattering including TDS, Compton scattering etc. This integrated background count is denoted as γ, and it is assumed that γ is linear in 2θ. (This assumption is particularly invalid for TDS, but a correction may be made later). Then

$$\gamma = \tfrac{1}{2}\eta[(\beta_1 - \alpha_1)+(\beta_2 - \alpha_2)]\ \Delta 2\theta$$

where η is a conversion factor related to the scanning rate used (0.5° per minute) and the time taken to record the fixed counts

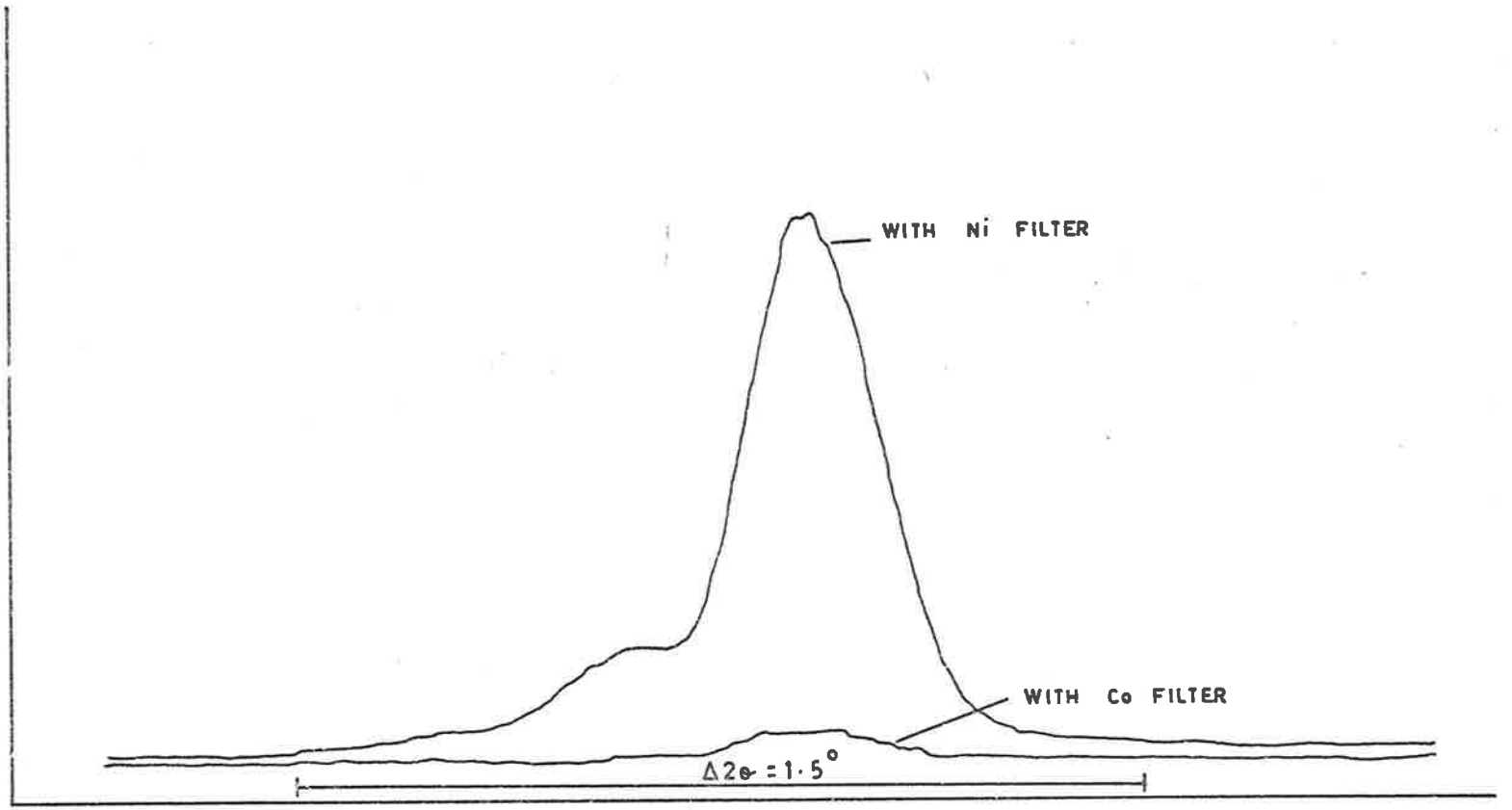

FIG. 6·5 SUPERIMPOSED TRACES OF 110 REFLECTION: θ - 2θ SCAN.

α_1, β_1, α_2, β_2 (100 secs). Its value is 1.2 obtained thus:

1.2 x no. of counts/100 secs = no. of counts/120 secs = counts/$1^o 2\theta$

The net count is then given by

$$N = \beta - \alpha - \gamma$$

with a statistical error of

$$\sigma_c = \sqrt{N_T}$$

where the "total" count N_T is given by

$$N_T = \beta + \alpha + \tfrac{1}{2}\eta\Delta 2\theta \ [\beta_1 + \alpha_1 + \beta_2 + \alpha_2]$$

If no beam attenuator is used, then E = N. The .5 mil aluminium foil was used for the 110, 211 and 220 reflections where the peak counting rate exceeded 2500 cps without an attenuator. In this case

$$E = N \times \text{attenuation factor}$$

$$\sigma_E = [N_T \times (\text{att. factor})^2 + \sigma^2_{(\text{att.factor})} \times N^2]^{\frac{1}{2}}$$

...(6.9.1)

6.10 Direct Beam Measurement

The energy falling on unit area per unit time in that part of

the beam received by the crystal was measured by replacing the crystal with a platinum aperture of nominal diameter 120 microns from a Philips electron microscope, and mounted in the centre of a 1 cm square lead plate about 1 mm thick. The average aperture diameter was measured with an optical comparator, and was found to be 121.4 microns (standard deviation 3.0 microns) from 12 measurements. The aperture was combined with eight of the .61 mil Ni foils. The absorption coefficient of each of these foils was 1.92 ± .03. The net recorded intensity was 1.50×10^{13} photons/metre^2/second, with a standard deviation of 4.8%.

The absorbing effect of the glass capillary tube used was found by setting the spectrometer crystal to CuK_α, and measuring the count rates obtained with and without the glass tube mounted over the receiving slit. No significant change in counting rate was observed.

6.11 Results

The integrated intensities recorded for a total of 17 reflections are given in Table 6.2. It can be seen that there is a marked variation in the intensities of symmetry related reflections at low angles. The spread in the 211 intensities, for example, is from -25% to +29% of the mean value. The lowest intensity for the 211 set and the two 330 reflections were remeasured after checking the alignment of the crystal, but no significantly different

TABLE 6.2

Integrated Intensities

Reflection	Intensity	Att. Factor	Corrected Intensity
110	93587	6.66	623290
110	123629	6.66	823370
211	24067	6.66	160290
211	20171	6.66	134340
211	28767	6.66	191590
211	34756	6.66	231470
220	11688	6.66	77842
220	19427	6.66	129380
330	10072		
330	8788		
411	10190		
411	5737		
411	7439		
332	5038		
332	4576		
422	3168		
422	3390		

measurements were obtained. Since the spread in measured intensities for the two pairs of high angle reflections is small, and is within the limits of experimental error (Section 6.12), it is probable that the large spread in the low angle symmetry related reflection intensities is due to extinction effects.

The averaged intensities for the seven independent reflections are listed in Table 6.3. These are the values taken as E in the equation (derived from equation 6.2.1)

$$|F| = k\,[E/A\,(\frac{1+\mathrm{Cos}^2 2\theta}{2\mathrm{Sin}2\theta})]^{\frac{1}{2}} \qquad \ldots(6.11.1)$$

where

$$k = [\omega/I_o N^2 \lambda^3 \,(\frac{e^2}{mc^2})^2\, V]^{\frac{1}{2}}$$

TABLE 6.3

Averaged Integrated Intensities

Reflection	Intensity
110	723330
211	179423
220	103611
330	9430
411	7789
332	4807
422	3279

The values of the transmission factor A were obtained assuming that the crystal was a sphere of radius .23 mm, and interpolating values of the absorption factor A* ($=A^{-1}$) at the relevant values of μR and θ (μ being the linear absorption coefficient and R the crystal radius) from the tables of A* for spherical crystals given in International Tables (1959). This was done using program BBSCORR as for the relative intensity measurements (Section 4.5 and Appendix 1).

Some experimental constants for the calculation of k in equation 6.11.1 were $\omega = .25^{o}$ min^{-1} = 7.27 x 10^{-5} radians sec^{-1}

$$I_o = 1.504 \times 10^{13} \text{ counts sec}^{-1}\text{m}^{-2}$$

$$V = 6.76 \times 10^{-11}\text{m}^3$$

The volume of the crystal, V, was determined from optical comparator measurements of the size of the crystal. This was found to approximate a cylinder, but with rounded ends. The total length was .464 ± .005 mm and diameter .462 ± .006 mm. The cylindrical section was ∿ .34 mm long. The volume was estimated as the volume of a cylinder of diameter .462 mm and length .34 mm, plus the volume of two sections of a sphere of base diameter .462 mm and height .061 mm. The volume of a cylinder of dimensions .46 mm x .46 mm is about 13% greater than that calculated above. It is not reasonable to assume, therefore, that the volume is known any more accurately than about 5%.

Values of the observed structure factors were calculated using equation 6.11.1. These were corrected for isotropic thermal motion by multiplying by the temperature factor $\exp(B\sin^2\theta/\lambda^2)$ where the value of B used was 8.16, the average of the five values obtained from the relative intensity sets (Section 5.3). Anomalous dispersion corrections were made to the structure factors as for the relative intensity sets (Section 4.8). TDS correction factors were calculated via program TDSCORR (Appendix 1), but in this case the volume integration in reciprocal space was defined by the θ-2θ scan, the size of the aperture used and the angle through which the crystal was rotated. The TDS correction factors α are presented in Table 6.4 together with the corrected observed structure factors F_o and the calculated Hartree-Fock structure factors F_c. It can be seen that there is evidence of anisotropy. An anharmonicity parameter P (Section 2.3) was calculated from the splitting of the 330-411 pair of reflections. Its value is -.00240. It can also be seen that the F_o values are low by a factor of about 2. Values of the observed structure factors multiplied by a scaling factor of 2.247, and of the calculated structure factors corrected for anharmonicity by the factor $\exp(-PD)$, where P and D are as defined in Section 2.3, are given in Table 6.5. Possible reasons for requiring the extra scaling factor of 2.247 will be discussed in Section 6.12.

TABLE 6.4

TDS Correction Factor; Observed and Calculated Structure Factors

Reflection	α	$\lvert F_o \rvert$	$\lvert F_c \rvert$
110	.099	4.84	17.65
211	.36	4.78	14.20
220	.50	4.77	12.90
330	1.25	4.00	8.71
411	1.25	3.64	8.71
332	1.51	3.72	7.68
422	1.53	3.47	7.36

TABLE 6.5

Observed and Calculated Structure Factors

Reflection	$2.247F_o$	$\lvert F_c e^{-PD} \rvert$
110	10.88	17.66
211	10.75	14.25
220	10.71	12.98
330	8.99	8.99
411	8.17	8.17
332	8.37	8.60
422	7.81	7.79

P = -.00240

The values of observed and calculated structure factors tabulated in Table 6.5 agree very well for the four higher angle reflections, but there is pronounced extinction for the three lower angle reflections. This is similar to the results given in Table 5.2 for the relative intensities of set 3. In both cases, the crystals were dipped in liquid air before the intensities were recorded. The anharmonicity parameter P in the present case is about twice that determined as an average of the five relative intensity set parameters.

6.12 Errors

Of the measured quantities involved in equation 6.11.1, an estimate of the error in V has already been given as 5%.

An estimate of the error in the absorption correction A* as a function of μR for a spherical crystal has been given by Burbank (1965) assuming a 10% error in μR. The distortion from spherical of the crystal used in this experiment was estimated at a maximum of 11%. For the value of $\mu R \sim .7$ applicable here, the errors inA* given by Burbank range from about 12% for $\theta = 0^{o}$ to about 7% for $\theta = 90^{o}$. It was estimated, therefore, that the error in A due to uncertainty in R was about 10%.

The error in measuring I_o was due solely to the errors in

calibration of the attenuating foils and measurement of the aperture size since the counting statistical errors were $\sim$ .1%. The standard deviation of the attenuation coefficient for each nickel foil was 1.6%, and the standard deviation of the aperture was 2.5%. The overall error in I_o was estimated at 4.8%.

Other sources of error may be multiple diffraction and TDS. The former can be disregarded for measurement on the zero layer of a non-symmetry axis in a crystal where there are relatively few reflections. The TDS correction factors calculated in the present case are larger than those calculated in the case of the photographically recorded relative intensities because the estimate of the volume swept out in reciprocal space as the aperture scans through a reflection is larger. It is possible, therefore, that the first order TDS correction is too large. This would make the structure factors too low. On the other hand, no correction has been made for higher order TDS. This would make the structure factors too high.

The statistical errors in E, given according to equation 6.9.1 are listed in Table 6.6. The corresponding calculated errors σ_F in the structure factors are given also. The σ_F values are all $\sim$ 6%. This is due almost entirely to the errors in A and V, which are due to the distortion of the crystal from spherical. The accuracy of the method depends therefore, not on the counting

statistical accuracy, but on the accuracy with which the size and shape of the crystal can be determined. In common with Burbank, we can conclude that more reliable information about thermal motion or density distortions can be obtained from a larger set of accurate relative intensity measurements than from a few absolute intensities.

TABLE 6.6

Reflection	σ_E(%)	σ_F(%)
110	1.7	6.1
211	1.8	6.1
220	1.9	6.2
330	1.8	6.1
411	2.0	6.2
332	3.2	6.3
422	4.4	6.5

None of the above errors can account for the scaling factor of 2.247 used in Table 6.5. Because the scaled observed structure factors show extinction and anisotropy to about the same degree as those measured previously (Table 5.2), it is unlikely that there are large errors in the measurement of the intensities. However, in order to check that there were no such errors due to crystal misalignment or electronics drift in the P.H.A., various intensities

were remeasured. The crystal alignment and P.H.A. were carefully readjusted before each reading. The results are shown in Table 6.7. The only major difference from those listed in Tables 6.2 and 6.3 was the intensity for 220, which can be explained as "annealing" as observed previously (Section 5.7). (The individual reflections in Table 6.7 are not necessarily the same as those in Table 6.2).

TABLE 6.7

Integrated Intensities

Reflection	Intensity	Att. Factor	Corrected Intensity
220	7906	6.66	52654
220	12190	6.66	81185
330	10464		
330	9027		
411	9632		
411	9245		
411	7117		
332	4571		
332	3620		
422	2805		
422	3411		

TABLE 6.7 (Continued)

Averaged Integrated Intensities

Reflection	Intensity	Errors(%)
220	66920	1.45
330	9746	1.75
411	8665	2.92
332	4096	3.71
422	3108	4.70

Similarly, the direct beam was remeasured using a larger (368 micron) pin hole punched in a large lead sheet. The remeasured value of I_o was in agreement with the original value to within the experimental error.

The need for a scaling factor is not due, then, to inaccurate measurement, but to factors which cannot be properly estimated in this case due to the type of crystal used. For example, there will be absorption of the incident and diffracted beams from the crystal by the glass capillary and the oil surrounding the crystal. There may also be systematic errors due to inaccurately known values of the linear absorption coefficient μ, and the other factors already mentioned. (The specimen is not suitable for an experimental measurement of μ).

In summary, the scaled observed structure factors obtained here confirm the observations of anisotropy and extinction discussed in Chapter 5. For example, the magnitude of each effect is about the same as observed for set 3 of the relative intensity sets. The isotropic Debye parameter $B' = 8.16$ obtained in Section 5.3, together with the calculated anisotropy parameter $P = -.00240$ gave an excellent account of the four higher angle structure factors. Evidence for room temperature annealing after liquid air chilling of the crystal was again observed. Finally, the method is not sufficiently accurate for absolute measurements for a crystal of this type.

CHAPTER 7

CONCLUSIONS AND DISCUSSION

Accurate experimental structure factors for metallic sodium have been presented for the first time. Probably the most striking aspect of the results is the anisotropy exhibited in the higher angle reflections, where deviations in intensity of more than 15% from the expected values for an isotropically vibrating spherically symmetric Hartree-Fock atom were recorded. This anisotropy is due to crystal field effects and has been described in terms of the generalised structure factor formalism of Dawson (1967a). Of the two possible physical interpretations of this phenomenon, the most probable is that the anisotropy is a result of anharmonic vibrations of the atoms. This might be expected given other known physical information about sodium which indicates large and possibly anisotropic thermal motion of the atoms in the solid. This information includes the high isotropic Debye parameter, low melting point, and the low values of the elastic constants and the anisotropy they show. A consequence of the observed anharmonicity is that anisotropy should be present in other measured quantities. In this respect, macroscopic experimental data relating to anharmonic vibrations is generally limited. For example, there is no data regarding anything other than isotropic thermal expansion coefficients of the alkali metals whereas thermal expansion is a

consequence of anharmonicity and can be expected to be anisotropic even for cubic sodium crystals. It is usual to calculate the linear expansion coefficient α (Kittel (1971)) as

$$< x > = \alpha T$$

where, using Boltzmann statistics,

$$< x > = \frac{\int_{-\infty}^{\infty} x \, e^{-\frac{V(x)}{k_B T}} \, dx}{\int_{-\infty}^{\infty} e^{-\frac{V(x)}{k_B T}} \, dx}$$

where x is the displacement of the atom from its equilibrium position, and V(x) is the potential. Since the coefficients of the potential expansion are known, it would be possible to calculate the expected anisotropy in the thermal expansion coefficient.

The anharmonic vibration theory due to Willis (1969) has been used in the analysis. Although this theory assumes an Einstein model of the crystal and has various mathematical simplifications, it has nevertheless been found to be a good model for this situation. This is the first analysis of anharmonicity in the body-centred-cubic environment using this theory; this is so because an atomic potential expansion to fourth order is needed to describe vibrational motion in sodium. Previous structures for which vibrational anisotropy has been studied have been adequately treated by the quasi-harmonic theory (for example KCl (Willis (1969)))

or a third order potential expansion (for example, the fluorite structures (Willis)). The sign of the anharmonicity parameter used in the analysis indicates that the atoms are vibrating, as might be expected, with greater amplitude toward the next nearest neighbours in the <100> directions, and with smaller amplitude toward the nearest neighbours in the <111> directions. As a result, the measured structure factors are greater than calculated Hartree-Fock values for those reflections near {111} and smaller than calculated values for reflections near {100}. A diagrammatic representation of this phenomenon showing those sections of reciprocal space which scatter more or less than for isotropically vibrating atoms is given in Figure 7.1.

The second possible explanation of the observed anisotropy, that of distortion of the electron density from spherical, with isotropic vibrations of the atoms, is improbable. The least tightly bound electrons in the sodium core, the six 2p electrons, have a binding energy of $\sim$ 39 eV. At a distance of $\sim$ 3Å from a charge of one electron, any electron is subject to a Coulomb potential of about 4 eV. It is unlikely, then, that the 2p electrons will be perturbed from spherically symmetric. The method, however, gives similar mathematical results to the first method. This indicates that it provides a good description of the time averaged electron density. Neither theory provides a means of determining the real space amplitude of vibration.

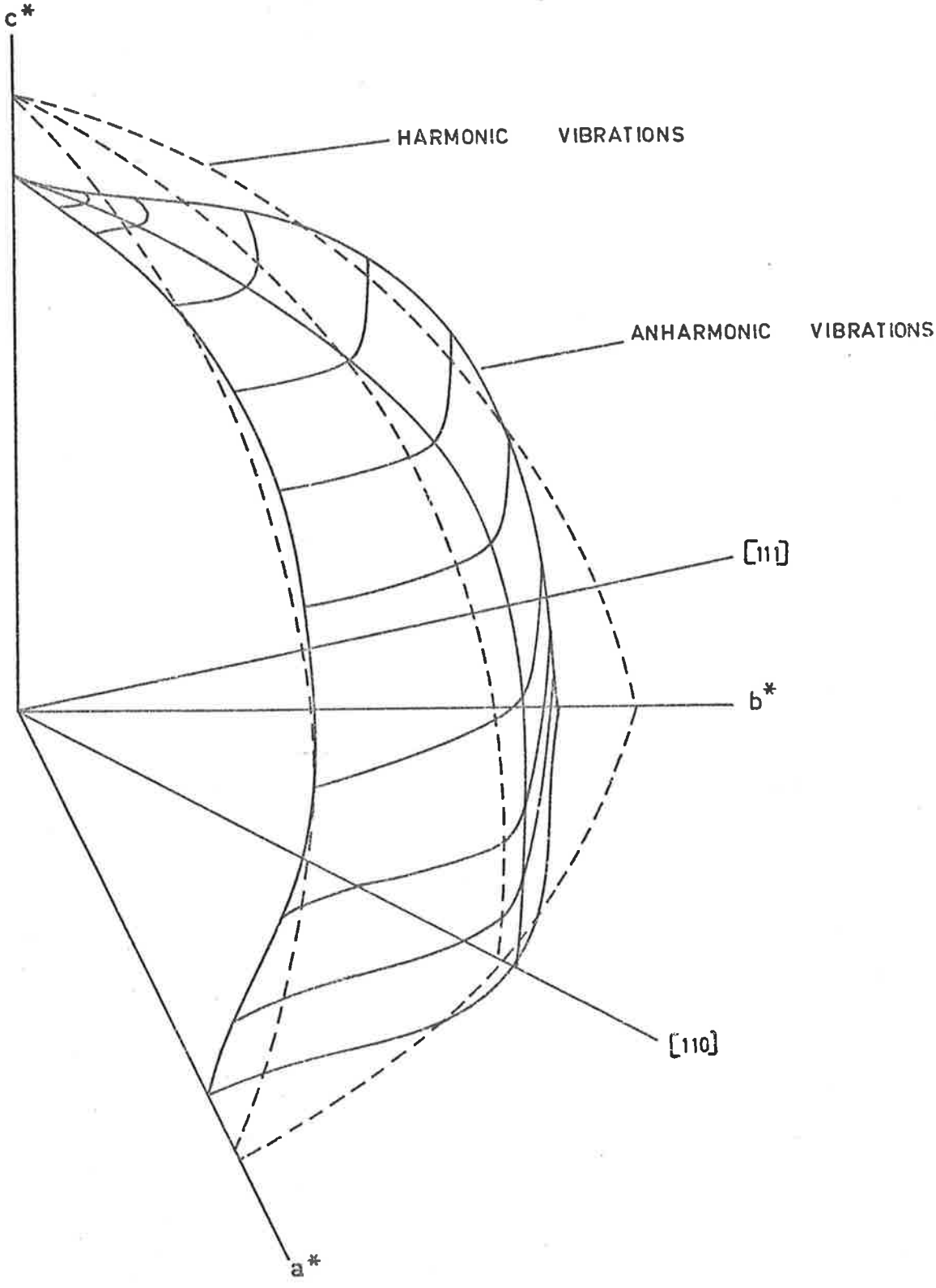

FIG. 7·1 SURFACES REPRESENTING THE ANGULAR DEPENDENCE OF RECIPROCAL SPACE INFORMATION FOR HARMONICALLY AND ANHARMONICALLY VIBRATING ATOMS IN A bcc STRUCTURE.

.

The potential parameters determined from a reanalysis of Dawton's work and in agreement with this work are

$$\alpha_o = .6 \text{ eV } \text{Å}^{-2}$$

$$\gamma_o = -.9 \text{ eV } \text{Å}^{-4}$$

$$\delta_o = -3. \text{ eV } \text{Å}^{-4}$$

It is expected that thermal vibrations "soften" at large amplitudes. This is indeed the case as seen in the negative sign of the isotropic fourth order parameter γ_o. An indication of the relative importance of the anisotropic vibrations, however, is given in the relative magnitudes of the two fourth order terms γ_o and δ_o. In addition, the effect of thermal expansion on the temperature factor appears to be small compared with the contribution from the γ_o parameter.

The physical properties of the Group I elements are such that higher atomic number elements have lower melting points, lower Debye temperatures and hence larger vibration amplitudes. Thus it might be expected that all the alkali metals would show significant anisotropy in structure factors due to thermal vibration. They should all be regarded, then, as highly anharmonic solids.

It is possible that anisotropic vibrations might be expected for the lighter alkali metals even in structures where the metal is in an ionic state. The alkali ion has only one bonding electron, but may be coordinated to six or more other atoms. In this case, it is likely to be relatively loosely bound and capable of large vibration amplitudes, which may be anisotropic depending on the surrounding coordinating atoms. Some evidence for this has been found in the alkali feldspars, for example (Bragg and Claringbull (1965)) and in some coordinated complex ions (Butler (1971)).

The large thermal vibrations appear to be in part the cause of the large extinction observed in sodium. Even after being dipped in liquid air, two crystals showed $\sim$ 70% extinction for the 110 reflection, but both crystals subsequently annealed at room temperature. This process of annealing may go on over a period of some weeks until the extinction for the 110 reflection is greater than 90%. There is not usually any suggestion in the literature of a connection between extinction and thermal motion. It is interesting to note, however, that Cooper and Rouse (1970) report almost 90% extinction in crystals of CaF_2 and SrF_2, both of which show anharmonic vibrations which may be accounted for by a third-order potential expansion (for example, Mair and Barnea (1971)). The extinction theory of Zachariasen (1967) modified by Cooper and Rouse was applied, but did not give reasonable results. The

reasons for this may be several. Firstly, the mathematical assumption that the crystal is made up of spherical mosaic domains with a Gaussian distribution of orientations is probably not true physically, and is not adaptable to the case of strong extinction. Secondly, the functional form of the extinction parameter y(x) may not have been suitable in the present case. For example, the final form of the function y(x) used by Cooper and Rouse (1970) to describe the extinction observed in SrF_2 was quite different from that used for sodium. Further, they conclude that "it is likely that some further improvement could be made in the exact form of the closed form expressions used". Thirdly, there may have been anisotropic extinction present in some form. For example, there was evidence of variation in intensity in low angle symmetry related reflections in sodium (Chapter 6). A similar effect has been observed by Cooper and Rouse in CaF_2, where it was attributed to anisotropy in extinction due to variation in the state of perfection in the crystal.

It has been shown that there are good theoretical and practical reasons why the contribution of the 3s electron cannot be observed in measured Bragg intensities for sodium. Most of the available supplementary evidence (for example on the Fermi surface) suggests that the valence electron in Na is indeed the most "free" of any of the alkali metals. There may still be some doubt over this matter, however, for two reasons. Firstly, the Harrison

(1966) pseudopotential calculation of the radial electron density distribution shows a significant departure from the free atom distribution. It has been shown by Medlin et al. (1969) that the experimental aluminium valence electron density distribution more closely resembles that calculated by Harrison than the free atom distribution. Secondly, it has been pointed out by Weiss (1967) that of the sequence of elements Ne (Z = 10), Mg (Z = 12), Al (Z = 13), and Si (Z = 14), only measured intensities from Al are at variance with values predicted by Hartree-Fock free atom theory. Weiss suggests that this may be connected with the fact that Al is the only odd Z element in the group. If this connection were true, then it would be expected that a similar effect might be observed in sodium (Z = 11), and in fact, in all the alkali metals. It should, then, be a worthwhile exercise to investigate the low angle scattering by means of a structure such as the clathrate type of Na_8Si_{46}, where the sodium atoms are virtually in the same valence state as in the metal.

APPENDIX 1

COMPUTER PROGRAMS

All programs referred to in this thesis were written by the author except the film- and layer-scaling programs AUFAC and AULAC respectively. These last are maintained in the crystallographic program library at Adelaide University. All computing was carried out on the CDC6400 computer of the University of Adelaide.

1. Program SCATFAC

This program was written to calculate atomic scattering factors for sodium from the Hartree-Fock wave functions of Hartree and Hartree (1948). The method used was essentially that of Berghuis et al. (1955).

The tabulated wave functions and radii were first converted to Angstrom units, then interpolated at 298 points, giving the wave function at a total of 354 points. The interpolation procedure used was an nth order polynomial fitting method described by Rollett (1965). It was found that n = 4 gave satisfactorily accurate results.

The scattering factors were then calculated by carrying out the numerical integration of the equation

$$f(s) = \int_0^Z R^2 \frac{\mathrm{Sin}(4\pi sr)}{4\pi sr}\, dr \qquad \ldots(1)$$

where R is the radial wave function as tabulated by Hartree and Hartree, and therefore

$$R^2 = 4\pi r^2 \rho(r)$$

where $\rho(r)$ is the electron density,

$$s = \frac{\mathrm{Sin}\theta_B}{\lambda}$$

and Z the maximum value of r at which the wave functions were tabulated. The numerical integration was carried out by Simpson's rule.

Equation 1 is the zeroth order example of a general set of equations

$$\langle j_n(4\pi sr)\rangle = \int_0^\infty R^2 j_n(4\pi sr)\, dr \qquad \ldots(2)$$

where $j_n(4\pi sr)$ are the spherical Bessel functions given by

$$j_0(4\pi sr) = \frac{\mathrm{Sin}(4\pi sr)}{4\pi sr}$$

$$j_1(4\pi sr) = \frac{\mathrm{Sin}(4\pi sr)}{(4\pi sr)^2} - \frac{\mathrm{Cos}(4\pi sr)}{(4\pi sr)} \qquad \ldots(3)$$

$$j_{n+1}(4\pi sr) = \frac{2n+1}{4\pi sr}\, j_n(4\pi sr) - j_{n-1}(4\pi sr) \quad \ldots(3)$$

This program was also adapted to calculate $\langle j_4(4\pi sr)\rangle$ using the wave function of Hartree and Hartree for the $2p^6$ electrons only. Here

$$j_4(4\pi sr) = \frac{105\mathrm{Sin}(4\pi sr)}{(4\pi sr)^5} - \frac{105\mathrm{Cos}(4\pi sr)}{(4\pi sr)^4} - \frac{45\mathrm{Sin}(4\pi sr)}{(4\pi sr)^3}$$

$$+ \frac{10\mathrm{Cos}(4\pi sr)}{(4\pi sr)^2} + \frac{\mathrm{Sin}(4\pi sr)}{(4\pi sr)} \quad \ldots(4)$$

2. Program PEDNA

This program was written to carry out the determination of the radial density distribution for the sodium valence electron from the Harrison (1966) pseudopotential data (see Section 2.4). The electron density is given by

$$\rho(r) = \frac{\Omega_o}{2\pi} \int_0^\infty dq\; q^2\; \rho_q\; \frac{\mathrm{Sin}qr}{qr} \quad \ldots(5)$$

where Ω_o is the volume per ion

ρ_q is a relative density form factor which is derived from the pseudopotential via Poisson's equation, and

q is the reciprocal space variable.

The radial density then becomes

$$Q(r) = \frac{4\pi r^2}{\Omega_o}\rho(r) = \frac{4r^2}{\pi}\int_o^\infty dq\ q^2\ \rho_q \frac{Sinqr}{qr} \qquad \ldots(6)$$

This equation can then be written as

$$Q(r) = \frac{2k_F^3 r^2}{\pi}\int_\bullet^\infty x^2\ \rho_x \frac{Sink_F xr}{k_F xr}\,dx \qquad \ldots(7)$$

where $x = q/k_F$ and k_F is the value of q at the Fermi surface. Values of ρ_x to x = 5.0 are tabulated by Harrison (1966) at intervals of $\Delta x = .1$. This range was extended to x = 10.0 with the same intervals by fitting a function of the form

$$f(x) = \frac{A}{x^3}\exp(-Bx) \qquad \ldots(8)$$

to the last two tabulated values of ρ_x. Equation 7 was then integrated by a simple trapezoidal method. Finally, a simple trapezoidal integral of Q(r) at intervals of $\Delta r = .1$ gave the area under the Q(r) curve, i.e. the effective number of valence electrons. This was found to be 1.01 electrons.

3. Program BBSCORR

This program was written to find absorption factors from the tabulated values of $A^*(\mu' R, \upsilon/2)$ given in International Tables

(1959). Here

$$\mu' = \mu \mathrm{Sec}\nu$$

$$\mathrm{Sin}\upsilon/2 = \mathrm{sec}\nu\sqrt{(\mathrm{Sin}^2\theta - \mathrm{Sin}^2\nu)} \qquad \ldots(9)$$

where μ, ν, R and υ have been described previously. (See Section 4.4.5) Values of μ' and $\upsilon/2$ were first calculated from these equations, then the tabulated values of A* were interpolated twice, first at the appropriate values of $\upsilon/2$ for six values of $\mu'R$ by means of a Lagrangian interpolation procedure described by Rollett (1965). Using the same procedure, the values of A* were then interpolated at the appropriate value of $\mu'R$ for the values of $\upsilon/2$.

4. Program TDSCORR

The first order TDS correction factor α_1 is given by (Rouse and Cooper (1969))

$$\alpha_1 = \frac{k_B T\, B^2}{\lambda^3 \mathrm{Cosec}^2\theta_B} \int \frac{1}{q^2} \sum_{j=1,3} \frac{\mathrm{Cos}^2\alpha_j^1(\underset{\sim}{q})}{\rho V_j^2(\underset{\sim}{q})}\, du\, dv\, dw \qquad \ldots(10)$$

where $\underset{\sim}{B}$ is a reciprocal lattice vector for Bragg reflection with

$$B = |\underset{\sim}{B}| = 4\pi \mathrm{Sin}\theta_B/\lambda$$

$\underset{\sim}{q}$ is the wave vector of the scattering phonon ($q = |\underset{\sim}{q}|$)

$(j,\underset{\sim}{q}), j = 1,3$ represents the mode of the phonon $\underset{\sim}{q}$

$V_j(\underset{\sim}{q})$ is the velocity of the mode $(j.\underset{\sim}{q})$

du is an element of angle through which the crystal is rotated during a scan, and dv and dw are elements of vertical and horizontal divergence angles respectively in the scattered beam

$\alpha_j^1(\underset{\sim}{q})$ is the angle between the polarisation direction of the mode $(j,\underset{\sim}{q})$ and $\underset{\sim}{B}$

and the other symbols have their usual meanings.

Cooper and Rouse (1968) have shown that the angles, du, dv, dw can be described in terms of a set of orthogonal axes x,y,z where z is in the direction of the scattering vector, and y is perpendicular to the plane containing the incident and scattered beams. The equation for α_1 then becomes

$$\alpha_1 = \frac{2k_BT}{\pi}\left(\frac{\mathrm{Sin}\theta_B}{\lambda}\right)^2 \int \frac{1}{q^2} \sum_{j=1,3} \frac{\mathrm{Cos}^2\alpha_j^1(\underset{\sim}{q})}{\rho V_j^2(\underset{\sim}{q})}\ dx\ dy\ dz \qquad \ldots(11)$$

Now the factor

$$S_q = \sum_{j=1,3} \frac{\mathrm{Cos}^2\alpha_j^1(\underset{\sim}{q})}{\rho V_j^2(\underset{\sim}{q})} \qquad \ldots(12)$$

$$= \mathrm{Cos}^2\theta_B(A^{-1})_{11} + \mathrm{Sin}^2\theta_B(A^{-1})_{33} + \mathrm{Sin}2\theta_B(A^{-1})_{13}$$

where

$$(A^{-1})_{11} = \begin{vmatrix} A_{22} & A_{23} \\ A_{23} & A_{33} \end{vmatrix} / \Delta \qquad \ldots(13)$$

$$(A^{-1})_{13} = \begin{vmatrix} A_{12} & A_{22} \\ A_{13} & A_{23} \end{vmatrix} / \Delta \qquad \ldots(14)$$

$$(A^{-1})_{33} = \begin{vmatrix} A_{11} & A_{12} \\ A_{12} & A_{22} \end{vmatrix} / \Delta \qquad \ldots(15)$$

$$\Delta = \begin{vmatrix} A_{11} & A_{12} & A_{13} \\ A_{12} & A_{22} & A_{23} \\ A_{13} & A_{23} & A_{33} \end{vmatrix} \qquad \ldots(16)$$

The matrices $A_{kl} = a_j \, a_m \, C'_{jklm}$ $\ldots(17)$

where $C'_{jklm} = b_{jn} b_{kp} b_{lq} b_{mr} C_{npqr}$ $\ldots(18)$

Here a_j, a_m are the direction cosines of $\underset{\sim}{q}$ ($j,m = 1,2$ or 3) and

C'_{jklm} the elastic constants of the medium referred to the x,y,z axes, i.e. b_{jn} etc. are the direction cosines of the x,y,z axes referred to the orthogonal axes for which the elastic constants C_{npqr} are given, i.e. the crystal axes.

A program was written to determine α_1 thus. The C'_{jklm} were calculated from the elastic constants of Martinson (1969) via

equation 18 after the b_{jn} etc. were calculated for each reflection. The values of u,v,w were determined from the least squares straight line fit of the spot sizes, and the reciprocal space volume swept out in the scan and determined by u,v,w was split up into an nxnxn grid for the purposes of numerical integration. The conversion to x,y,z coordinates was made via the equations

$$x = kw - z\tan\theta$$

$$y = kv$$

$$z = 2ku\ \mathrm{Sin}\theta\ \mathrm{Cos}\theta$$

for the ω scan, or

$$x = kw + z\ \cot\theta$$

$$y = kv$$

$$z = 2ku\ \mathrm{Sin}\theta\ \mathrm{Cos}\theta$$

for the θ-2θ scan. Values of q and a_j, a_m were calculated and the values of A_{kl} calculated via equation 17. These were then used to calculate the inverse matrix elements $(A^{-1})_{kl}$ via equations 13, 14 and 15. The calculation of S_q was then a straightforward procedure for each reflection via equation 12. The numerical integration involved in equation 11 was then carried out over the nxnxn grid, using a Simpson's rule procedure adapted for three dimensions. The minimum value of n needed for the results to converge was 11. For this grid size, the program required 70000_8 words of core space and took about four seconds per reflection.

5. Program EXTINCT

This program was written to calculate extinction corrections to the observed structure factors according to the modifications of Cooper and Rouse (1970) to the theory of Zachariasen (1967, 1968) (see Section 5.8).

The physical basis for the Zachariasen theory is that the crystal is assumed to consist of spherical mosaic domains of mean radius r, with their orientations characterised by a Gaussian function

$$W(\Delta) = \sqrt{2}\ g\ \exp(-2\pi^2 g^2 \Delta^2) \qquad \ldots(19)$$

Then the extinction correction factor for the intensities for a spherical crystal is given by

$$y = (1+2x)^{-\frac{1}{2}} \qquad \ldots(20)$$

where

$$x = \left(\frac{p_2}{p_1}\right) Q_o \lambda^{-1}\ \bar{T}r^* \qquad \ldots(21)$$

$$Q_o \lambda^{-1} = \left| \frac{e^2 \lambda F_c}{mc^2 V} \right|^2 / \mathrm{Sin}2\theta_B \qquad \ldots(22)$$

$$p_n = [1 + \mathrm{Cos}^{2n} 2\theta_B]/2 \qquad \ldots(23)$$

$$\bar{T} = RAdA^*/d(\mu R) \qquad \ldots(24)$$

$$r^* = r\left[1 + \left(\frac{r}{\lambda g}\right)^2\right]^{-\frac{1}{2}} \qquad \ldots(25)$$

where A(μR) is the transmission factor and the other symbols have their usual meaning. If determinations of r_1^* and r_2^* at two different wavelengths λ_1 and λ_2 are available, then the two parameters r and g for the crystal can be found via

$$\left.\begin{aligned} r &= r_1^* r_2^* [(\lambda_1^2-\lambda_2^2)/(\lambda_1^2 r_2^{*2} - \lambda_2^2 r_1^{*2})]^{\frac{1}{2}} \\ g &= (r_1^* r_2^*/\lambda_1\lambda_2)[(\lambda_1^2-\lambda_2^2)/(r_1^{*2}-r_2^{*2})]^{\frac{1}{2}} \end{aligned}\right\} \quad \ldots(26)$$

The relation between "observed" and "calculated" structure factors (F_o and F_c respectively) is then given by

$$|F_o| = K|F_c|[1+2x]^{-\frac{1}{4}} \quad \ldots(27)$$

or

$$|F_c| = K^{-1}|F_o|[x^* + (1+x^{*2})^{\frac{1}{2}}]^{\frac{1}{2}} \quad \ldots(28)$$

where

$$x^* = x/(1+2x)^{\frac{1}{2}} \quad \ldots(29)$$

Cooper and Rouse (1970) have extended this theory of Zachariasen in two ways. Firstly, they make allowance for an angle dependent effect by replacing the factor y by

$$y^1 = [1 - \frac{1}{f(\theta)}] + \frac{1}{f(\theta)}[1+2xf(\theta)]^{-\frac{1}{2}} \quad \ldots(30)$$

where

$$f(\theta) \simeq 1 + \frac{1}{3}\,\mathrm{Sin}^{2.5}(\theta) \quad \ldots(31)$$

Secondly, the theory has been extended for corrections to a cylindrical crystal by taking a slightly different form for equation 20 of (ignoring the angle dependence)

$$y = \left[\frac{\sqrt{\pi}}{2}(\mathrm{erf}\sqrt{3x})/\sqrt{3x}\right]^{5/4} \qquad \ldots(32)$$

If the angle dependence modification is now combined with the form of y for cylindrical crystals, the modified extinction factor becomes

$$y^1 = \left[1 - \frac{1}{f(\theta)}\right] + \frac{1}{f(\theta)}\left[\frac{\sqrt{\pi}}{2}(\mathrm{erf}\sqrt{3xf(\theta)})/\sqrt{3xf(\theta)}\right]^{5/4} \qquad \ldots(33)$$

In programming, first the values of $f(\theta)$ given by equation 31 were calculated for each of the two sets of intensities collected with two different wavelengths. The values of the scaling constants K in the equation

$$|F_o| = K|F_c|[y^1]^{\frac{1}{2}} \qquad \ldots(34)$$

were then calculated by averaging over higher angle reflections where the extinction factor was ~ 0. Values of y^1 for the lower angle reflections were then calculated via equation 34, and values of the extinction parameter x for each set were calculated as an average of values of x found for several extinction affected low angle reflections via equation 33. The values of the error function erf(t) were read in for 313 values of t, and the table

searched for the nearest value of t to correspond to the particular value of $3xf(\theta)$ being used. The values of x found via equation 33 were those given by

$$x = 0.01\ (1.1)^{n};\quad n = 1,100$$

which gave the closest solution for y^1 to that obtained from the experimental values via equation 34.

Next the quantities $p_1, p_2, Q_o\lambda^{-1}$ and $\overline{T}$ were calculated. The values of A* were calculated as for the absorption correction program BBSCORR, and the numerical differentiation of A* with respect to μR was done by the method of forward differences over 8 values of μR. Values of r* were then calculated via equation 21 for each of the intensity sets. The parameters r and g were then calculated via equation 26.

Having found the parameters r and g, the procedure was reversed to find, for each wavelength, values of the correction factor r* from equation 25, x from equation 21, y^1 from equation 33 and finally, corrected values of the observed structure factors from equation 34.

APPENDIX 2

TABLES AND FIGURES FOR DATA SETS 1,2,4,5 AND 6

In general, only tables and figures for data set 3 were presented in the text. Various corresponding tables and figures are presented in this Appendix for all data sets not presented in the main thesis.

Table 1 gives the relative intensities after film factor scaling and spot shape correction (see Table 4.1 for set 3). The averaged intensities after correction for Lorentz-polarisation, absorption and TDS are shown in Table 2 (see Table 4.3 for sets 3 and 4). The intensities after layer scaling, and correction for anomalous dispersion are shown in Table 3 (the corresponding values for set 3 are shown in Table 4.6).

The Wilson plot figures corresponding to that for set 3 (Figure 5.1) are shown in Figures 1 to 5.

Finally, observed and calculated structure factors, standard errors and reliability indices are given in Table 4. These correspond to the values for set 3 given in Table 5.2.

TABLE 1

RELATIVE INTENSITIES AVERAGED AFTER FILM FACTOR SCALING AND SPOT SHAPE CORRECTIONS

Set 1

Reflection	Layer 0	Layer 1	Layer 2
110	2682.8	4210.6	
200	1380.2		
211		1113.6	1590.1
220	857.4		911.8
310	430.4	431.0	
222			247.6
321		242.8	220.3
400	95.1		
(330	96.8		
(			
(411		86.2	
420	58.1		55.9
332			44.4
422			27.1
(431		26.4	
(			
(510	16.2	21.7	
521		17.9	9.3

TABLE 1 (Continued)

Set 2

Reflection	Layer 0	Layer 1	Layer 2	Layer 3	Layer 4
110	3715.5	4698.5			
200	2373.8				
211		1667.3	3187.6		
220	1204.3		1625.4		
310	632.4	513.5		2045.3	
222			391.3		
321		250.5	222.9	432.0	
400	81.1				
(330	55.7			109.8	
(					
(411		43.4			120.2
420	22.7		29.5		49.0
332			17.8	24.1	
422			10.2		16.4
431				7.5	12.9

TABLE 1 (Continued)

Set 4

Reflection	Layer 0	Layer 1	Layer 2	Layer 3	Layer 4	Layer 5
110		484.5	340.9	872.7		
200	332.7		201.6		257.9	
211	232.5	197.9		155.7	178.8	202.6
220			90.94		100.7	
310		69.93	47.08	58.90		51.17
222			37.71			
321	40.27	29.77		22.05	22.69	22.34
400	21.10				15.82	
(330				10.09		
(411		14.23	8.60	7.65		
420	10.85		8.14		7.08	
332		7.49		5.48	4.85	
422	5.72		2.91			
(431		3.22	2.24			2.52
(510		2.40	1.94	2.14		2.47

TABLE 1 (Continued)

Set 5

Reflection	Layer 0	Layer 1	Layer 2	Layer 3	Layer 4
110		204.0	159.7	331.1	
220	117.9		107.7		236.0
211	91.53	94.74		89.47	135.0
220			43.12		70.10
310		42.78	23.79	27.99	
222			18.72		
321	15.24	14.90		10.61	14.51
400	6.2				6.41
(330				3.17	
(411		2.81	2.97	2.25	
420	2.09				2.394

TABLE 1 (Continued)

Set 6

Reflection	Layer 0	Layer 1	Layer 2	Layer 3
110	226.1	237.2		
200	162.3			
211		90.51	138.7	
220	81.98		75.42	
310	52.27	36.94		99.38
222			33.70	
321		13.84	18.37	24.61
400	11.06			
(330	6.928			7.12
(411		3.860		
420	3.254			

TABLE 2

RELATIVE INTENSITIES AFTER ABSORPTION,

LORENTZ-POLARISATION AND TDS CORRECTIONS

Set 1

Reflection	Layer 0	Layer 1	Layer 2
110	5978.6	6871.7	
200	4558.7		
211		4411.4	4431.8
220	4285.8		3656.9
310	2446.3	2387.2	
222			1382.1
321		1534.2	1324.3
400	584.5		
(330	583.6		
(411		501.7	
420	312.6		293.4
332			204.8
422			109.9
(431		72.23	
(510	42.98	57.12	
521		21.06	10.84

TABLE .2 (Continued)

Set 2

Reflection	Layer 0	Layer 1	Layer 2	Layer 3
110	975.2	872.0		
200	891.6			
211		694.2	840.5	
220	617.1		590.5	
310	358.3	276.1		368.5
222			197.5	
321		169.5	124.7	171.4
400	56.0			
(330	40.8			57.1
(411		30.5		
420	17.2		20.0	
332			12.9	14.9
422			7.4	
431				5.1

TABLE 2 (Continued)

Set 5

Reflection	Layer 0	Layer 1	Layer 2	Layer 3	Layer 4
110		50.16	29.14	26.76	
200	43.20		35.38		38.74
211	40.69	40.03		33.13	40.98
220			20.59		27.68
310		23.83	12.50	14.09	
222			8.87		
321	9.68	9.74			8.28
400	4.21				3.98
(330				2.26	
(411		2.07	2.11	1.59	
420	1.55				1.65

TABLE 2 (Continued)

Set 6

Reflection	Layer 0	Layer 1	Layer 2	Layer 3
110	56.75	41.37		
200	58.53			
211		36.23	35.14	
220	41.17		26.84	
310	29.49	19.79		17.81
222			17.23	
321		9.14	10.67	10.13
400	9.09			
(330	5.55			4.05
(411		2.98		
420	2.79			

TABLE 3

AVERAGE RELATIVE INTENSITIES AFTER LAYER SCALING AND ANOMALOUS DISPERSION CORRECTIONS

Reflection	Set 1	Set 2	Set 4	Set 5	Set 6
110	6159.4	1035.1	793.9	40.33	585.6
200	4587.7	947.3	762.8	46.23	579.4
211	4477.5	947.5	734.1	44.31	514.6
220	4006.4	722.2	588.6	29.94	392.8
310	2314.1	343.3	373.3	19.44	282.9
222	1479.8	258.7	273.4	12.41	247.8
321	1444.5	172.0	182.2	9.742	148.7
400	576.0	59.08	112.6	4.424	89.35
(330	572.9	53.61	78.91	3.142	56.66
(411	474.7	35.44	67.36	2.357	43.99
420	307.3	24.22	52.51	1.668	27.47
332	215.3	15.47	32.40		
422	115.1	9.684	17.59		
(431	67.31	5.081	8.764		
(510	42.05		7.552		
521	13.33				

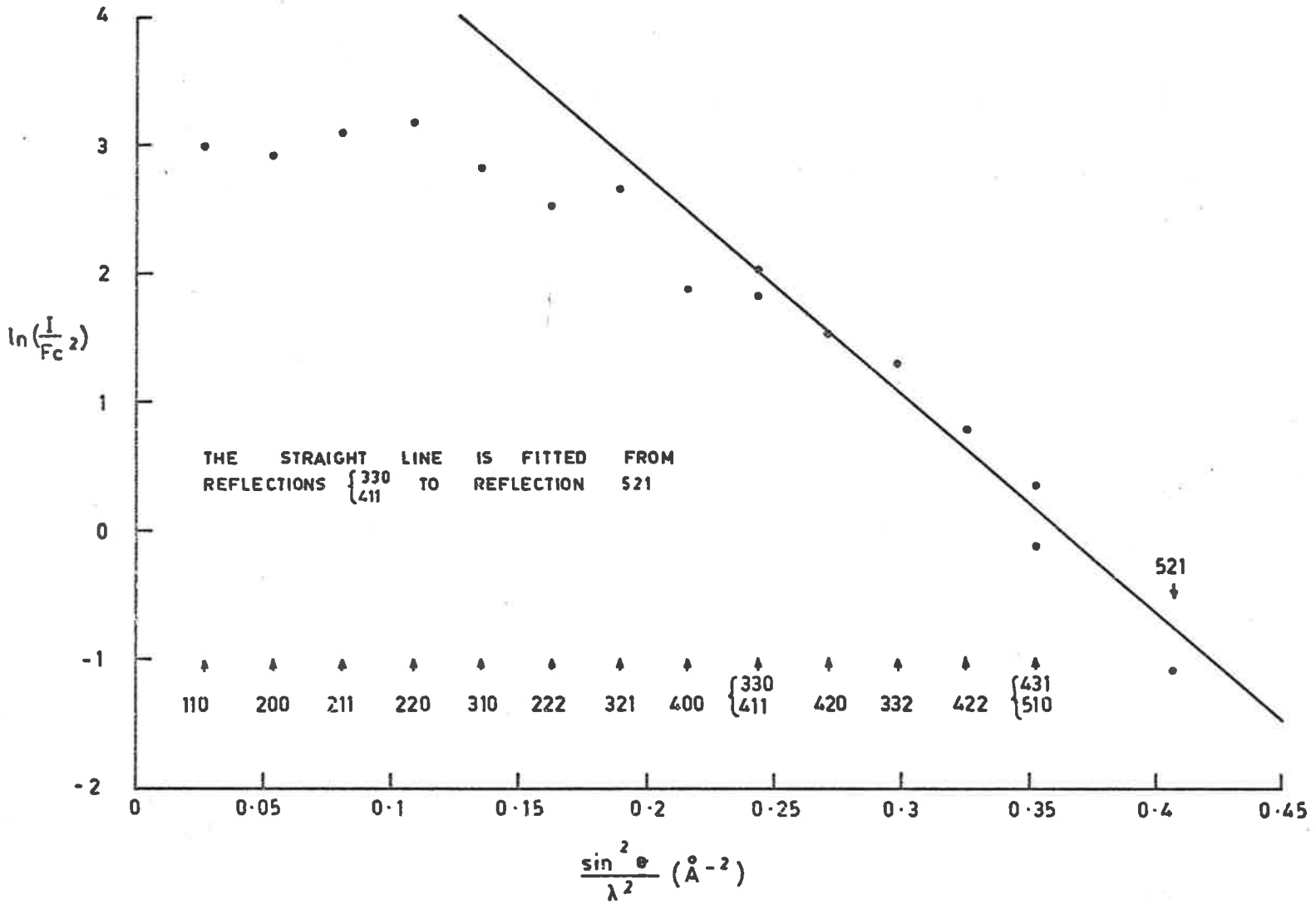

FIG. 1 WILSON PLOT FOR DATA SET 1.

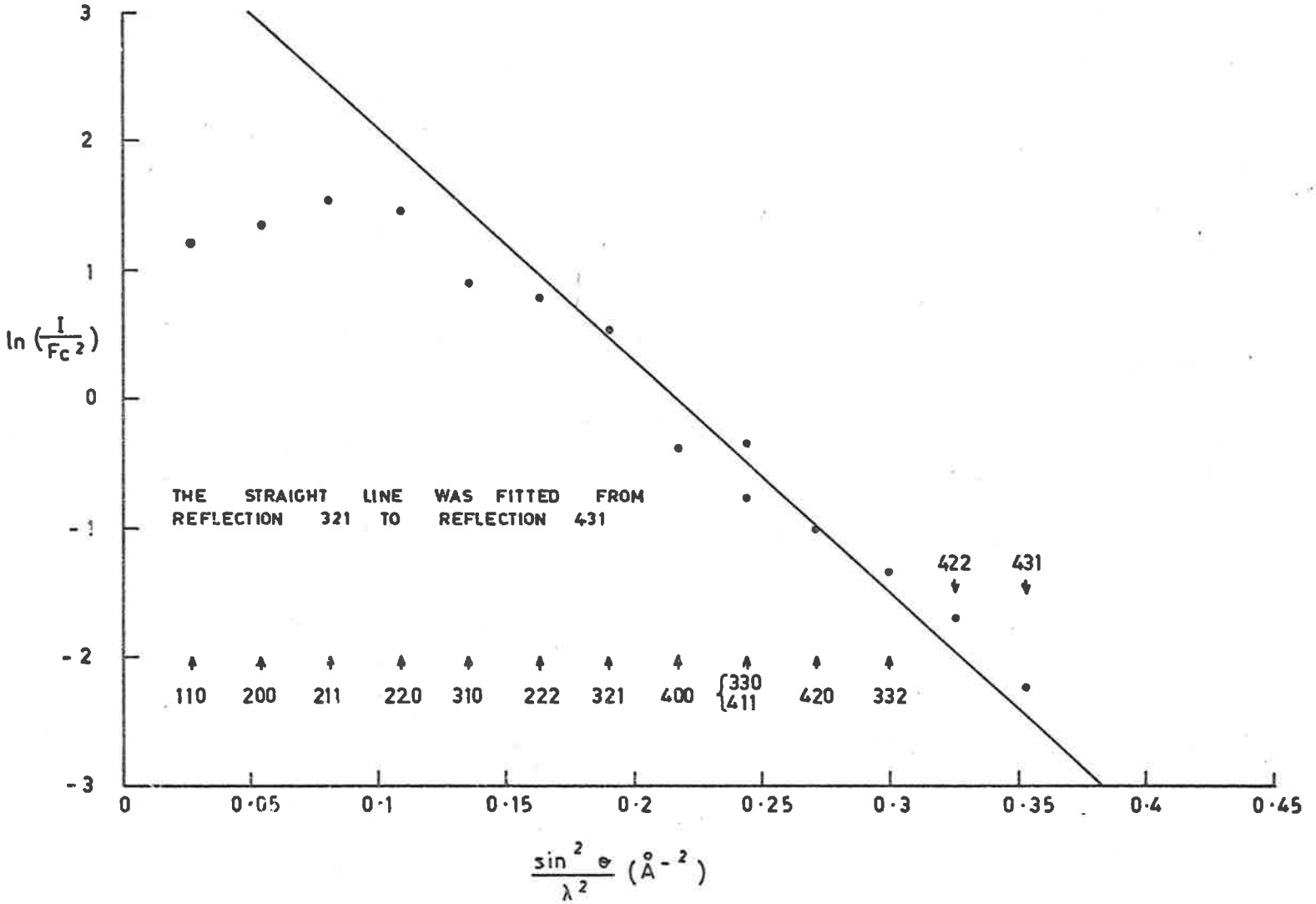

FIG. 2 WILSON PLOT FOR DATA SET 2.

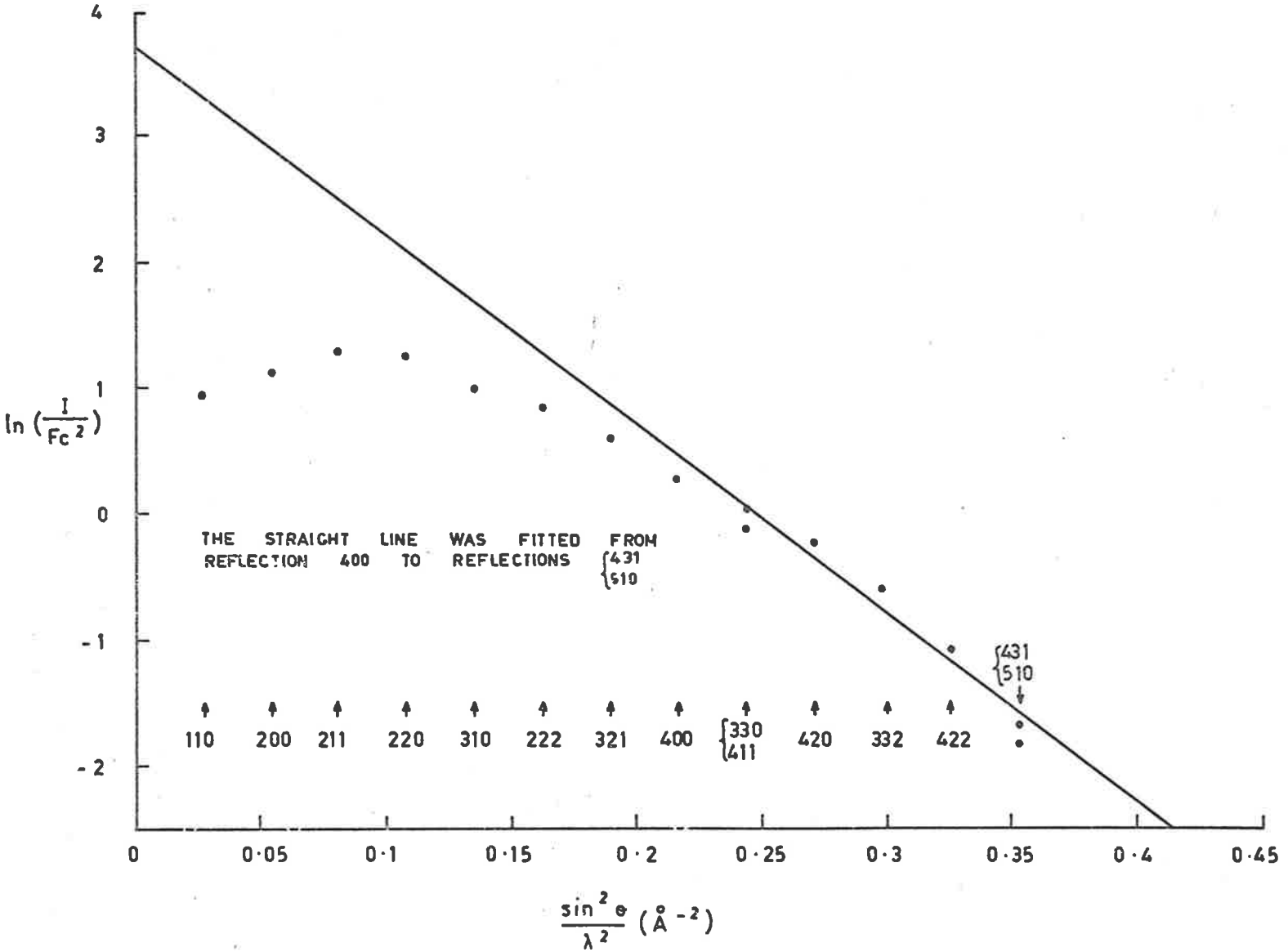

FIG. 3 WILSON PLOT FOR DATA SET 4.

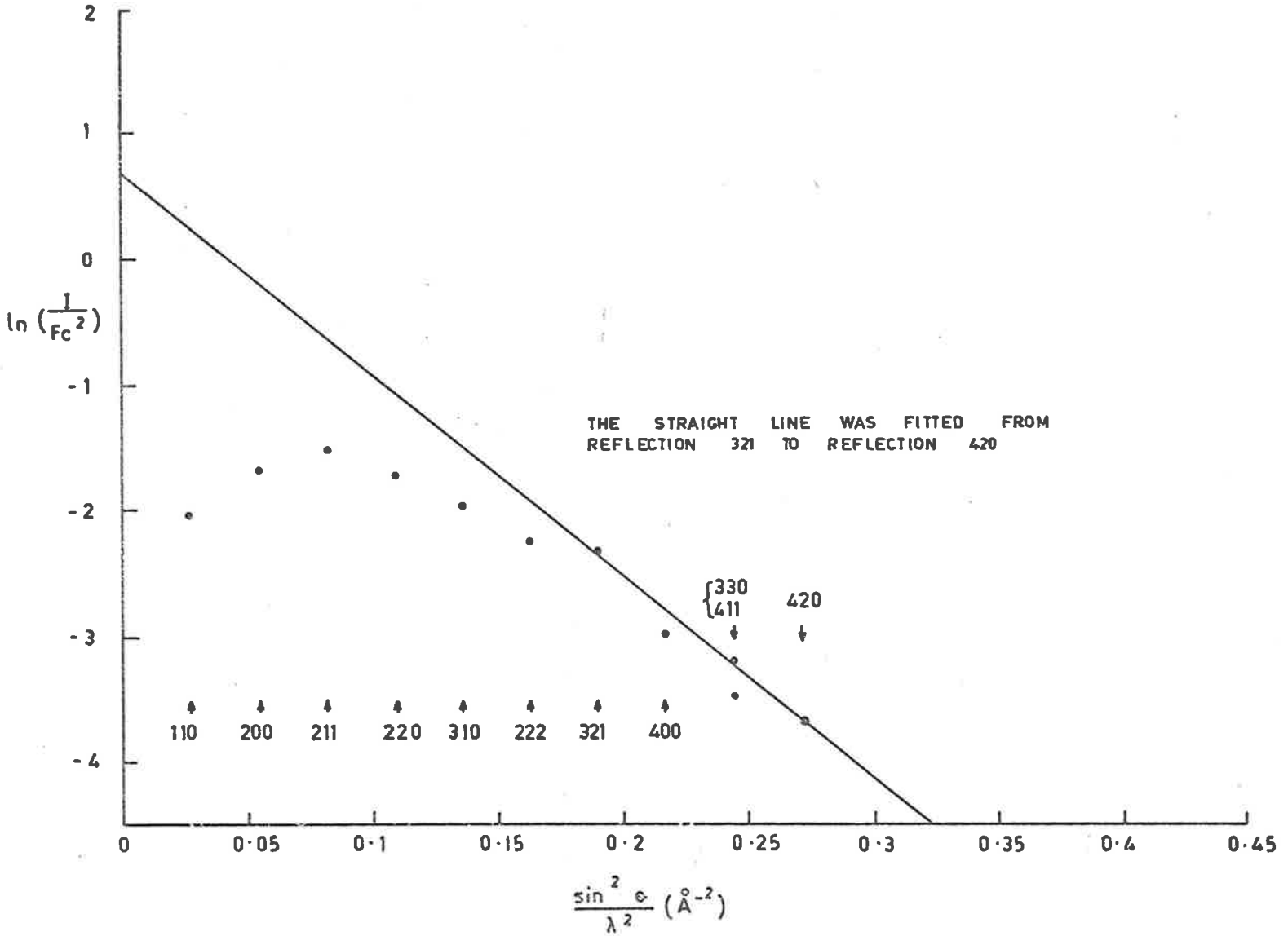

FIG. 4 WILSON PLOT FOR DATA SET 5.

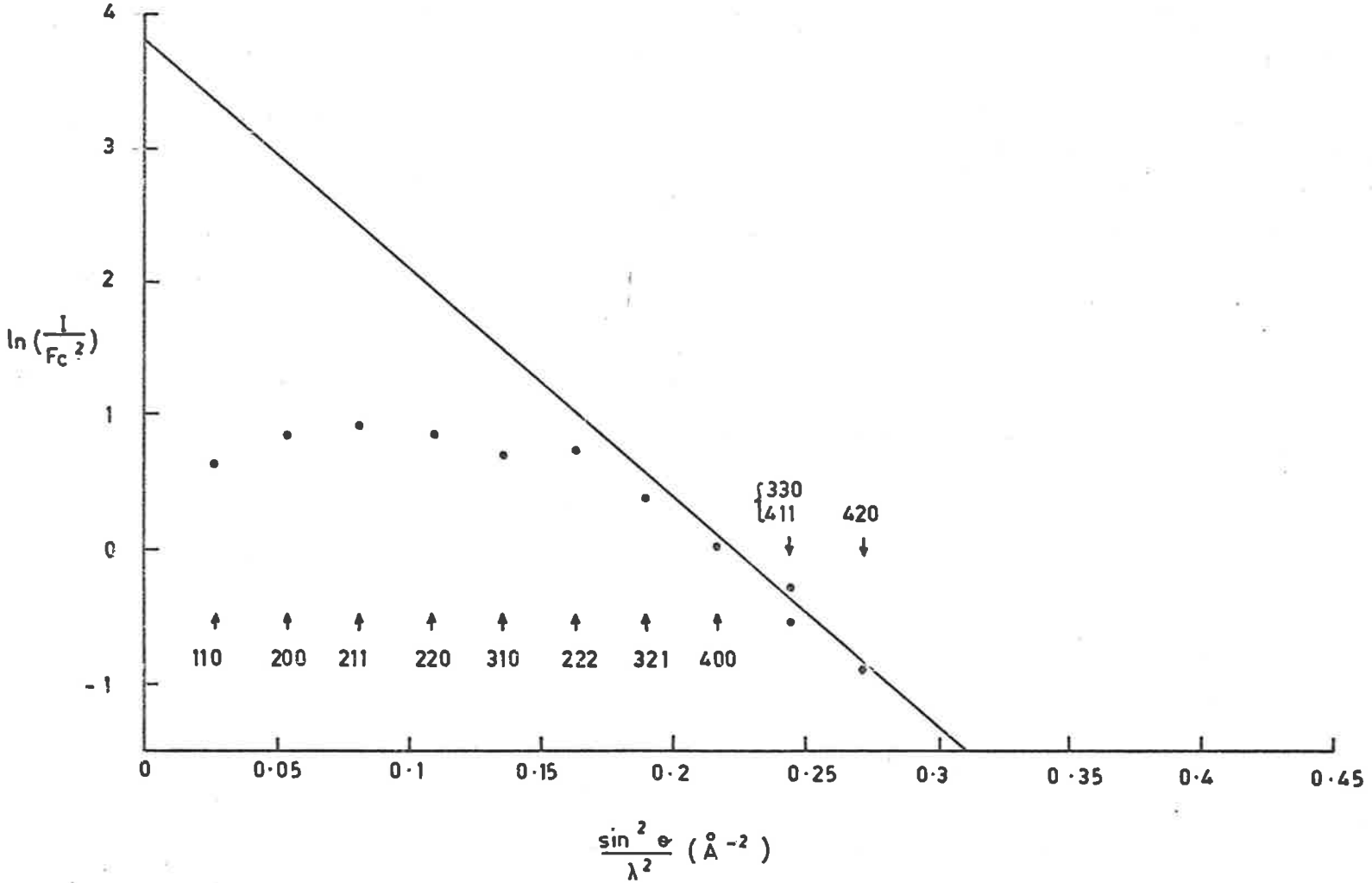

FIG. 5 WILSON PLOT FOR DATA SET 6.

TABLE 4

OBSERVED AND CALCULATED STRUCTURE FACTORS,

STANDARD ERRORS AND RELIABILITY INDICES

Set 1

Reflection	$\|F_o\|$	$\|F_c\|$	$\|F_1\|$	$\|F_2\|$	α_F(%)
110	4.54	17.65	17.66	17.66	3.4
200	4.93	15.74	15.66	15.58	2.9
211	6.13	14.20	14.24	14.27	3.3
220	7.30	12.90	12.97	13.02	5.5
310	6.99	11.80	11.59	11.47	4.4
222	7.04	10.85	11.11	11.35	10.2
321	8.75	10.03	10.19	10.26	3.2
400	6.96	9.32	8.54	8.30	5.3
330	8.74	8.71	8.94	8.99	5.6
411	7.95	8.71	8.25	8.14	5.5
420	8.06	8.16	7.95	7.91	2.8
332	8.49	7.68	8.39	8.47	8.3
422	7.81	7.36	7.71	7.62	4.7
431	7.52	6.88	7.26	7.27	5.7
510	5.95	6.88	5.64	5.63	4.5
521	5.31	6.25	5.72	5.77	3.7

$R = .080$

$R_1 = .030$

$R_2 = .031$

TABLE 4 (Continued)

Set 2

Reflection	$\lvert F_o \rvert$	$\lvert F_c \rvert$	$\lvert F_1 \rvert$	$\lvert F_2 \rvert$	α_F (%)
110	5.93	17.65	17.66	17.67	4.4
200	7.23	15.74	15.58	15.51	14.4
211	9.23	14.20	14.28	14.31	4.3
220	10.27	12.90	13.04	13.07	4.7
310	9.03	11.80	11.38	11.32	2.7
222	10.00	10.85	11.35	11.58	4.1
321	10.39	10.03	10.35	10.36	1.8
400	7.77	9.32	7.80	7.82	4.9
330	9.44	8.71	9.16	9.13	2.8
411	7.67	8.71	7.82	7.88	4.4
420	8.09	8.16	7.74	7.79	3.2
332	8.24	7.68	9.07	8.84	4.2
422	8.32	7.36	8.04	7.79	12.8
431	7.68	6.88	7.63	7.45	9.2

$R = .091$

$R_1 = .030$

$R_2 = .033$

TABLE 4 (Continued)

Set 4

Reflection	$\|F_o\|$	$\|F_c\|$	$\|F_1\|$	$\|F_2\|$	α_F(%)
110	5.36	17.65	17.66	17.66	1.6
200	6.45	15.74	15.66	15.64	3.3
211	7.77	14.20	14.24	14.25	2.1
220	8.54	12.90	12.97	12.98	3.5
310	8.34	11.80	11.60	11.58	7.8
222	8.76	10.85	11.10	11.18	5.3
321	8.78	10.03	10.19	10.18	1.8
400	8.47	9.32	8.58	8.64	5.8
330	8.70	8.71	8.78	8.90	2.6
411	8.04	8.71	8.27	8.33	1.9
420	8.71	8.16	7.96	7.99	2.3
332	8.40	7.68	8.36	8.21	3.0
422	7.60	7.36	7.69	7.50	11.2
431	6.58	6.88	7.25	7.14	2.8
510	6.11	6.88	5.70	6.05	2.8

$R = .067$

$R_1 = .038$

$R_2 = .036$

TABLE 4 (Continued)

Set 5

Reflection	$\|F_o\|$	$\|F_c\|$	$\|F_1\|$	$\|F_2\|$	α_F(%)
110	5.69	17.65	17.66	17.66	1.2
200	7.56	15.74	15.64	15.60	.7
211	9.19	14.20	14.25	14.27	2.6
220	9.38	12.90	12.99	13.01	1.7
310	9.38	11.80	11.54	11.50	2.9
222	9.31	10.85	11.16	11.31	7.8
321	10.24	10.03	10.23	10.24	2.0
400	8.57	9.32	8.38	8.38	2.3
330	8.97	8.71	8.98	8.97	5.4
411	7.77	8.71	8.16	8.19	4.3
420	8.11	8.16	7.90	7.93	7.1

$R = .051$

$R_1 = .019$

$R_2 = .018$

TABLE 4 (Continued)

Set 6

Reflection	$\lvert F_o \rvert$	$\lvert F_c \rvert$	$\lvert F_1 \rvert$	$\lvert F_2 \rvert$	α_F(%)
110	4.57	17.65	17.66	17.66	1.8
200	5.72	15.74	15.65	15.64	5.1
211	6.79	14.20	14.24	14.25	4.4
220	7.48	12.90	12.97	12.97	2.5
310	7.99	11.80	11.58	11.59	2.5
222	9.42	10.85	11.11	11.16	4.5
321	9.19	10.03	10.20	10.17	1.5
400	8.98	9.32	8.53	8.69	2.0
330	9.01	8.71	8.94	8.88	2.0
411	7.94	8.71	8.24	8.36	2.9
420	7.90	8.16	7.94	8.01	1.8

$R = .050$

$R_1 = .026$

$R_2 = .028$

BIBLIOGRAPHY

Abrahams, S.C., Hamilton, W.C. and Mathieson, A. McL. (1970); Acta Cryst. A26, 1.

American Institute of Physics Handbook, 2nd Ed. (1963).

Andrade, E.N. da C. and Tsein, L.C. (1937); Proc. Roy. Soc. A163, 1.

Annaka, S. (1962); J. Phys. Soc. Japan 17, 846.

Barrett, C.S. (1956); Acta Cryst. 9, 671.

Berghuis, J., Ijbertha M. Haanapel, Potters, M., Loopstra, B.O., MacGillavry, Caroline, H. and Veenendaal, A.L. (1955); Acta Cryst. 8, 478.

Blackman, M. (1955); Handbuch der Physik vii, Pt. 1, 325.

Bragg, W.L. and Claringbull, G.F. (1965); Crystal Structures of Minerals, Bell.

Brill, R. (1967); Solid State Physics 20, 1.

Burbank, R.D. (1964); Acta Cryst. 17, 434.

Burbank, R.D. (1965); Acta Cryst. 18, 88.

Butler, K.R. (1971); Private Communication.

Cade, P.E., Bader, R.F.W., Henneker, W. and Keaveny, I. (1969); J. Chem. Phys. 50, 5313.

Calder, R.S., Cochran, W., Griffiths, D. and Lowde, R.D. (1962); J. Phys.Chem. Solids 23, 621.

Canut, M.L. and Amoros, J.L. (1961); Proc. Phys. Soc. 77, 712.

Chipman, D.R. and Jennings, L.D. (1963); Phys. Rev. 132, 728.

Cohen, M.H. and Heine, V. (1958); Adv. in Phys. 7, No. 28.

Cooper, M.J. and Rouse, K.D. (1968); Acta Cryst. A24, 405.

Cooper, M.J. and Rouse, K.D. (1970); Acta Cryst. A26, 214.

Coulthard, M.A. (1967); Proc. Phys. Soc. 91, 44.

Cromer, D.T. (1965a), Acta Cryst. 18, 17.

Cromer, D.T. (1965b); Acta Cryst. 19, 224.

Cromer, D.T. and Mann, J.B. (1968); Acta Cryst. A24, 321.

Daniels, W.B. (1960); Phys. Rev. 119, 1246.

Davies, P.T. (1950); J. Sci. Inst. 27, 338.

Dawson, B. (1967a); Proc. Roy. Soc. A, 298, 255.

Dawson, B. (1967b); Proc. Roy. Soc. A, 298, 264.

Dawson, B., Hurley, A.C. and Maslen, V.W. (1967); Proc. Roy. Soc. A, 298, 289.

Dawton, R.H.V.M. (1937); Proc. Phys. Soc. 49, 294.

Diederich, M.E. and Trivisonno, J. (1966); J. Phys. Chem. Solids 27, 637.

Dingle, R.E. and Medlin, E.H. (1972); Acta Cryst., in the press.

Donaghy, J.J. and Stewart, A.T. (1967); Phys. Rev. 164, 396.

Doyle, P.A. and Turner, P.S. (1968); Acta Cryst. A24, 390.

Feder, R. and Charbnau, H.P. (1966); Phys. Rev. 149, 464.

Freeman, A.J. (1959); Acta Cryst. 12, 261.

Fuchs, K. (1936); Proc. Roy. Soc. A, 153, 622.

Furnas, T.C. (1957); Single Crystal Orienter Instruction Manual, General Electric.

Gammer, R.E. and Heer, C.V. (1960); Phys. Rev. 118, 955.

Geshko, E.I., Kushta, G.P. and Mik'halchenko, V.P. (1968); Ukrainskii fiz. zhurnal, 13, 1788.

Grimes, C.C. and Kip, A.F. (1963); Phys. Rev. 132, 1991.

Hamilton, W.C. (1969); Acta Cryst. A25, 102.

Handbook of Chemistry and Physics (1967-8); 48th Ed., Chemical Rubber Co.

Harrison, W.A. (1966); Pseudopotentials in the Theory of Metals, Benjamin.

Hartree, D.R. (1928); Camb. Phil. Soc. Proc. 24, 89, 11.

Hartree, D.R. and Hartree, W. (1948); Proc. Roy. Soc. 193, 299.

Honeycombe, R.W.K. (1959); Metallurgical Reviews 4, No. 13.

Hull, A.W. (1917); Phys. Rev. 10, 661.

International Tables for X-ray Crystallography; Vol. I (1952), Vol. II (1959) and Vol. III (1962); Kynock.

James, R.W. (1965); The Optical Principles of the Diffraction of X-rays, Bell.

James, R.W. and Brindley, G.W. (1931); Phil. Mag. 12, 81.

Jeffery, J.W. and Whitaker, A. (1965); Acta Cryst. 19, 963.

Jeffery, J.W. (1969); Acta Cryst. A25, 153.

Kasper, J.S., Hagenmuller, P., Pouchard, M. and Cros. C. (1965); Science 150, 1713.

Kittel, C. (1971); Introduction to Solid State Physics (Fourth Edition), Wiley.

Konti, A. and Varshni, Y.P. (1969); Can. J. Phys. 47, 2021.

Kurki-Suonio, K. (1968); Acta Cryst. A24, 379.

Lien, W.H. and Phillips, N.E. (1960); Phys. Rev. 118, 958.

Lonsdale, K. (1942); Proc. Phys. Soc. 54, 314.

Lonsdale, K. (1948); Acta Cryst. 1, 142.

Lucas, B.W. (1968); Acta Cryst. A24, 336.

Lucas, B.W. (1969); Acta Cryst. A25, 627.

Lucas, B.W. (1970); Acta Cryst. A26, 354.

Mair, S.L. and Barnea, Z. (1971); Phys. Lett. 35A, 286.

Mann, J.B. (1967); Los Alamos Scientific Laboratory Reports LA-3690 and LA-3691.

Maradudin, A.A. and Flinn, P.A. (1963); Phys. Rev. 129, 2529.

Martin, D.L. (1965); Phys. Rev. 139A, 150.

Martinson, R.H. (1969); Phys. Rev. 178, 902.

Medlin. E.H., Dingle, R.E. and Field, D.W. (1969); Nature 224, 581.

Meissner, E. (1935); Handbuck d. exp. Physik 11, Pt. 2, 50.

Michell, D. (1968); Private Communication.

Milledge, H.J. (1969); Acta Cryst. A25, 173.

Nilsson, N. (1957); Arkiv fur Fysik 12, 247.

Phillips, D.C. (1954); Acta Cryst. 7, 746.

Phillips, W.C. and Weiss, R.J. (1968); Phys. Rev. 171, 790.

Raccah, P.M. and Arnott, R.J. (1967); Phys. Rev. 153, 1028.

Raccah, P.M. and Henrich, V.E. (1969); Phys. Rev. 184, 607.

Roberts, L.M. (1957); Proc. Phys. Soc. 70, 744.

Rollett, J.S. (1965); Computing Methods in Crystallography, Pergamon.

Rouse, K.D. and Cooper, M.J. (1969); Acta Cryst. A25, 615.

Sanger, P.L. (1969); Acta Cryst. A25, 694.

Schwartz, L.H. (1964); Acta Cryst. 17, 1614.

Seitz, F. (1940); Modern Theory of Solids, McGraw-Hill.

Sharma, P.K. and Mehrota, K.N. (1969); An Real Soc. Espan. Fis. Quin. 65, 189.

Shoenberg, D. and Stiles, P.J. (1964); Proc. Roy. Soc. A281, 62.

Simon, F. and Zeidler, W. (1926); Zeits. f. phys. chem. A, 123, 383.

Suzuki, T. (1960); Acta Cryst. 13, 279.

Togawa, S. (1965); J. Phys. Soc. Japan 20, 742.

Tokonami, M. (1965); Acta Cryst. 19, 486.

Truter, M.R. and Pedersen, C.J. (1971); Endeavour 30, 142.

Walford, L.K. and Schoeffel, J.A. (1970); Phil. Mag. 21, 375.

Weiss, R.J. and De Marco, J.J. (1965); Phys. Rev. 140A, 1223.

Weiss, R.J. (1966); X-ray Determination of Electron Distributions, North-Holland.

Weiss, R.J. (1967); Phil. Mag. 16, 141.

Weymouth, J.W. and Soepano, R. (1962); J. App. Phys. 33, 454.

Willis, B.T.M. (1969); Acta Cryst. A25, 277.

Wilson, A.J.C. (1942); Nature 150, 152.

Wilson, R.H., Skelton, E.F. and Katz, J.L. (1966); Acta Cryst. 21, 635.

Wolfe, G.A. and Goodman, B. (1969); Phys. Rev. 178, 1171.

Wolfe, J. (1969); Electronics 42, 42.

Yakel, H.L. and Fankuchen, I. (1962); Acta Cryst. 15, 1188.

Young, R.A. (1969); Acta Cryst. A25, 55.

Zachariasen, W.H. (1965); Acta Cryst. 18, 705.

Zachariasen, W.H. (1967); Acta Cryst. 23, 558.

Zachariasen, W.H. (1968); Acta Cryst. A24, 212.

Zener, C. and Bilinsky, S. (1936); Phys. Rev. 50, 101.